CANADIAN THESES ON MICROFICHE

THÈSES CANADIENNES SUR MICROFICHE

National Library of Canada
Collections Development Branch

Canadian Theses on
Microfiche Service

Ottawa, Canada
K1A 0N4

Bibliothèque nationale du Canada
Direction du développement des collections

Service des thèses canadiennes
sur microfiche

NOTICE

The quality of this microfiche is heavily dependent upon the quality of the original thesis submitted for microfilming. Every effort has been made to ensure the highest quality of reproduction possible.

If pages are missing, contact the university which granted the degree.

Some pages may have indistinct print especially if the original pages were typed with a poor typewriter ribbon or if the university sent us an inferior photocopy.

Previously copyrighted materials (journal articles, published tests, etc.) are not filmed.

Reproduction in full or in part of this film is governed by the Canadian Copyright Act, R.S.C. 1970, c. C-30. Please read the authorization forms which accompany this thesis.

AVIS

La qualité de cette microfiche dépend grandement de la qualité de la thèse soumise au microfilmage. Nous avons tout fait pour assurer une qualité supérieure de reproduction.

S'il manque des pages, veuillez communiquer avec l'université qui a conféré le grade.

La qualité d'impression de certaines pages peut laisser à désirer, surtout si les pages originales ont été dactylographiées à l'aide d'un ruban usé ou si l'université nous a fait parvenir une photocopie de qualité inférieure.

Les documents qui font déjà l'objet d'un droit d'auteur (articles de revue, examens publiés, etc.) ne sont pas microfilmés.

La reproduction, même partielle, de ce microfilm est soumise à la Loi canadienne sur le droit d'auteur, SRC 1970, c. C-30. Veuillez prendre connaissance des formules d'autorisation qui accompagnent cette thèse.

THIS DISSERTATION
HAS BEEN MICROFILMED
EXACTLY AS RECEIVED

LA THÈSE A ÉTÉ
MICROFILMÉE TELLE QUE
NOUS L'AVONS REÇUE

Canada

NL 339 (r. 85/09)

The Nature of Gold Deposits in Shear Zones in the Cordova Gabbro, Grenville Province, Ontario.

by

Peter B. Thomas

A thesis
presented to the University of Ottawa
in partial fulfillment of the
requirements for the degree of
Master of Science
in
Geology

OTTAWA, Ontario, 1985

UNIVERSITÉ D'OTTAWA
UNIVERSITY OF OTTAWA

The University of Ottawa requires the signatures of all persons using or photocopying this thesis. Please sign below, and give address and date.

ABSTRACT

The Cordova Pluton, a small gabbroic body of approximately 30 square kilometres area, intruded Precambrian marble and volcanic rocks at the southern exposed margin of the Grenville Province.

The pluton has been divided into three lithologic units: (1) a medium-grained gabbro with an igneous layering, (2) a fine-grained, massive gabbro, and (3) a pegmatoid gabbro.

Layers in the medium-grained gabbro consistently parallel the margin of the pluton and generally dip toward the centre. This suggests a cone shape for the intrusion.

The only deformational features seen in the pluton are shear zones. These shear zones are defined by a well developed foliation of chlorite and lesser biotite. The shears occur mostly in two areas: in the northern tip of the pluton, where they generally strike east to north-eastward, and in the eastern area of the pluton where they strike approximately northward. The shear zones are characterized by the presence of flattened lenses of quartz, calcite and ankerite which in the northern tip of the pluton host the Cordova and Ledyard gold deposits.

Geochemical variation across the shear zones is generally irregular. The deposition of quartz lenses appears to have

strongly enriched the surrounding sheared gabbro in potassium and to a lesser extent sodium. The sheared gabbro is depleted overall in calcium in relation to the neighboring unsheared gabbro. No geochemical signature characteristic of the gold-bearing shear zones was noted.

Three types of fluid inclusions occur in the shear zone quartz: simple 2 phase inclusions containing saline H2O and vapour (Type 1), 3 phase inclusions containing saline H2O, vapour and a daughter mineral (Type 2), and 3 phase inclusions containing CO2 liquid, CO2 gas, and saline H2O (Type 3).

Gold mineralization is thought to have precipitated from the same fluid which was trapped to form Type 3 inclusions. This fluid averages 11 wt % NaCl, 20 wt % CO2, and was trapped at a temperature between 320 and 450 degrees C. The estimated pressure at trapping is between .85 and 1.25 kilobars.

The Ottawan episode of metamorphism and orogeny is thought to be responsible for both the shear zone formation and the generation of fluids which transported gold to them.

ACKNOWLEDGEMENTS

I am very grateful to Dr. W. K. Fyson for his guidance and support of this thesis through N.S.E.R.C. grant number A 3409. Thanks also to Dr. Ralph Kretz who acted as interim supervisor during Dr. Fyson's sabattical leave.

I would also like to thank Dr. J. S. Springer and Dr. M. E. Cherry of the Mineral Deposits Section of the Ontario Geological Survey for their interest and assistance throughout this project.

The field work for this thesis was funded equally by the Federal Department of Regional Economic Expansion and the Ontario Ministry of Natural Resources under the Minerals Program of the Eastern Ontario Subsidary Agreement, and was administered through the Mineral Deposits Section of the Ontario Geological Survey.

Thin and polished sections used in this study were prepared by Robert Taylor of the University of Ottawa Geology Department. Ore sample assays were provided by the Geoscience Laboratories of the Ontario Geological Survey. Electron microprobe analyses were performed by Peter Jones of the Department of Geology, Carleton University.

CONTENTS

LIST OF FIGURES

LIST OF TABLES

Chapter I

INTRODUCTION

1.1 GENERAL STATEMENT

The Cordova Gabbro is one of several small mafic and ultramafic plutons within the Central Metasedimentary Belt of the Grenville Province. The pluton is host to the Cordova and Ledyard gold deposits, which produced in the early part of this century.

Detailed mapping of the Cordova Gabbro has not previously been undertaken. This thesis provides a detailed report of the geology and mineral deposits of the Gabbro on the basis of field and labratory work.

1.2 GEOGRAPHY

The Cordova Gabbro, latitude 44 29'- 44 32'N, longitude 77 43'- 77 48'W, is located in Marmora and Belmont Townships about 5 kilometres northwest of the village of Marmora (Figure 1.1).

Access to the area is excellent, the Trans-Canada Highway runs immediately to the south, paved roads encircle the pluton, and several dirt roads provide access to its centre. The nearest population centre providing all major services is Peterbourough, some 45 kilometres to the west.

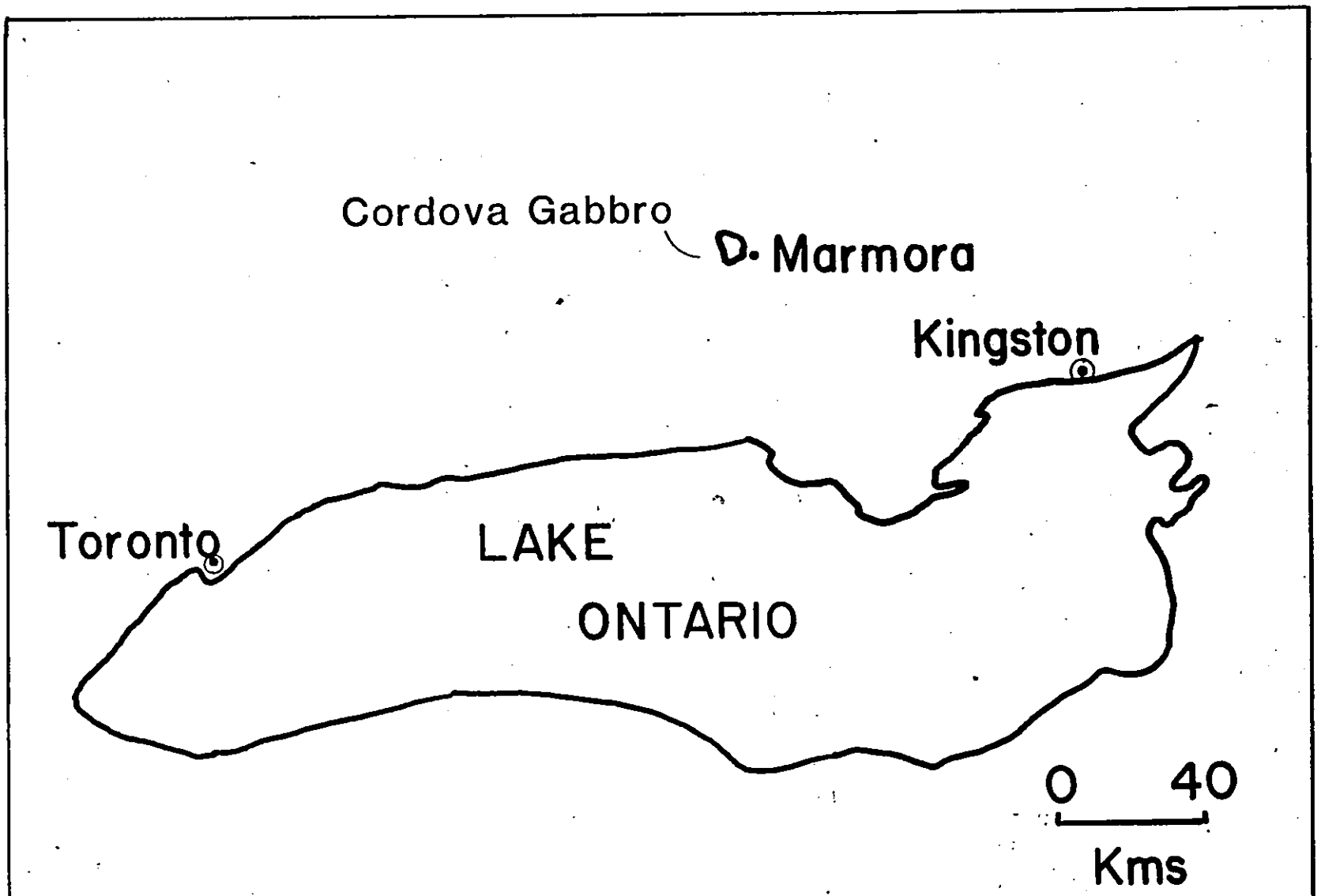

FIGURE 1.1 Location of study area.

The Cordova Gabbro forms a small topographic high, resulting in good drainage and little surface water. Except for a few swampy areas and some farm land, the study area is covered with an open decidious forest.

1.3 PREVIOUS GEOLOGICAL WORK

Most of the previous geological work on the Cordova Gabbro was in the period 1890-1940 and was related to the development of the Cordova and Ledyard gold deposits (Figure 1.2). The following summary draws freely from the Assessment Files and the Annual Reports of the Department of Mines of Ontario from the years 1893-1943.

In 1890 gold-bearing quartz veins in a shear zone were discovered on surface near where the Cordova Mine is now located (Figure 1.2). Between the years 1890-1893, three shafts: No.1, No.2, and No.3 were sunk. In 1897 the property was leased to the Cordova Exploration Company, which later became Belmont Gold Mines Limited. Five new shafts were sunk, none to great depth, and the three original shafts were deepened. By 1903 mining activity by Belmont Mines stopped. The mine was reopened in 1911 by Cordova Mines Limited and mining resumed on the No. 3 shaft on two levels. The mine site was largely destroyed by fire in 1917 and the mine was closed once again.

In 1933 Consolidated Mining and Smelting Ltd. (Cominco) optioned the property and began assessment of its potential.

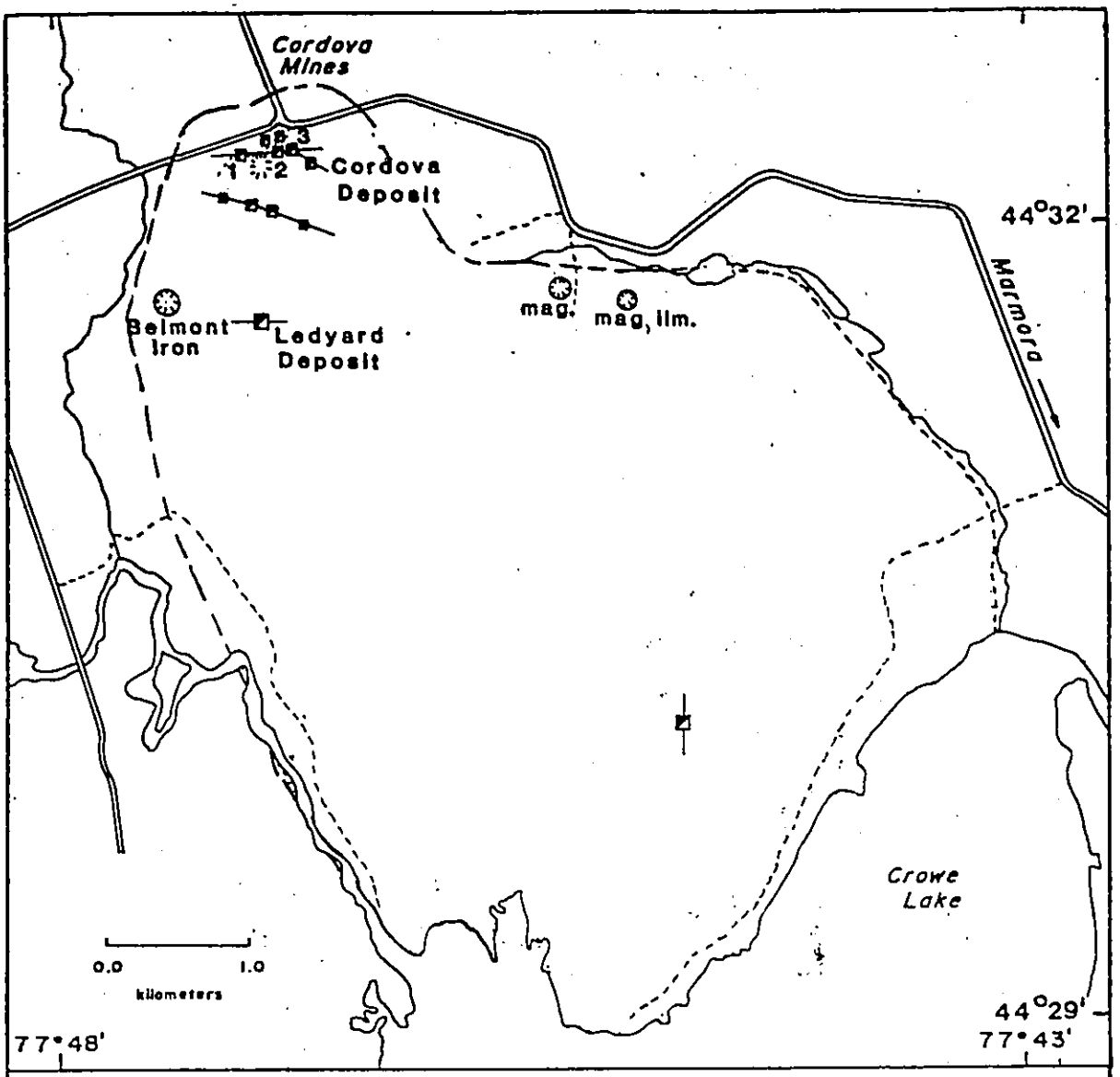

Geologic Boundary, (defined, approximate, assumed)

Shear Zone

2,3 Cordova Deposit Shaft Numbers

Shaft

Tailings

Pit

Roads, (paved, unpaved)

FIGURE 1.2 Mineral deposits and occurances in the Cordova Gabbro.

Cominco purchased the mine outright in 1935 and began to develop the original No. 3 shaft. All work ceased in 1940, at which time the workings consisted of; the No.1 shaft, 122 metres deep with 4 levels, the No.2 shaft, 56 metres deep with 2 levels, and the No.3 shaft, 320 metres deep on the incline with 9 levels. Total production from the mine between the years 1890-1940 was 22,744 ozs of gold and 687 ozs of silver from 120,670 tons of ore.

In 1965 the property was optioned by Orvana Mines which drilled and sampled the waste dumps. Since 1979 the rights have been held by Lasir Gold Incorporated, which has been developing and practicing a heap leaching technique to recover gold from the surface ore reserves and mill tailings.

The Ledyard gold deposit, located near the Cordova deposit (Figure 1.2) is geologically similar but much smaller. It was also discovered in the early 1890's and was worked until 1896, at which time the workings consisted of a single 33 metre shaft with a 25 metre crosscut. The total production from this deposit was 13 ozs of gold from 55 tons of ore.

Also within the Cordova Gabbro is the Belmont Iron Mine located approximately 200 metres from the western contact with Precambrian marbles (Figure 1.2). It was worked in the period 1906-1914, and approximately 20,000 tons of magnetite ore were shipped from surface and underground workings.

About 3,500 tons of ore remain stockpiled on the surface (R. Young, personal communication 1981).

The Cordova Gabbro is within areas mapped by Miller and Knight (1914) at a scale of 1:15,840, by Wilson (1940) at a scale of 1:63,360 and by Hewitt and Satterly (1957) at a scale of 1:126,720. Bartlett and Moore (1983) produced a 1:15,840 scale map of Marmora Township and Bartlett, Moore, and Murray (1982) produced a 1:15,840 scale map of Belmont and southern Meuthen Townships. In 1983 a MSc thesis was completed at Carleton University by Bartlett who studied the Belmont Lake metavolcanic complex which is in contact with the Cordova gabbro to the west. In the course of his study Bartlett examined samples from the western edge of the Cordova Gabbro, and provided a brief petrographic description.

Boyle (1979) compared elemental variation in samples from the main vein and the unaltered host rock of the Cordova Deposit. A thermochronometric and paleomagnetic study of plagioclase and amphibole from the Cordova Gabbro was performed by Dunlop et al (1980) and Lopez-Martinez and York (1983).

1.4 PURPOSE AND METHODOLOGY OF THIS THESIS

The purpose of this thesis is to describe and understand the distribution of rock units, structures, and mineral deposits in the Corvova Gabbro. Conclusions are made as to the processes involved in the formation of the gold deposits.

Field work for this study was carried out during May to October of 1981 with support from the Mineral Deposits Section of the Ontario Geological Survey.

From samples collected 65 thin sections were cut for mineralogical and textural examination, 6 thin sections of vein quartz from shear zones were cut and doubly polished for fluid inclusion studies, 3 thin sections were cut and polished for microprobe study, and 70 samples were prepared for X-ray fluorescence analysis of major and trace element variation in major rock units and shear zones.

The samples collected for X-ray fluorescence analysis were washed and crushed to chips 0.5 cm or less in size. The sample was then split until about 75 grams remained. This portion was then powdered to 80 mesh or less. 1.5 gms of the sample was then mixed with 4.5 gms of lithium borate and .5 gms of lithium carbonate and fused into a glass pellet. Pellets produced in this manner were analysed at the University of Ottawa using a Philips Model 1410 automated XRF unit with a chromium tube and alpha cofficients of De Jongh (1973). Accuracy (based on

comparison with the results presented by Abby (1972)), and precision of the analyses has been determined to be (plus or minus); 2% for SiO2, Al2O3, Fe2O3 and K2O, 3% for MgO, TiO2 and CaO, 3.5% for NaO, and 10% for P2O5, MnO, Rb, Sr, Ba and Zr.

Fluid inclusion studies were proformed using a Linkam Th 600 Heating-Cooling Stage. The apparatus and procedure is described in Appendix 2.

Microprobe analyses were made at Carleton University's Geology Department using a Cambridge Mark 5 electron probe. The electron probe was operated at 15 kilovolts acclerating potential and a specimen current of 50 nanoamperes as measured on pure iron. Raw X-ray data were reduced using a computer program of Rucklidge and Gasparini (1969). The accuracy of the analyses is within 1% for major elements and 5% for minor elements with slightly higher uncertainties for analyses of very low value, (pers. comm. Peter Jones, Carleton University 1985).

Chapter II

REGIONAL GEOLOGY

2.1 INTRODUCTION

The Cordova Gabbro lies within the Hastings 'Basin' segment of the Grenville Province's Central Metasedimentary Belt (Figure 2.1) as defined by Wynne-Edwards (1972). The Hastings 'Basin' (which is better referred to as the Hastings Lowland or Metamorphic Low) consists mainly of carbonate, metavolcanic and clastic metasedimentary rocks of the Grenville Supergroup which have been intruded by a wide variety of plutonic rocks (Figure 2.2).

2.2 STRATIGRAPHY

Lumbers (1967) has divided the Grenville Supergroup in the Hastings Lowland into two groups (Figure 2.3). The elder is the Hermon group, which includes the Tudor Metavolcanic formation, the Oak Lake formation, the Vansickle formation, the Turriff Metavolcanic formation and the Burnt Lake formation. The basal Tudor Metavolcanic formation consists mainly of mafic metavolcanics and is exposed over a wide area (6400 sq km). Over 8,000[1] metres

---

[1] Due to complex deformation estimated thicknesses are highly suspect.

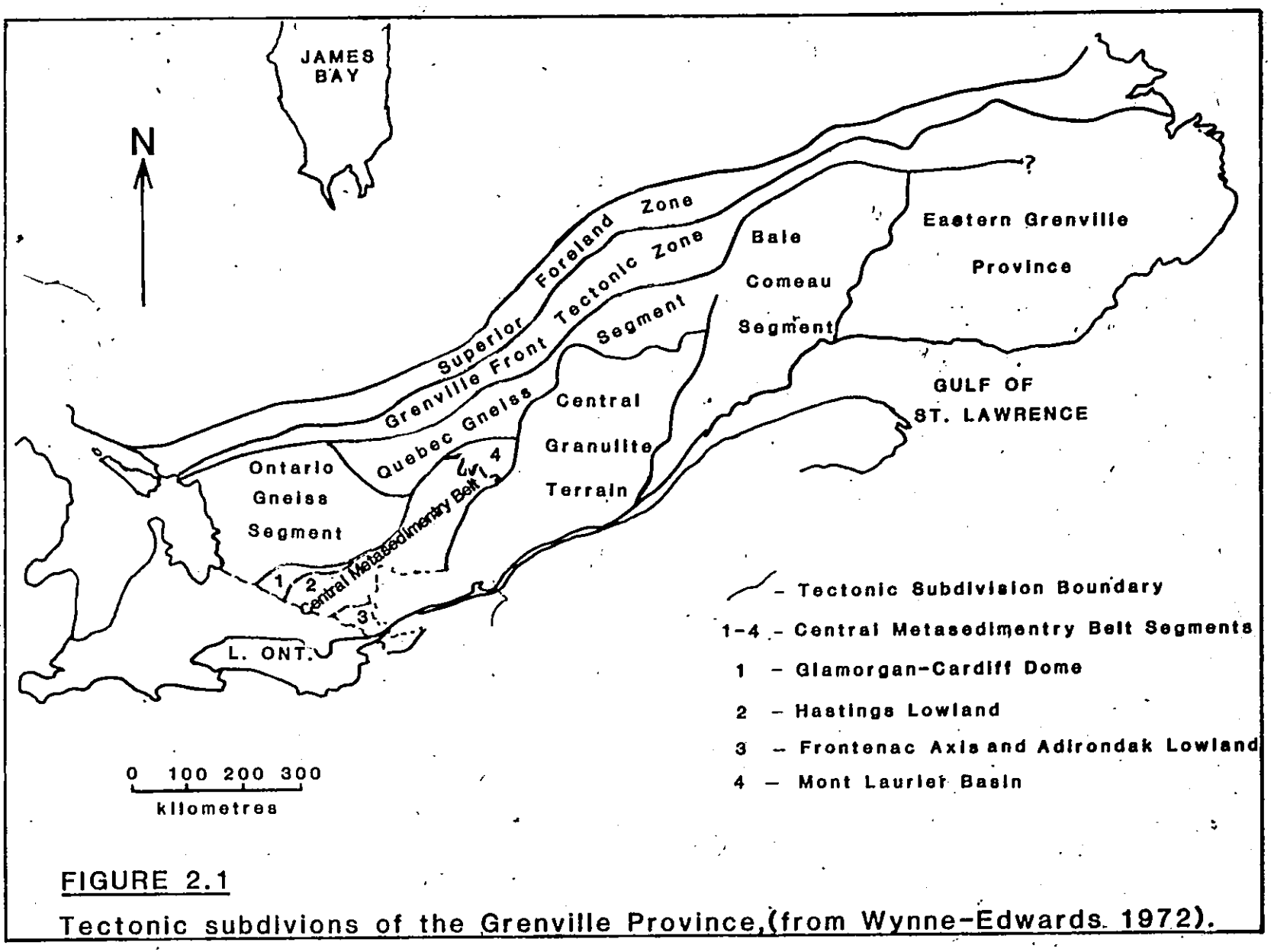

FIGURE 2.1

Tectonic subdivions of the Grenville Province,(from Wynne-Edwards. 1972).

FIGURE 2.2 Geological map of the Hasting's Lowland, (after Freeman 1979).

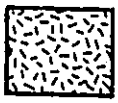

Felsic intrusive rocks, (granite, granophyre, granodiorite, quartz diorite, quartz monzonite, syenite, trondjemite, and derived gneisses)

Mafic and ultramafic intrusions, (gabbro, gabbroic anorthosite, norite, diorite, ultramafic rocks, and derived metamorphic rocks)

Grenville Supergroup

Carbonate and clastic metasediments, (marble, calc-silicate rocks, skarn, conglomerate, greywacke, arkose, calcareous sandstone and siltstone, shale, and derived metamorphic rocks)

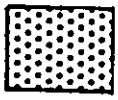

Metavolcanics, (flows, tuff, agglomerate, minor iron formation and metasediments)

Hasting's Lowland Boundary

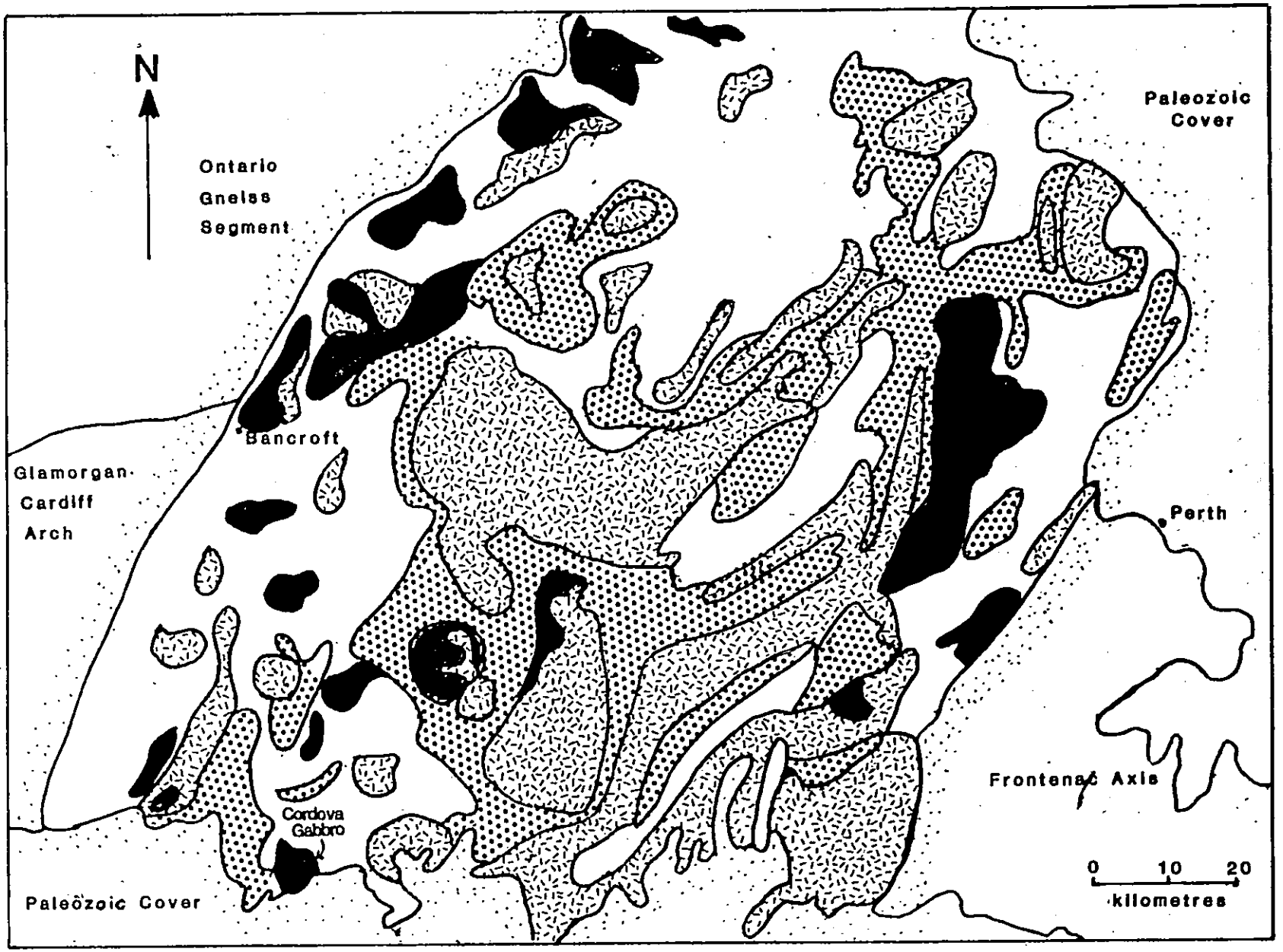
N
Ontario
Gneiss
Segment
Paleozoic
Cover
Bancroft
Glamorgan-
Cardiff
Arch
Perth
Frontenac Axis
Cordova
Gabbro
Paleozoic Cover
0 10 20
kilometres

GROUP	FORMATION	LITHOLOGY
		UNCONFORMITY
Mayo	Lasswade	marble, minor calcareous metasandstone and metasiltstone, rare recrystallized chert.
	Apsley	fedspathic metasandstone or acid metavolcanics with upper and lower members of calcareous metasandstone and metasiltstone
	Dungannon	80 per cent marble; remainder mainly calcareous metasandstone and metasiltstone, poorly sorted feldspathic metasandstone, well sorted quartz-rich metasandstone, and rare recrystallized chert; mafic metavolcanic flows and iron-formation rare near base of formation overlying Tudor metavolcanics.
Hermon	Burnt Lake	mainly rhyolitic, trachytic, dacitic, and andesitic metavolcanics with minor metabasaltic flows; lensoid marble units and sandy siliceous metasediments found locally
	Turriff	75 per cent pillowed basaltic and andesitic metavolcanic flows; remainder dacitic and felsic flows and pyroclastic rocks, and minor iron-formation.
	Vansickle	mainly poorly sorted feldspathic metasandstone locally with abundant marble, felsic and mafic metavolcanics, metaconglomerate, and well sorted quartz-rich metasandstone; arkosic metasediments commonly associated with felsic metavolcanics.
	Oak Lake	mainly metamorphosed felsic pyroclastic rocks and arkose with some mafic and felsic metavolcanic flows; rare marble and metaconglomerate in upper part of formation.
	Tudor	mainly metamorphosed, pillowed, basaltic and andesitic flows; minor dacitic and felsic metavolcanics and rare iron-formation.

FIGURE 2.3 Table of formations for the Grenville Supergroup in the Hasting's Lowland, (from Wynne-Edwards 1972, modified after Moore and Thompson 1980).

have been mapped by Lumbers (1967) who suggests that these rocks represent the lower section of a subsiding submarine shield volcano complex. The expected evolution of such a complex to one supplying felsic volcanics can be seen in the overlying formations. These formations generally have limited distribution. The Oak Lake formation overlies the Tudor formation and consists of felsic pyroclastics with minor metaarkose and metavolcanic flows. Next in the series is the Vansickle formation composed mostly of feldspathic graywacke with lesser carbonate metasediments and felsic and mafic metavolcanics. The Vansickle formation is overlain by the Turiff formation which consists of 75% basalt and andesite derived metavolcanics and 25% pyroclastics, dykes and flows of various composition. The upper member of the Hermon group is the Burnt Lake formation, a deformed sequence of felsic and pyroclastic flows.

Interfingering with and probably overlying the Hermon group is the Mayo group, comprising the Dungannon formation, the Apsley formation, and the Lasswade Marble. The Dungannon formation is dominated by carbonate metasediments, which with minor feldspathic graywacke have an apparent thickness of about 3,300 metres (Lumbers 1967). The Apsley formation and the Lasswade marble overlie the Dungannon formation, and consist respectively of feldspathic metagraywacke and carbonate metasediments. Lumbers (1967) considers these formations to represent a marine basin

assemblage of clastic detritus from volcanic and distal sources with carbonates either biochemically or chemically precipitated.

An age of 1286[2] Ma +-15 has been assigned to the Grenville Supergroup in the Hastings area on the basis of two U-Pb dates on zircons from metarhyolites of the Tudor Metavolcanics (Silver and Lumbers 1966).

Plutonic rocks intrusive into the Grenville Supergroup were emplaced over a wide time span but generally can be divided into two temporal groups of major plutons and a third group of minor intrusions of varied ages (Lumbers 1967).

The oldest group was termed the Biotite-Diorite Series and was emplaced about 1250 Ma +-25 (Silver and Lumbers 1966). It is made up of felsic intrusives such as granites, syenites, tronjhemites and dioritic intrusives (of which the Cordova Gabbro is one). The second group of intrusives was emplaced around 1104 +-25 Ma (Silver and Lumbers 1966) and consists of quartz monzonite. The third, less important group of intrusives are of a varied composition, most were probably intruded between 1250 and 1104 Ma but some may pre-date or post-date this time period. Among the rock types of this group are nepheline syenite, potassic syenite, monzonite, gabbro and diorite (considered to be later than the diorites of the 1250 Ma group) and mafic sills and

[2] All dates quoted have been recalculated by Davidson et al (1979) who used decay constants from Jaffey et al (1971).

dykes.

Uncomformably overlying metamorphosed volcanic, clastic, and carbonate rocks and large granitic plutons of the Grenville supergroup, is the Flinton group. This group, consisting of carbonate and clastic rocks of deepwater origin, and nonmarine to shallow marine clastic rocks forms a small northeasterly trending belt near the southeastern border of the Hastings Lowland (Moore and Thompson 1972). The age of these rocks is uncertain. Moore and Thompson (1980) suggest they were deposited during a break in orogenic activity between 1050 and 1080 +-25 Ma.

2.3 METAMORPHISM AND DEFORMATION

Moore and Thompson (1980) have grouped the volcanism, plutonism and regional metamorphism which affected the Hastings Lowland within the Grenville Orogenic Cycle. This cycle spans the interval 1300-1000 Ma. They have divided the tectonic history of the Central Metasedimentary Belt of Eastern Ontario into two periods of orogeny: the Elzevirian and the Ottawan Orogeny. The Elzevirian Orogeny (1225-1100 Ma) was a time of major plutonism. Both the Biotite Diorite and the Quartz Monzonite Series of Lumbers (1967) were emplaced during this time.

The Ottawan Orogeny closely followed the Elzevirian. Radiometric dates vary between 1,100 Ma and 950 Ma. A date of 1,000 Ma is generally accepted (Bell 1981).

During this orogeny the major period of regional metamorphism and polyphase deformation occurred. The effects of the regional metamorphism are most evident in the rocks of the Grenville Supergroup upon which is imposed a generally north to north-easterly trending fabric. The plutonic masses in the Hastings Lowland commonly do not show this regional fabric although within the Grenville Supergroup it wraps around both the Biotite-Diorite and the Quartz Monzonite group of major plutons (Wynne-Edwards 1972, Hewitt and Satterly 1957). This is good evidence of emplacement before or at least during deformation.

Within the Hastings Lowland the metamorphic grade is greenschist in the centre grading outward into two flanking zones of amphibolite facies. Carmichael et al (1978) and Lumbers (1964) have defined several metamorphic isograds (Figure 2.4).

2.4 GABBROIC ROCKS IN THE HASTINGS LOWLAND

The Cordova Gabbro is one of about 40 dioritic-gabbroic bodies in the Hastings area (Figure 2.4) of which 10 are of equal or greater size. Including the Cordova Gabbro, four such bodies within the greenschist facies zone have been studied previously. The other bodies are the Lake Metagabbro (Lumbers 1967), the Tudor Gabbro (Laakso 1968 and Brown and Thivierge 1976a), and the Lingham Lake Complex (Lumbers 1967, Brown and Thivierge 1976b). In the adjacent

FIGURE 2.4 Mafic and ultramafic rocks, and metamorphic isograds in the southern portion of the Hasting's Lowland. Geology after Freeman (1979), metamorphic isograds from Carmichael et al (1979).

Previously studied gabbroic bodies:

A - Lake Metagabbro (Lumbers 1967)

B - Tudor Gabbro (Laakso 1968, Lumbers 1967)

C - Lingham Lake Complex (Brown and Thivierge 1976, Lumbers 1967)

D - Umphraville Gabbro (Lumbers 1967)

E - Jocko Lake Complex (Lumbers 1967)

F - Thanet Complex (Lumbers 1967)

Metamorphic isograds (dashed where approximate):

1 - garnet-muscovite-chlorite
staurolite- biotite- quartz

2 - kyanite
sillimanite

3 - muscovite- plagioclase- quartz
sillimanite- K feldspar

4 - garnet- hornblende- quartz-
orthopyroxene- clinopyroxene- plagioclase

- Paleozoic cover rocks

- Mafic and ultramafic rocks

- Tectonic subdivision boundary

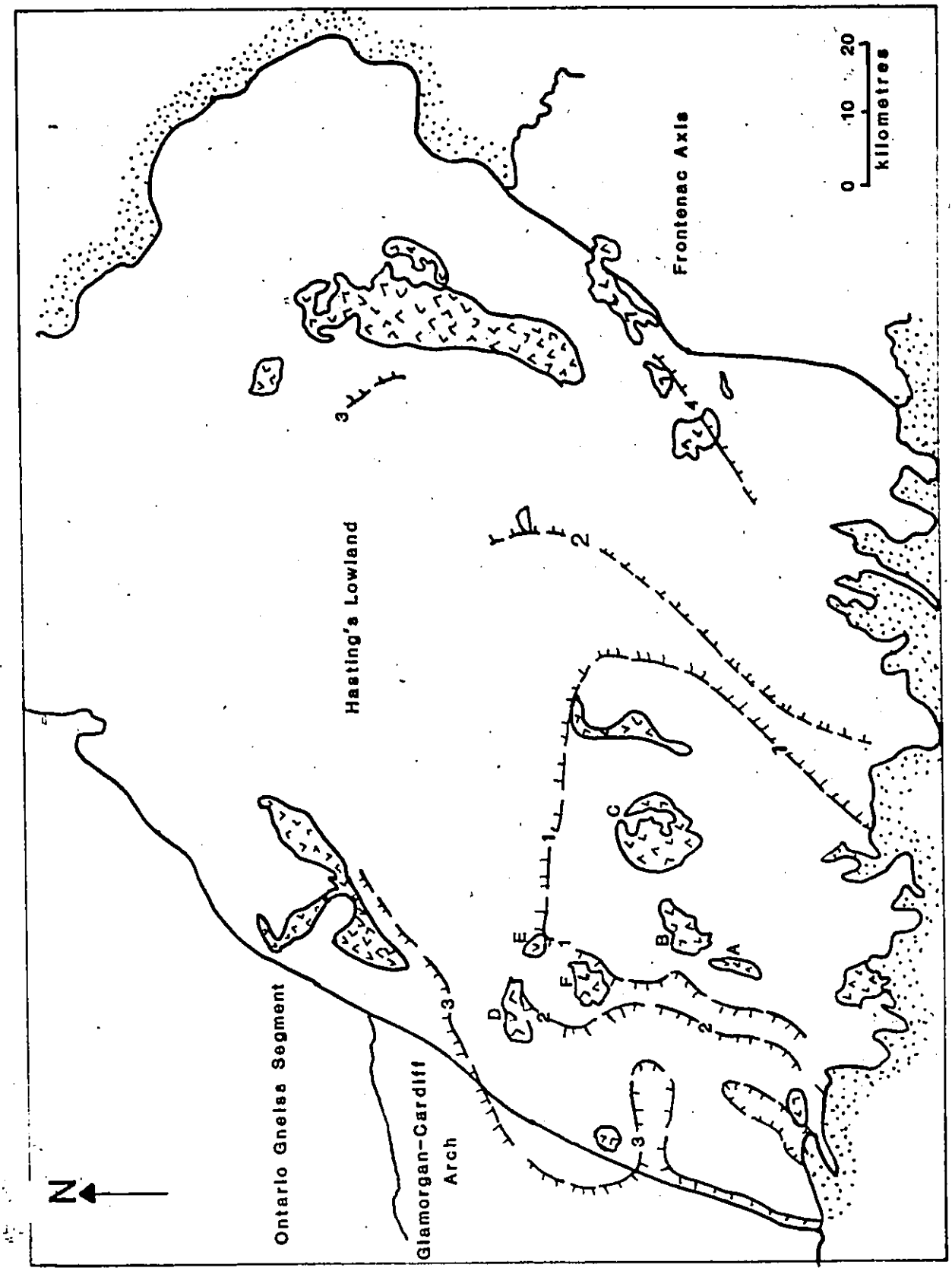
Frontenac Axis
Hasting's Lowland
Ontario Gneiss Segment
Glamorgan–Cardiff Arch
N
0 10 20
kilometres
A
B
C
D
E
F

amphibolite grade zone the Umfraville gabbro, the Jocko Lake Complex, and the Thanet Complex were investigated by Lumbers (1967, 1969). Except for the Umfraville Gabbro, which belongs to the third group of plutonic rocks of uncertain age, the gabbros previously studied belong to the 1250 Ma Biotite-Diorite Series of Lumbers (1967).

The gabbroic plutons were mainly composed of phases rich in pyroxene and plagioclase in varying proportions with lesser amounts of olivine and hornblende. However, the rocks have been extensively altered, pyroxene partially or totally to amphibole, and plagioclase to epidote group minerals. Present in all the gabbros is a primary mineral layering developed to varying degrees, which usually is confined to the marginal areas. Most plutons consist of several phases showing a variety of grain size and composition, for example commonly reported rock units are: gabbro, diorite, pyroxenite and anorthosite.

The gabbro plutons in the greenschist zone are generally undeformed except for the presence of shear zones where the original mineral assemblage has been replaced by fine-grained quartz, mica and feldspar.

Chapter III

GEOLOGY OF THE CORDOVA GABBRO

3.1 ROCK UNITS

3.1.1 Introduction

The Cordova Gabbro is a small pluton of approximately 30 square kilometres. It lies along the southern margin of the Hastings Lowland where it is in contact with Paleozoic limestones. To the east, north, and northwest it is in contact with carbonates and to the west with volcanics of the Grenville Supergroup. The Cordova Gabbro and the Grenville Supergroup rocks in contact with it have been regionally metamorphosed to greenschist grade. The contacts between these rocks and the Cordova Gabbro are generally not well exposed. Where visible the Grenville carbonates have been altered to a greenish, fine-grained calc-silicate rich rock.

Rock units have been defined mostly by textural criteria, principally changes in grain size from aphanitic to pegmatitic, and from the presence in some areas of a primary igneous layering. On this basis the pluton has been divided into three major units; medium-grained layered gabbro (Unit 1), fine-grained massive gabbro (Unit 2), and pegmatoid gabbro (Unit 3), (Figure 3.1 and Figure 3.1a (in pocket)).

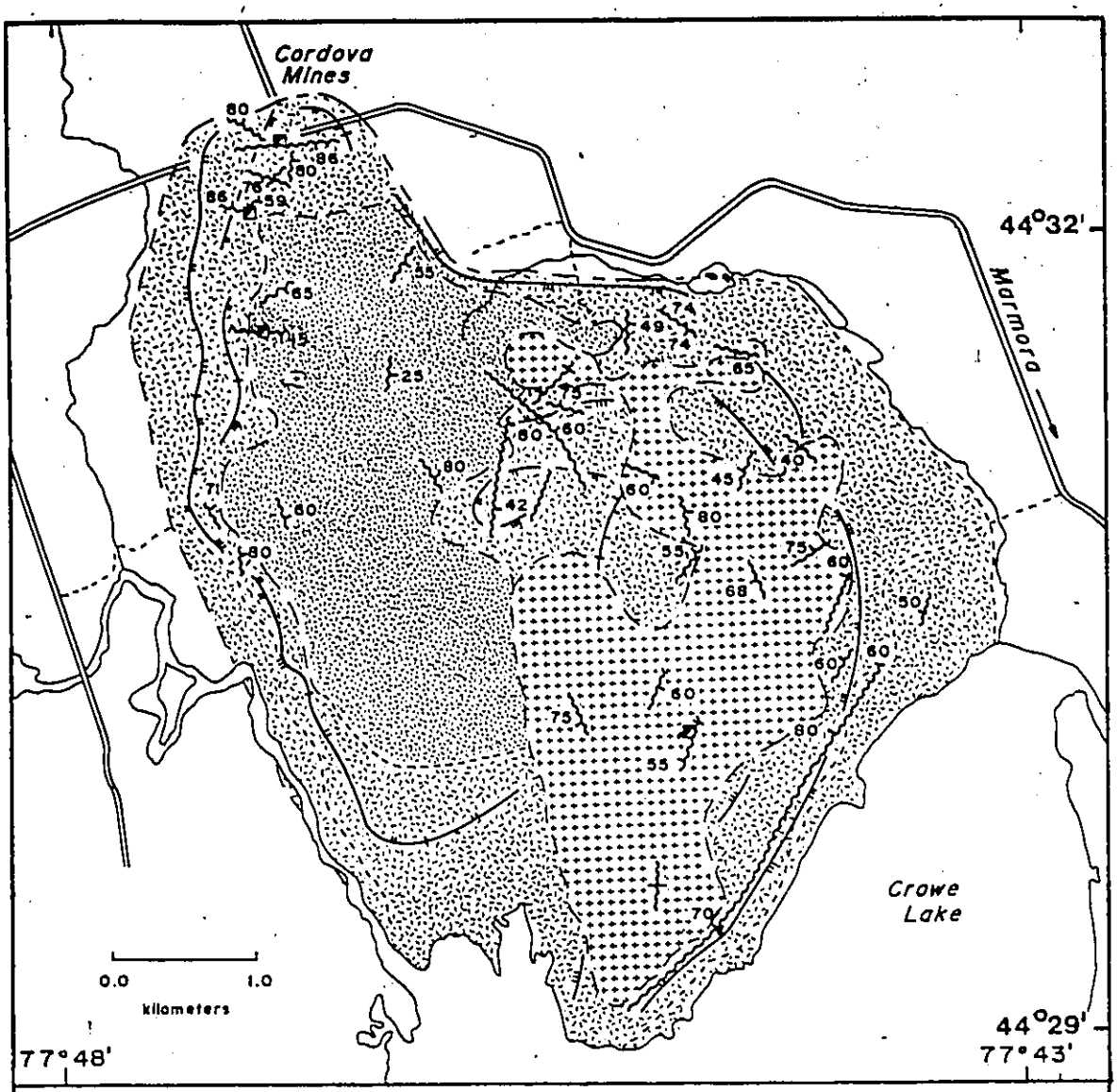

UNIT 3 Pegmatoid Gabbro.

UNIT 2 Fine Grained, Massive Gabbro.

UNIT 1 Medium Grained Layered Gabbro.

Mine shaft.

Shear zone with quartz ± ankerite ± pyrite ± gold.

Trend of primary layers Dip: 60°, 60-80°, 80-90°, 90°.

Geologic boundary Defined, approximate, assumed.

Road, paved, unpaved.

FIGURE 3.1 Geology of the Cordova Gabbro. (from Thomas and Cherry 1981)

The dominant minerals in each of the units are plagioclase and amphibole (derived from pyroxene) in proportions varying from 10 to 50 percent. Anorthite content of plagioclase was determined petrographically to be from An 33 to 44, (Bartlett 1983). Microprobe analyses of amphiboles has indicated that they are Ca rich and Na and K poor and fall in Section A of Leake's (1978) classification of calcic amphiboles (Figure 3.2). Also present, in lesser amounts, are calcite, quartz, biotite, chlorite, apatite, magnetite, pyrite, ilmenite, muscovite, and epidote group minerals.

3.1.2 Unit 1 - Medium-Grained Layered Gabbro

This unit forms an outer rim to the pluton as well as a small central area (Figure 3.1). A primary igneous layering varies in thickness from that of a single crystal to a maximum of about 15 centimetres. The layers consist alternatively of 80-90 percent mafic or felsic minerals. Occationally layered rocks have a primary mineral alignment in the plane of layering. Rocks which have not developed a primary layering often have a similar primary mineral alignment (Figure 3.3). Within the rim area of the pluton the strike of the primary layering generally parallels the outer contact and dips steeply toward the centre (Figure 3.1 and Appendix C) suggesting a bowl shape.

Layering is commonly best seen on weathered surfaces and is not always visible in thin section. When seen in thin

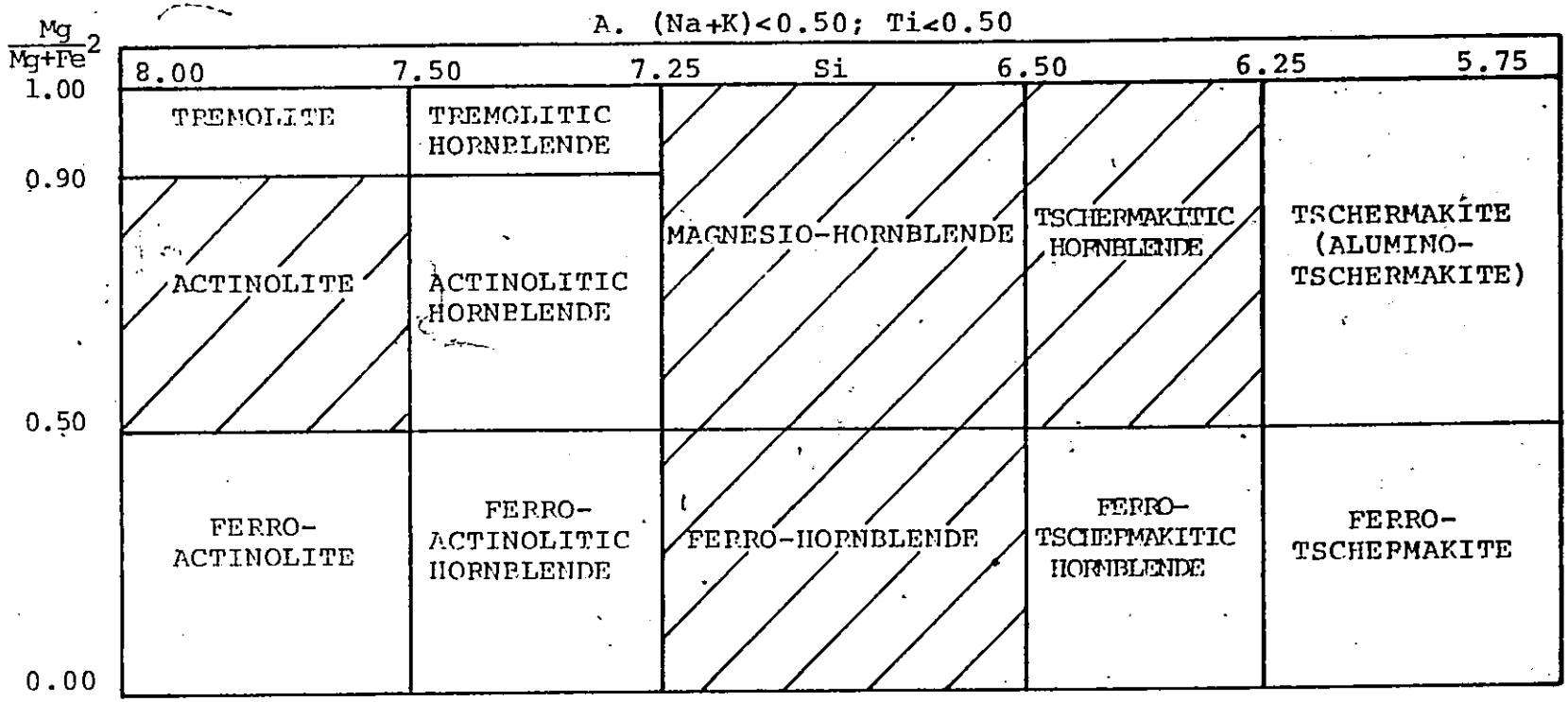

FIGURE 3.2 Amphibole types found in the Cordova Gabbro. Shown above is part A of the Calcic Amphibole Group of Leake's (1978) classification scheme. Shaded areas show the amphibole types determined using electron microprobe analysis.
All elements represent atoms per formula unit containing 23 oxygen atoms.

FIGURE 3.3 Photographs of hand specimens* of Unit 1 - Medium Grained Layered Gabbro.
The upper photograph shows amphibole (black) defining a primary mineral foliation (vertical in photograph). The remainder of the sample is composed of plagioclase (white). The lower photograph shows primary layering (horizontal in photograph). One centimetre layers are composed alternately of 80-90 % amphibole or plagioclase. Scales are graduated in centimetres.

*Sample locations for all hand specimens, thin sections sections, analyses, and outcrops referred to with the prefix CG-81 may be found on Figure 3.1a (in pocket).

CG-81-95

COLOURED PICTURES
Images en couleur

CG-81-11

section the layers consist of alternations of large parallel amphibole grains and finer masses of plagioclase (Figure 3.4).

Unit 1 is composed almost entirely of plagioclase and amphibole and their alteration products. Amphiboles usually are about 5 mm in size. They occur as clear, strongly pleochroic grains that are pseudomorphs of pyroxene or grains with many fine striations in the 001 crystallographic direction. This represents the initial stages of alteration (Deer, Howie, Zussman, 1963). Amphibole may also be heavily altered to a fine mass of pleochroic grains with small rounded grains of calcite and scaly masses of chlorite.

Plagioclase usually occurs in lath like crystals ranging in long dimension from 1-5 millimetres. Alteration is also quite variable. Grains may be unaltered with distinct twinning or heavily altered to a fine mass of clinozoisite and epidote. Often biotite and chlorite are intimately associated with the altered plagioclase. The chlorite commonly has an anomalous purple interference colour under crossed polars indicating a high chromium content, (Kerr 1977).

3.1.3 Unit 2 - Fine-Grained Massive Gabbro

Rocks of this unit occupy the western central area of the pluton (Figure 3.1). The rocks generally are dark green to black, massive, with a grain size of about 1 mm.

FIGURE 3.4 Thin section photograph of a sample of Medium Grained Layered Gabbro (Unit 1). Large green amphiboles (black in sketch) with altered cores are surrounded by a finer matrix of altered plagioclase. A primary layering is defined by alternations of parallel groups of coarse amphibole and finer plagioclase. Photographed in plane polarized light.

COLOURED PICTURES
Images en couleur

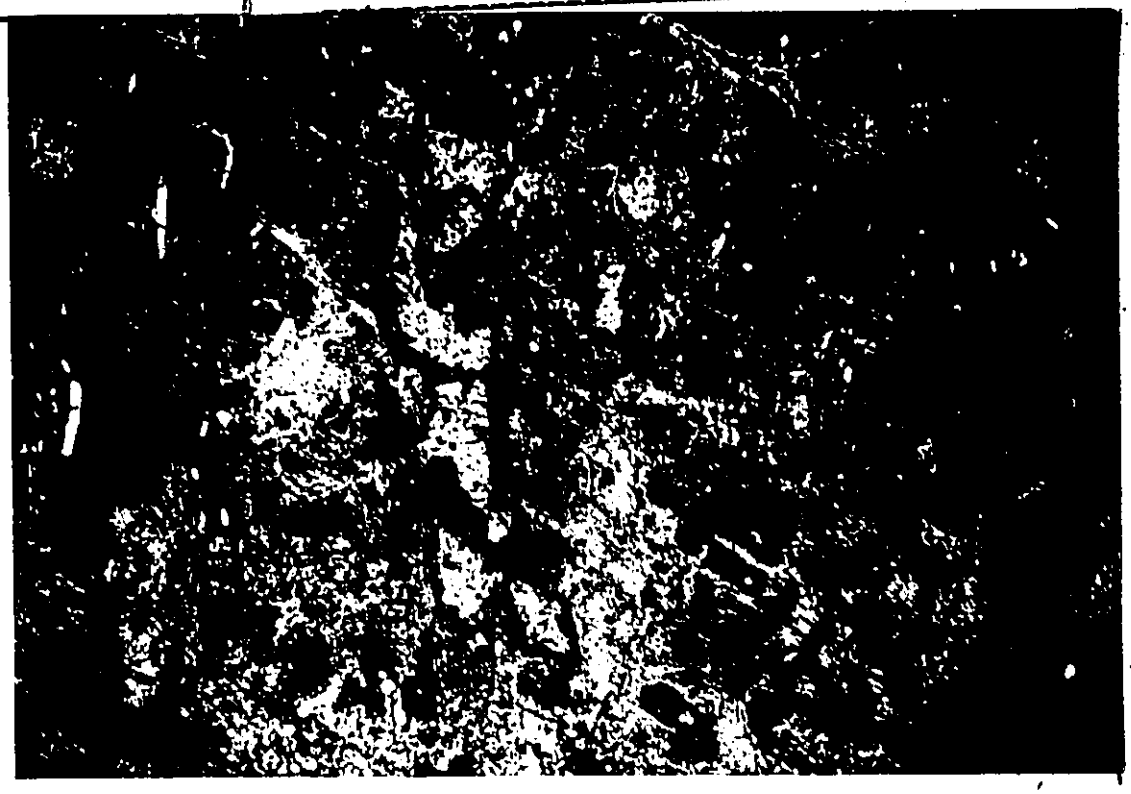

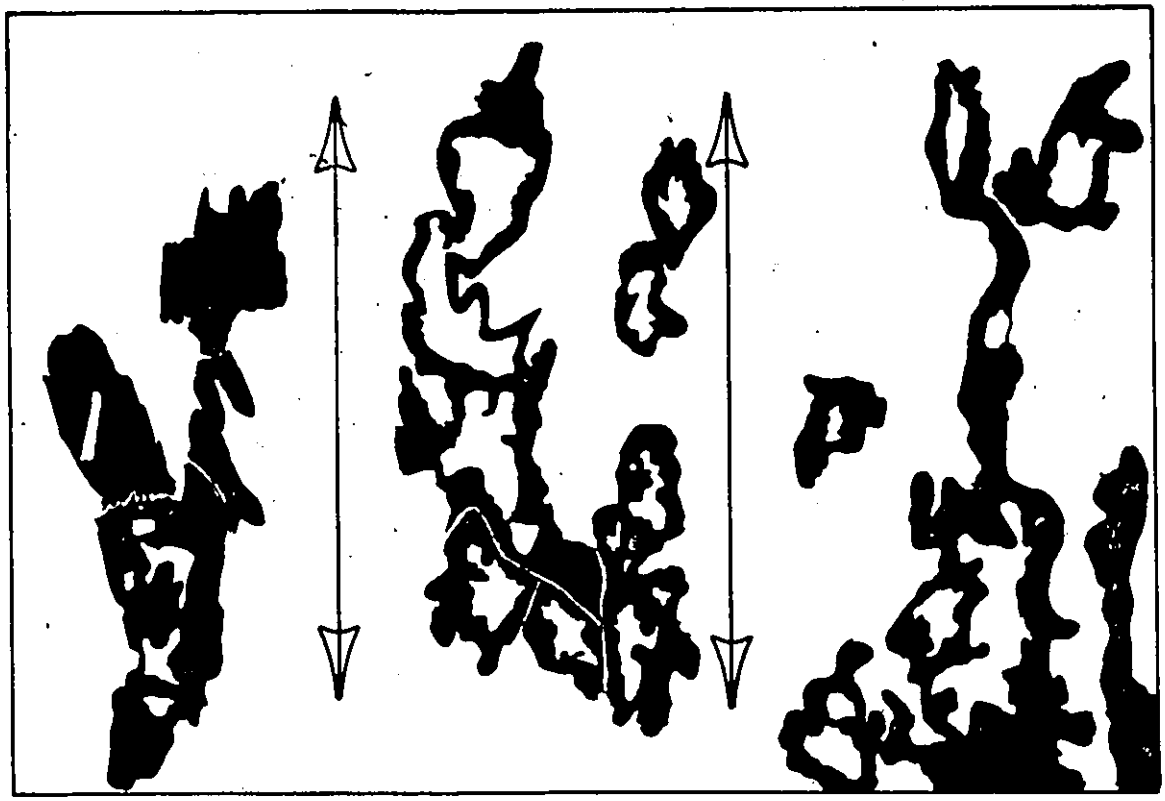

FIGURE 3.4

0 1 2 3
millimetres

CG-81-48

They are composed of equal parts of amphibole and plagioclase totaling 80-90 percent with minor apatite, biotite and opaque minerals.

The effects of regional metamorphism are variable. The plagioclase may be fresh or heavily altered to masses of epidote group minerals. The amphibole varies from fresh to masses of chlorite, calcite and opaques.

Blastoporpryitic amphiboles occur occasionally throughout this unit. Grains average 1 to 2 centimetres across and are ophitic in texture (1 mm laths of plagioclase are included within the crystals) (Figure 3.5).

3.1.4 Unit 3 - Pegmatoid Gabbro

Coarse grained rocks of this unit are located in the southwestern portion of the pluton (Figure 3.1). The rocks may be dark or light in colour, and consist of 1-2 centimetre plagioclase and amphibole grains surrounding very large (up to 10 centimetres) amphibole crystals which include 1 to 3 mm plagioclase laths (Figure 3.6).

Microprobe analyses of plagioclase from this unit indicated a anorthite content of about 60. This is a rather high value for rocks metamorphosed in the greenschist facies especially in view of the findings by Bartlett (1983), (An 33 to 44). It is possible that this discrepency is due to the choice of the least altered grains for analysis, especially since they are coarse grained and hence less suseptible to alteration.

FIGURE 3.5 Thin section photograph of ophitic texture in a sample of Fine Grained Massive Gabbro (Unit 2). Plastoporphyritic amphiboles (1 cm) enclose fine (1 mm) laths of unaltered plagioclase. Photographed in cross polarized light.

COLOURED PICTURES
Images en couleur

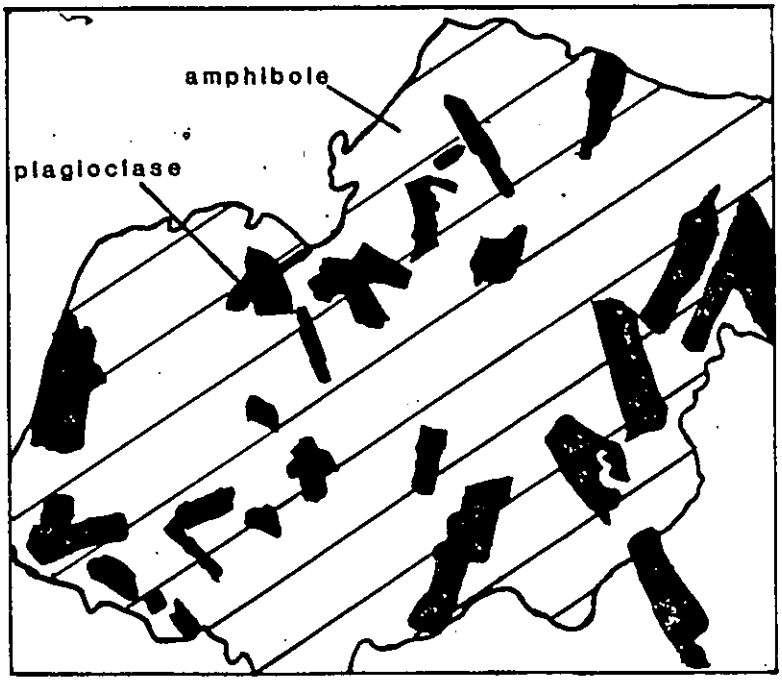

FIGURE 3.5

COLOURED PICTURES
Images en couleur

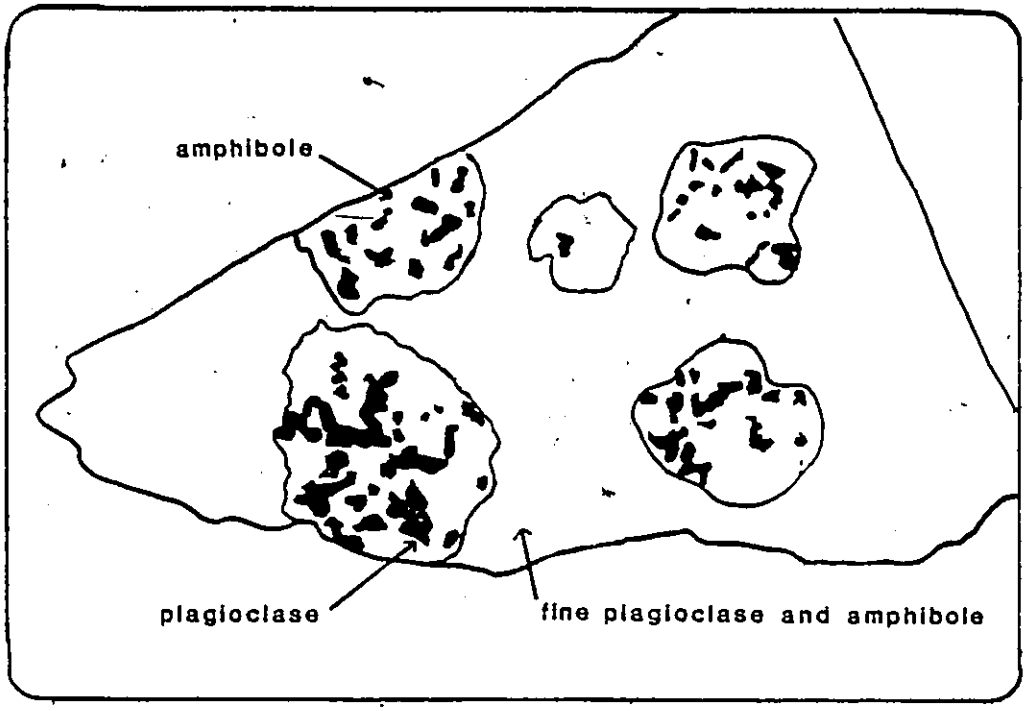

CG-81-272

FIGURE 3.6 Hand specimen photograph of Pegmatoid Gabbro (Unit 3). This sample consists of 2-3 cm amphibole grains (enclosing 1-3 mm laths of plagioclase) in a fine matrix of plagioclase and amphibole.
Scale in photograph is graduated in cm.

Some amphibole grains have a zonal structure defined by a dark to olive green pleochroic core surrounded by a rim of non-pleochroic material with higher birefringence (Figure 3.7). Microprobe analyses of these grains (Appendix A.5) indicate they are calcic amphiboles. The rim material corresponds to actinolite and the core to magnesio, ferro or tschermakitic hornblende of Leake's (1978) classification scheme (Figure 3.2). Grains with zoning in reverse to this also occur, that is, actinolite forms the core instead of the rim.[3]

Ilmenite is often present in rocks of Unit 3 as interstitial grains rimmed by titanite (sphene). More rarely grains along cleavage planes of amphibole form a well defined 120/60 degree pattern (Figure 3.8).

Locally rocks of Unit 3 may be very leucocratic consisting mostly of 1 to 2 centimetre plagioclase grains with rare large amphibole crystals, which in thin section show well developed ophitic texture (Figure 3.9). Large grains of optically continuous amphibole, (in various stages of alteration) enclose laths of fresh or heavily altered plagioclase.

Corona textures are also apparent in thin section. Purple chlorite forms a double shell or rim, surrounded and separated by plagioclase (Figure 3.10).

---

[3] A similar zoning of amphibole is apparent in Units 1 and 2, usually where the grain size is large or ophitic texture is developed.

FIGURE 3.7 Thin section photograph of a zoned amphibole in a sample of Pegmatoid Gabbro (Unit 3). Electron microprobe analysis revealed that the cores correspond to ferro-hornblende and the rim to actinolite of Leake's (1978) classification scheme.
Photographed in cross polarized light.

COLOURED PICTURES
Images en couleur

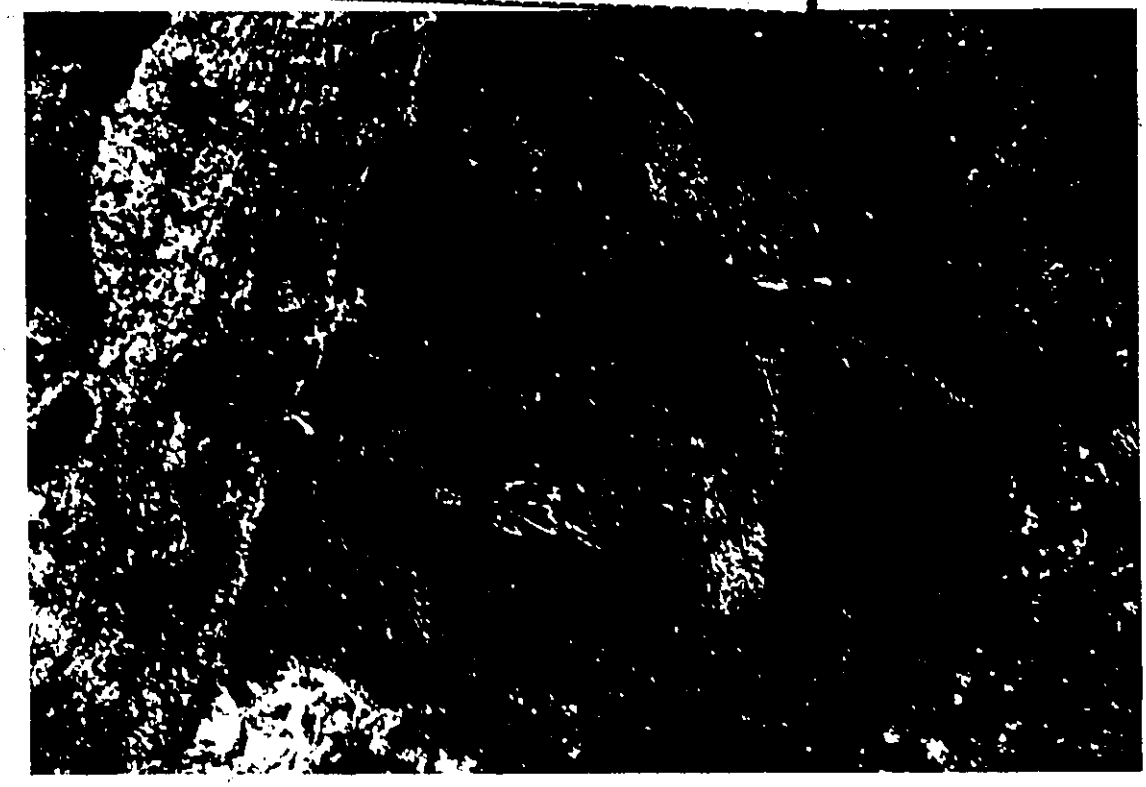

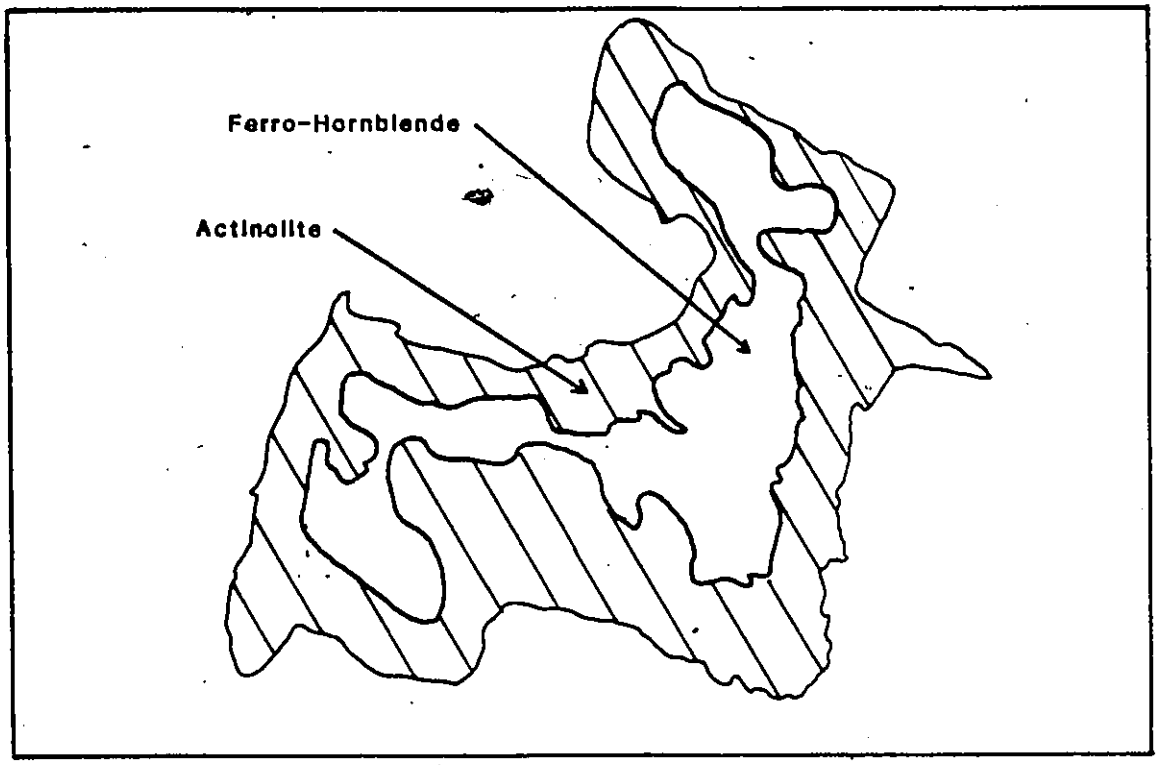

FIGURE 3.7

CG-81-30

COLOURED PICTURES
Images en couleur

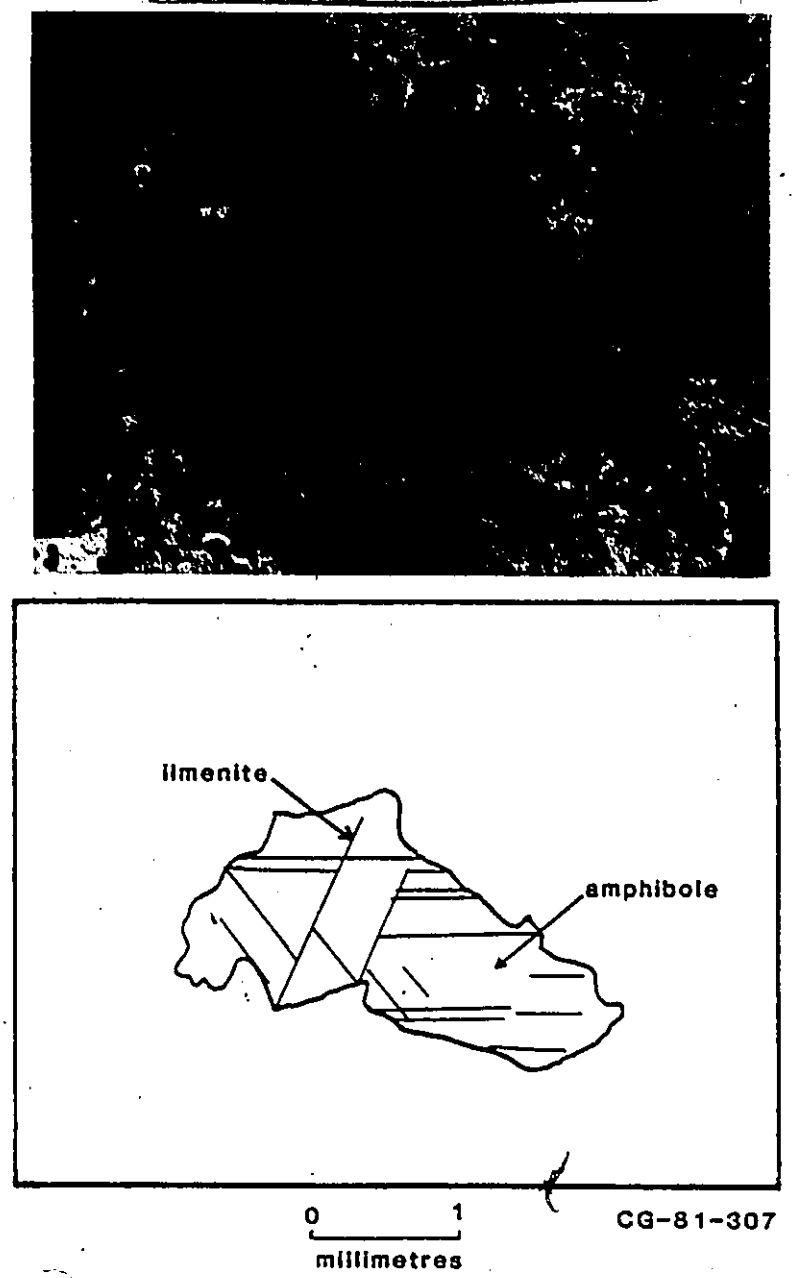

FIGURE 3.8 Thin section photograph of ilmenite grains along the cleavage planes of amphibole in a sample of Pegmatoid gabbro (Unit 3). Photographed in plane polarized light.

FIGURE 3.9 Thin section photograph of ophitic texture in a sample of Pegmatoid Gabbro (Unit 3). In this sample large greenish amphiboles enclose laths of plagioclase. In the upper portion of the photograph the variation in alteration affecting the plagioclase is evident. The portion of a plagioclase crystal within amphibole is not heavily altered whereas the remainder has been altered to a fine mass of epidote group minerals. Photographed in crossed polarized light.

COLOURED PICTURES
Images en couleur

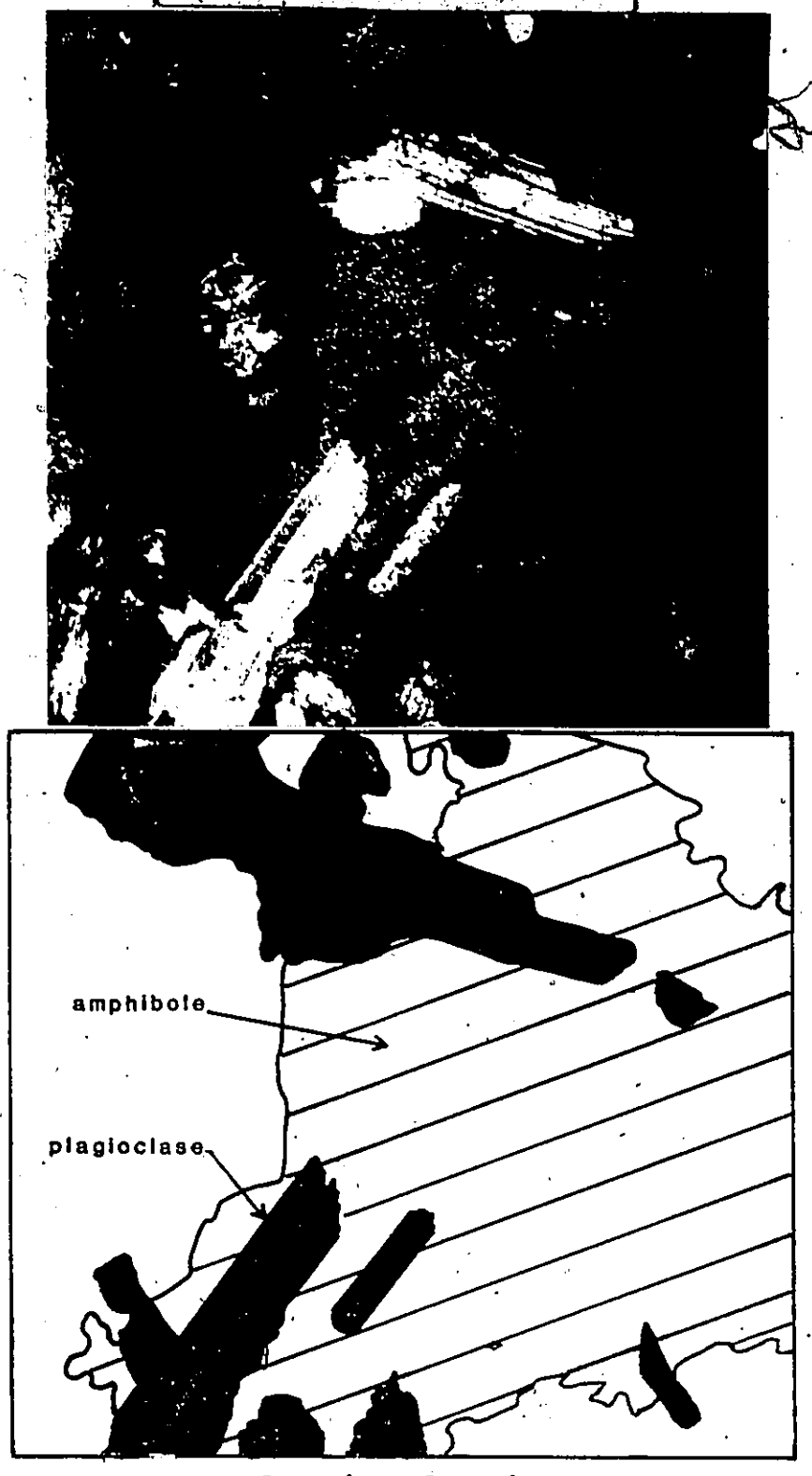

FIGURE 3.9

CG-81-243

FIGURE 3.10 Thin section photograph of corona texture in a sample of Pegmatoid Gabbro (Unit 3). Corona textures in this sample are formed by a double rim of chlorite which surrounds and separates plagioclase. The central core of plagioclase and the thin rim of plagioclase separated from it by chlorite are optically continuous, suggesting they were originally part of a single grain.
Photographed in crossed polarized light.

COLOURED PICTURES
Images en couleur

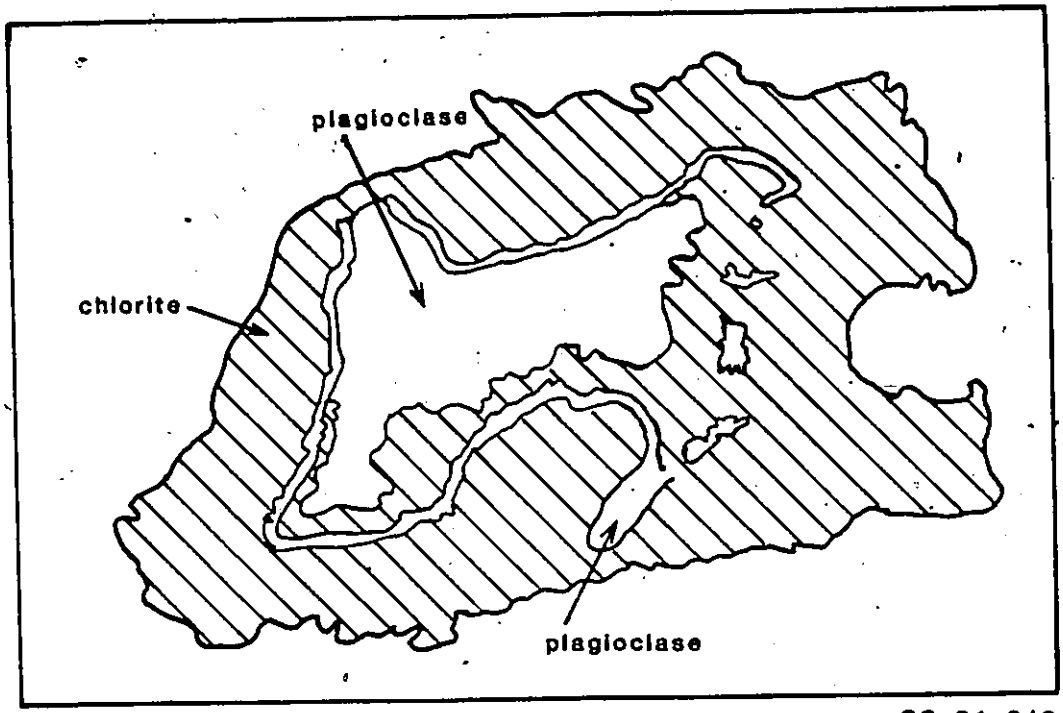

FIGURE 3.10

1 0
millimetres

CG-81-343

3.1.5 Age Relations

Contacts between Units 1,2 and 3 are gradational. Within each, isolated outcrops of the other are found and features common to one unit may be present in the others. For example a crude primary layering is occasionally seen in the fine-grained massive gabbro, as is ophitic texture, which is more typical of the pegmatoid unit.

Units 1,2 and 3 are crosscut by many granitic dykes. Rocks in these dykes are usually fine-grained, pink and are composed of approximately 50 percent potassic feldspar, 30-40 percent quartz and 10 percent plagioclase. Commonly these dykes are about 10 centimetres wide but they may reach widths of 3 metres and have a coarser grain size. Also present are narrow (about 10 cm) fine-grained, white granitic dykes. These dykes are composed of plagioclase, quartz and minor mafic minerals.

All of the dykes are considered to be late stage differentiates of the gabbro magma. Evidence of the late emplacement of the dykes is shown in outcrop where both layered and massive gabbro have been disrupted and brecciated by the intrusion of granitic material (Figure 3.11).

The large grain size of the pegmatoid unit (3) and its locally leucocratic nature suggest that it was late forming. The presence of primary layering (which is usually associated with the roof or lower levels of mafic intrusions

COLOURED PICTURES
Images en couleur

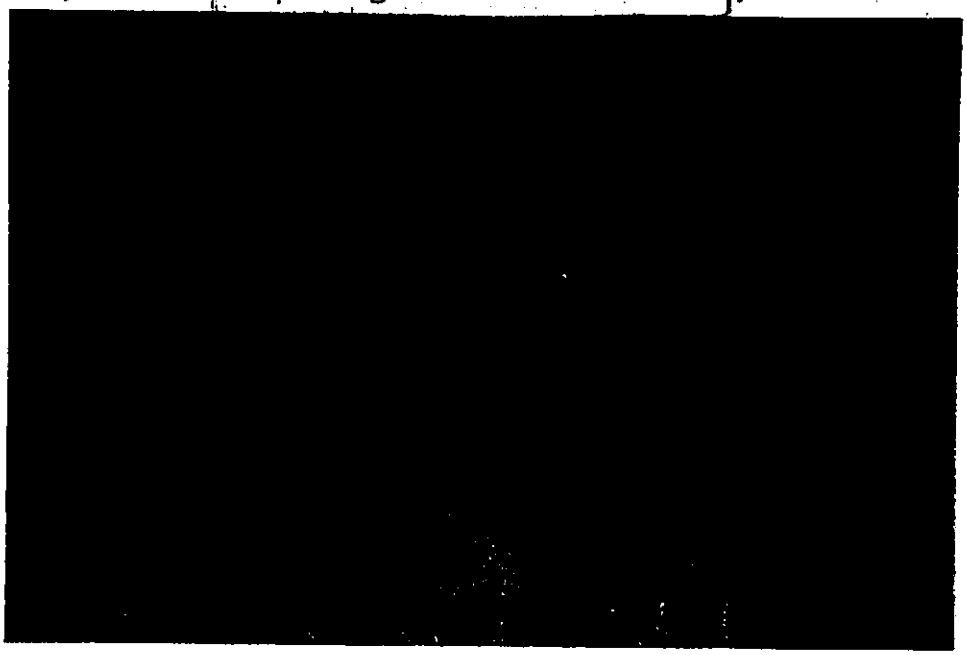

CG-81-137

FIGURE 3.11 Photograph of an outcrop of Medium-Grained Layered Gabbro (Unit 1), (dark grey) disrupted and brecciated by the intrusion of granitic dykes (white).
Hammer in photograph is 35 centimetres long.

(Wager and Brown 1967)), together with its probable bowl shape suggests that the medium-grained layered unit (1) crystallized first. However the fine grain size of unit 2 is suggestive of it being the first to have crystallized. The lack of clear intrusive relationships between the units make a definite sequence of cooling difficult to propose.

3.2 GEOCHEMISTRY OF THE ROCK UNITS

A total of 23 samples were analysed from Units 1,2 and 3 using X-ray fluorescence. The analyses can be seen in Appendix A.1.

Averages of chemical compositions for each unit are very similar (Figure 3.12). On average the layered unit (1) has slightly more TiO_2 than the other units. The pegmatoid unit (3) has slightly more SiO_2, Al_2O_3, and CaO than the other units. These variations are probably due to a slightly higher overall percentage of plagioclase in Unit 3 and a slightly higher percentage of ilmenite in Unit 1.

When the analyses are plotted on an AFM diagram (oxides) they lie within the theoliitic field defined by Irvine and Baragar (1971), (Figure 3.13).

Comparison of the average analyses for each unit with analyses from other gabbroic bodies (Figure 3.12) reveals only slight compositional variation. This suggests the heavy alteration which affected the Cordova Gabbro occurred under isochemical conditions (with the possible exception of H_2O).

	1*	2*	3*	4	5
SiO_2	47.06	48.63	50.38	48.36	48.08
Al_2O_3	15.34	16.52	18.12	16.84	17.22
Fe_2O_3	14.20	12.72	11.15	11.47	9.76
MgO	8.64	7.04	7.65	8.06	8.62
CaO	9.33	9.22	10.68	11.07	11.38
Na_2O	3.00	2.76	2.43	2.26	2.37
K_2O	0.40	0.49	0.37	0.56	0.25
TiO_2	2.52	1.33	1.02	1.32	1.17
P_2O_5	0.69	0.03	0.13	0.24	0.10
MnO	0.21	0.02	0.17	0.18	0.16
S	0.02	0.03	0.02	ND	ND
Ba	64	111	96	ND	25
Cr	145	238	307	ND	170
Zr	41	71	16	ND	50
Sr	254	291	352	ND	267
Rb	3	12	5	ND	4
Y	26	30	11	ND	ND
Nb	1	0	0	ND	ND
Zn	92	116	61	ND	ND
Ni	45	86	98	ND	180
Total	100.00	100.00	100.00	99.36	100.17
No. of analyses	8	6	8	160	1

Explanation of column headings:

1 Average analysis of Unit 1 - Medium Grained Layered Gabbro

2 Average analysis of Unit 2 - Fine Grained, Massive Gabbro

3 Average analysis of Unit 3 - Pegmatiod Gabbro

4 Average gabbro composition (Nockolds 1954)

5 Skaergaard marginal gabbro (Wager and Brown 1967)

FIGURE 3.12 Chemical composition of Units 1,2 and 3 of the Cordova Gabbro, the Skaergaard marginal gabbro (probable liquid composition), and an average of 160 gabbros collected worldwide. Oxide abundances are reported in weight percent, trace elements in ppm. ND - not determined

* Recalculated volatile free

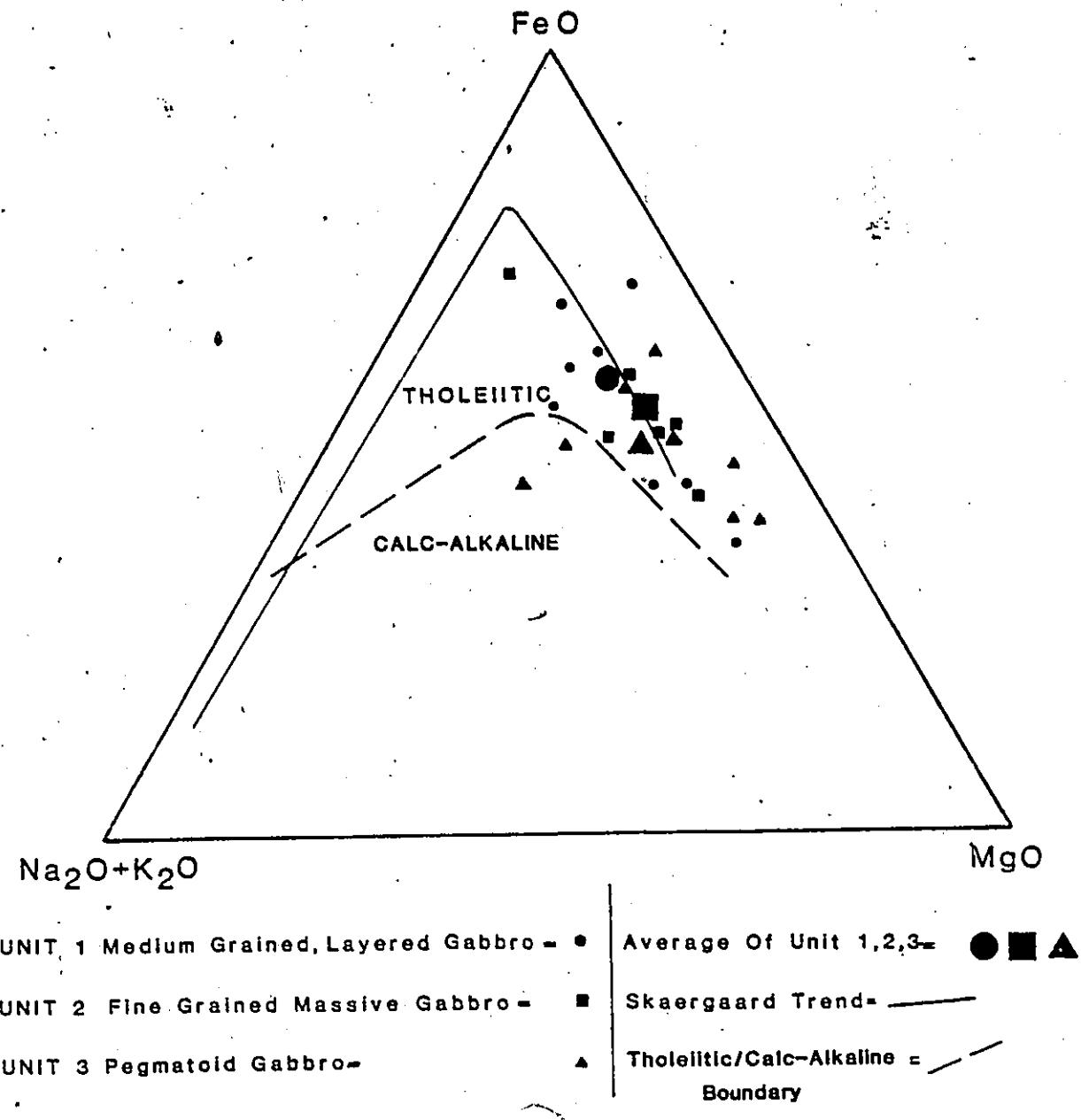

FIGURE 3.13 AFM diagram with analyses of samples from Unit 1,2 and 3 and their averages plotted. The majority of the samples plot in the tholeiitic field of Irvine and Baragar (1971). The average analyses of each unit plot on or near the beginning of the Skaergaard trend which represents undifferentiated parental magma.

When compared to the Skaergaard trend of Wager and Brown (1967) the average analysis for each unit plots close together near the point that represents the composition of the parental Skaergaard magma (Figure 3.13). This may indicate a lack of differentiation during the crystallization of the Cordova Gabbro.

3.3 STRUCTURE

Structures within the Cordova Gabbro are both primary and secondary. The primary layering and the parallel mineral foliation have been described above. Many theories have been suggested for the formation of similar rhythmic layering in other intrusions ranging from gravity segregation (Wager and Brown 1967) to in-situ crystallization (McBirney and Noyes 1979). According to McBirney and Noyes, within intrusions that are cooling from the outside, variations in the rates of chemical and thermal diffusion may cause the crystallization of alternating layers of minerals along the floor, walls and roof. This theory may be applicable to the Cordova Gabbro, the steep dip of the primary layering toward the centre of the pluton reflecting the initial steep floor.

The only obvious deformational features in the Cordova Gabbro are shear zones. These zones cut all rock units and are scattered throughout the pluton. They are most abundant in the northern and eastern parts (Figure 3.1). The zones

vary in strike, but in general trend easterly in the northern part and north to north-easterly in the eastern part of the pluton. The zones dip steeply, mostly between 65 and 90 degrees, dips less than 45 degrees are rare. The zones curve markedly along strike, both in outcrop and map scale, which may indicate a high dip slip component for the shear movements. Bell and Bell (1936) in an investigation of the underground workings of the Cordova Mine reported that individual shear zones vary in dip whereas the strike is constant. This may be a local feature.

The shear zones could not be traced for more than 100 metres along strike, but mine reports from the Cordova Deposit state that shears are continuous for several hundred metres. Springer (1982) has interpreted a map published by Thomas and Cherry (1981) and suggests that the Cordova Gabbro is cut by a long northerly trending shear zone extending 8 kilometres and the pluton has been block faulted. There is however, little field evidence to support this theory.

The transition from unsheared host rock into the shear zones is very sharp (Figure 3.14). The zones are usually narrow (1-3 metres wide) and consist of dark green to black well foliated, aphanitic material, often with lense shaped veins of quartz, calcite and ankerite lying parallel to the foliation. It is within these veins that the gold mineralization of the Cordova and Ledyard Deposits is found.

FIGURE 3.14 Photograph of a hand specimen showing the sharp tranisition from unsheared gabbro (Unit 1) to sheared gabbro.

The medium-grained layered gabbro is separated from the well foliated shear zone by a narrow transition zone. The medium-grained layered gabbro consists of about equal parts plagioclase and amphibole with minor opaques. A 1 cm layering defined by a local variation in the proportion of amphibole and plagioclase is faintly visible.

The tranisition zone is unfoliated and consists of 1 to 2 mm rounded grains of calcite and biotite with fine interstitial plagioclase, chlorite and opaques.

The shear zone has a strong foliation defined by parallel aggregates of chlorite separated by fine calcite, biotite and plagioclase.

The upper scale in the photograph is graduated in centimetres.

COLOURED PICTURES
Images en couleur

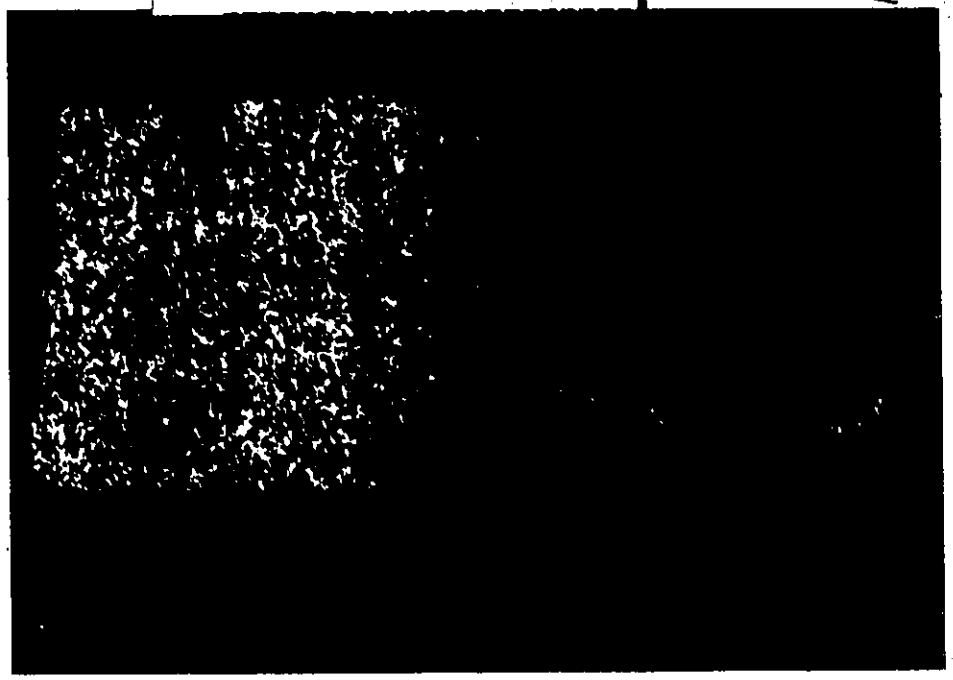

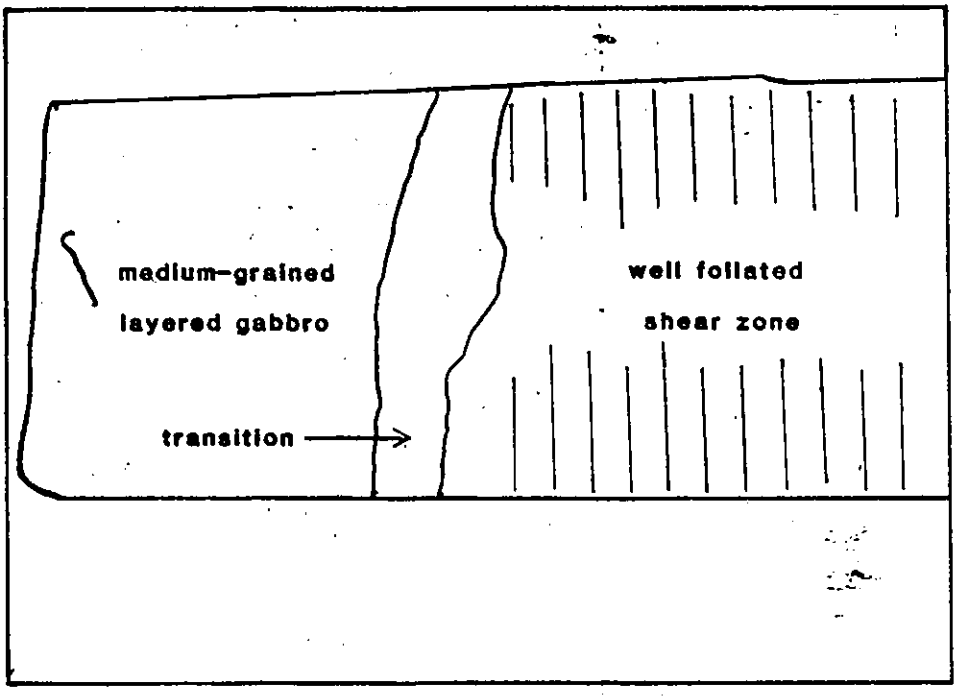

CG-81-258

The shear zone foliation is formed by the parallel alignment of chlorite flakes which form aggregates about 1 to 2 millimetres wide and one centimetre long. The chlorite aggregates are separated by a fine-grained mass of quartz, chlorite, plagioclase, microcline, and opaque minerals (Figure 3.15). More rarely the foliation is defined by the parallel alignment of chlorite and biotite or by parallel layers of randomly oriented biotite grains. In a few places foliation planes have been cut by very thin (1mm) stringers of quartz and calcite.

Within some shear zones the foliation is variably developed. A central well foliated core is flanked by aphanitic, poorly foliated material which contains isolated, rounded grains of plagioclase and occasionally amphibole. Foliation in the flanking zones wraps around the porphyroclasts and twin lamallae in porphyroblasts of plagioclase are bent or offset suggesting the plagioclase grains pre-date shearing and are remnants of the original unsheared parent rock (Figure 3.16).

Variations in the textures and mineral content were noted for a shear zone 5 metres across in the medium grained layered unit (1) near the southern border of the pluton. An abrupt boundary lies between typical primary layering in the gabbro and the shear zone. The material for two to three centimetres into the shear zone consists of 1 to 2 millimetre rounded grains of calcite and biotite surrounded

FIGURE 3.15 Thin section photograph of chlorite aggregates defining foliation in sheared gabbro. Parallel aggregates of chlorite (green in photograph) up to 1 mm thick are separated by a fine mass of quartz, plagioclase, calcite, and opaque minerals.
Photographed in plane polarized light.

COLOURED PICTURES
Images en couleur

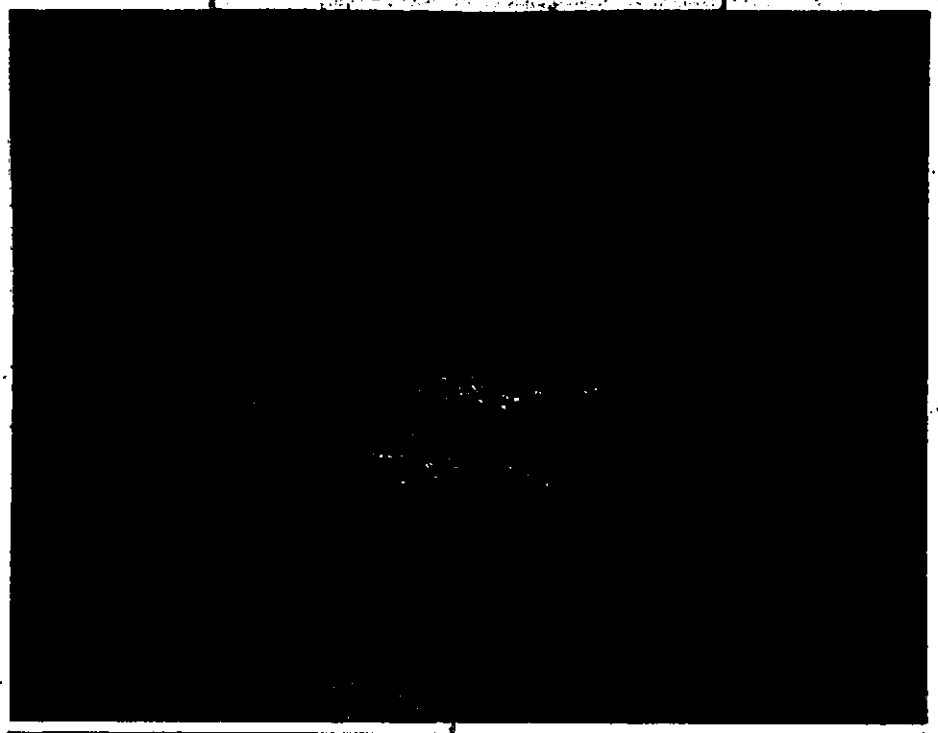

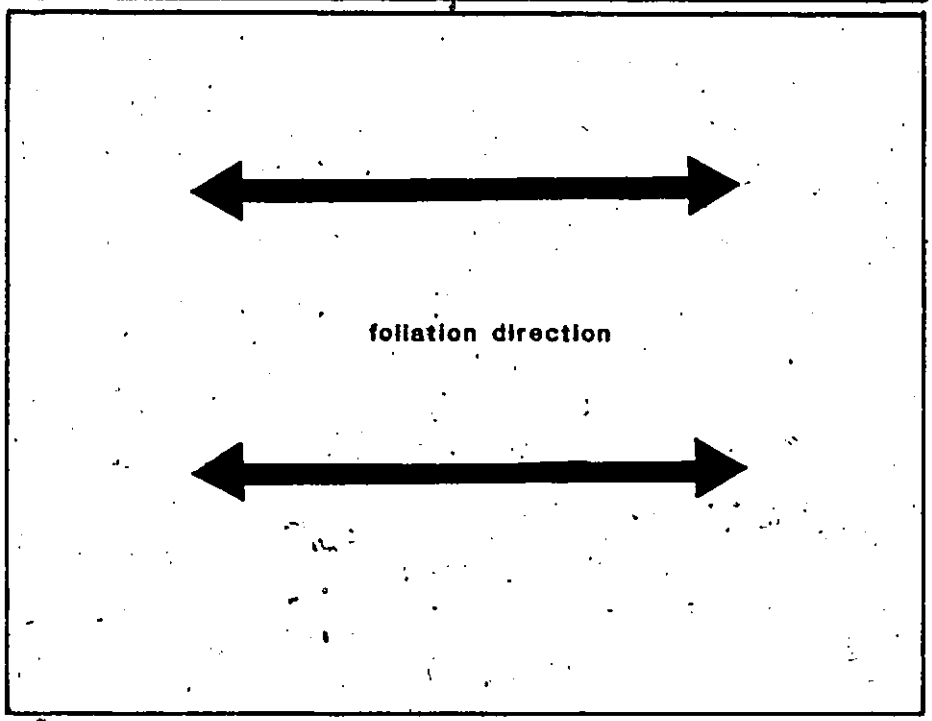

FIGURE 3.15 CG-81-4

COLOURED PICTURES
Images en couleur

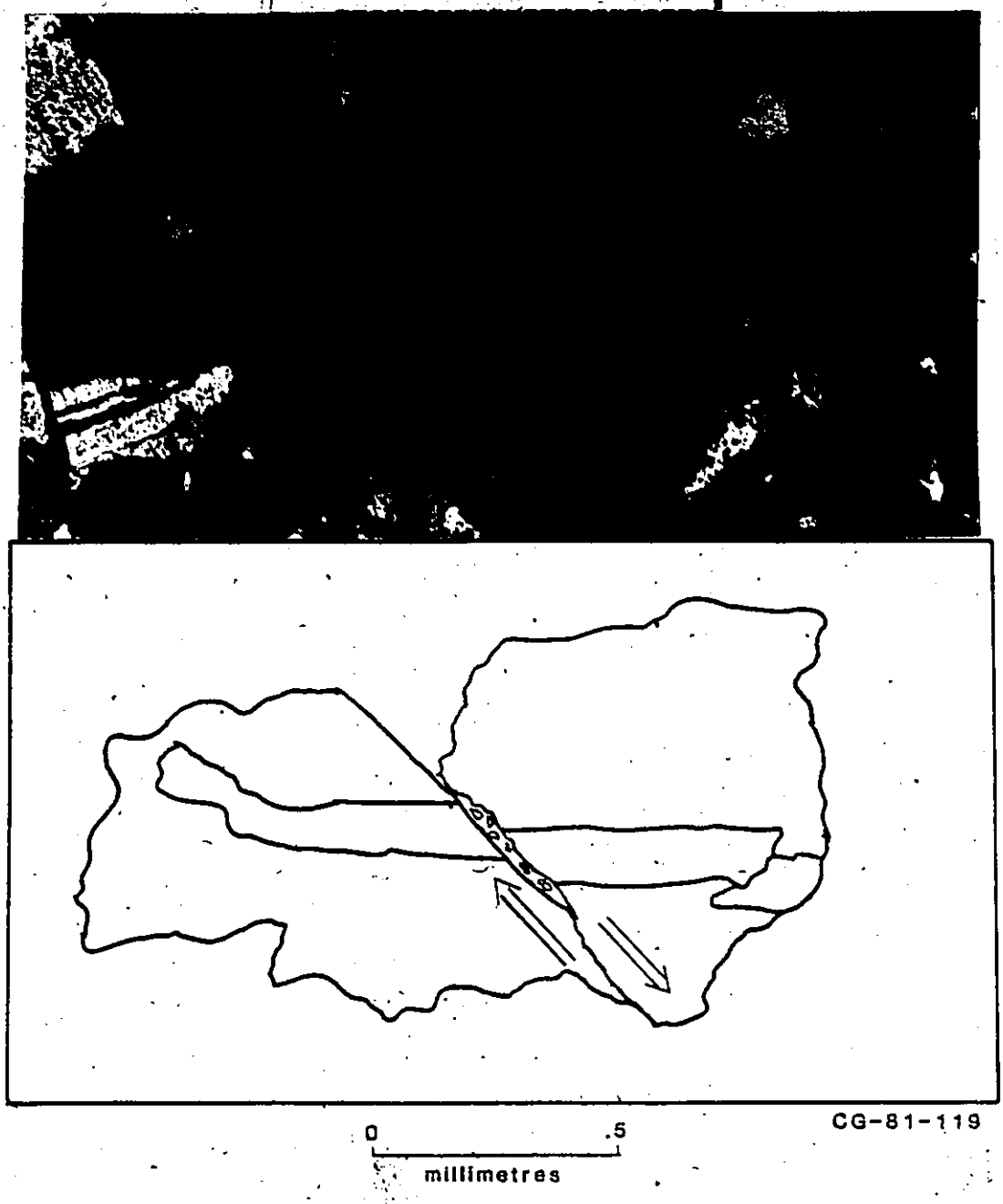

FIGURE 3.16 Thin section photograph of a faulted grain of plagioclase in sheared gabbro. Twin lamellae of the plagioclase have been cut and offset suggesting the grain predates shearing. Photographed in cross polarized light.

by a very fine matrix rich in plagioclase, chlorite and opaque minerals. Further into the shear zone the chlorite content increases accompanied by an decrease in plagioclase. At about 2 cm from the margin a prominent foliation is formed, defined by chlorite and calcite in parallel elongate masses.

Lineations are often visible on sheared surfaces. They appear as very fine parallel ridges, or more rarely as more widely spaced (1 to 2 millimetre) micro crenulations on the shear surface. These lineations consistently pitch between 45 and 60 degrees, usually to the south in northerly trending shear zones and to the east in easterly trending shear zones.

Where examined in thin section the fine parallel lineations appear to follow the intersection of the main foliation plane lying parallel to the shear zone and a second plane oblique to it (Figure 3.17). These planes may to correspond to C and S structures described by Berthe et al (1979). Due to insufficient data the sense of shear has yet to determined from these structures.

Coarser lineations, occationally present are the hinges of asymmetric crenulation folds whose axial planes are oblique to the shear zone and almost horizontal.

FIGURE 3.17 Thin section photograph of C and S structures in sheared gabbro. The main foliation planes (black in sketch) are composed of chlorite and biotite. Fine planes of chlorite (dashed in sketch) are oblique to the main foliation direction possibly representing the S component of C and S structures described by Berthe' et al (1979). Photographed in plane polarized light.

COLOURED PICTURES
Images en couleur

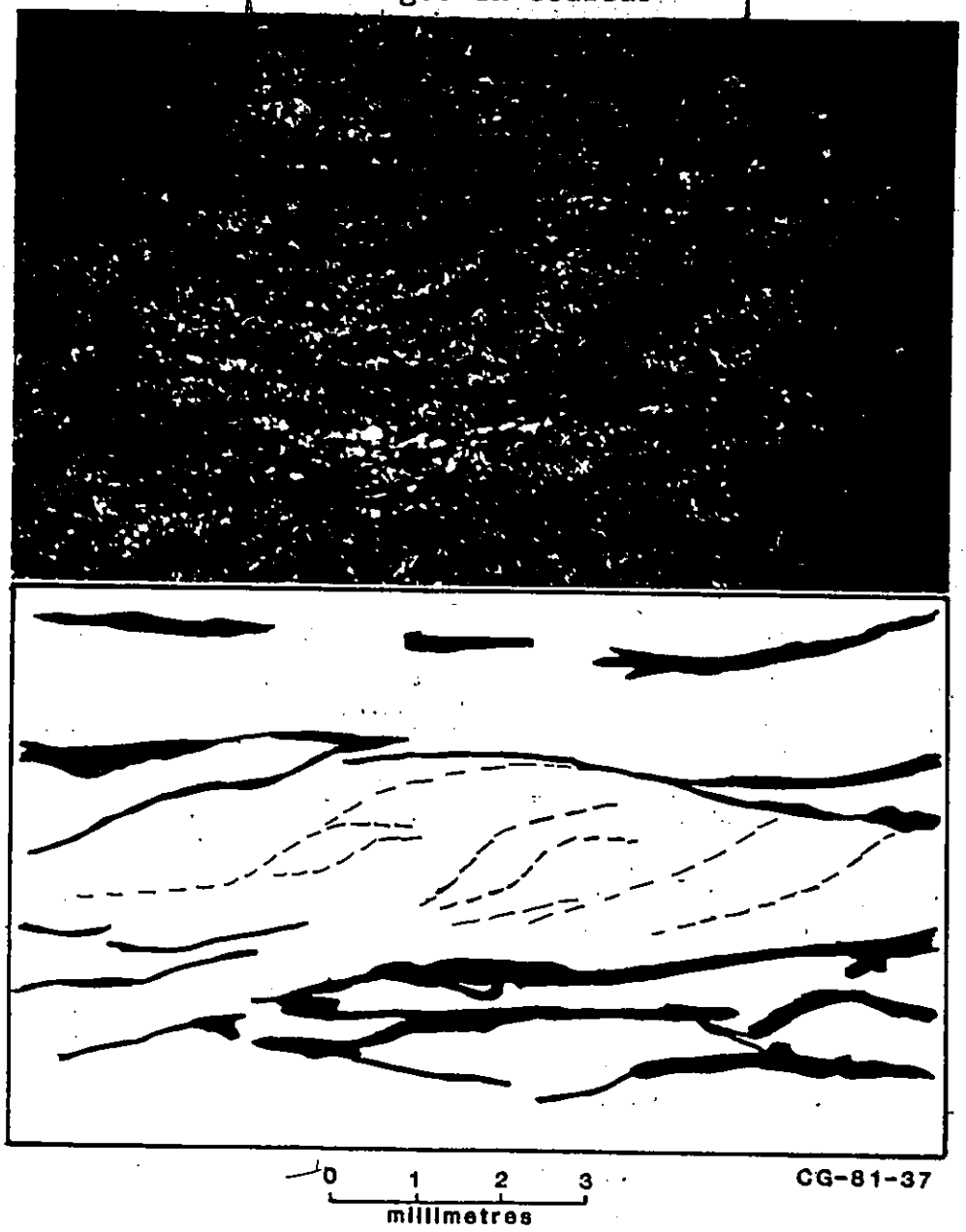

3.4 MINERALIZATION

Gold mineralization within the Cordova Gabbro occurs in four easterly trending shear zones of the Cordova deposit and the single, easterly trending shear zone of the Ledyard deposit (Figure 1.2). Gold is in a gangue of quartz, ankerite, calcite and pyrite. Pyrrhotite, chalcopyrite, and galena occasionally occur as accessory minerals in the ore. Arsenopyrite, seen in other deposits in this area hosted by granitic rocks, is absent. Ontario Department of Mines reports from early in the century indicate feldspar is a gangue mineral. None, however, was observed in this study. Ontario Department of Mines reports also indicate gold occurs in pyrite and may occur in small amounts in pyrrhotite. Minor amounts of silver were recovered from the ore, but its mode of occurrence is unknown. The quartz in ore with a high gold content is reported as having a bluish tint due to small inclusions of sulphides. White quartz is considered barren.

The gold ore in the Cordova and Ledyard Deposits occurs in lense shaped quartz bodies lying parallel to the shear zones. The lenses of quartz vary in width in outcrop from 1 cm to 1 metre. Similar lenses of quartz, calcite and pyrite occur in shear zones elsewhere in the pluton, but none are known to be mineralized. Foliation within enclosing dark, fine-grained, sheared gabbro deflects and wraps around the quartz lenses.

Mine closure and flooding preclude access underground, but company files from Cominco Limited and the reports from the Ontario Department of Mines provide useful information. The mine records state that ore lenses as wide as 15 metres occur in the underground workings. Records also state that very large blocks of ore occur where shear zones intersect. Ore may be present in a wide zone rich in narrow anastomosing quartz-calcite-pyrite veinlets. The amount of blue-grey quartz in the ore increases with depth, with a corresponding increase in pyrite and gold. The sheared gabbro is often impregnated with pyrite at depth, but it is not known if this pyrite is auriferous.

Twenty-one quartz samples from shear zones throughout the pluton were assayed for 15 elements (Appendix A.4). Twenty had gold values below the detection limit of two parts per billion. One sample taken from the main vein at the Number 3 shaft contained abundant pyrite and has relatively high values for gold (2450 ppb), Co,Cu,Ni and Zn. Polished slabs of quartz and pyrite from the vein at Number 3 shaft (Figure 1.2) were examined but no gold was visible. Small amounts of chalcopyrite occur within the pyrite grains.

Three bodies of magnetite are present within the medium-grained layered gabbro (Unit 1) near the contact with the Precambrian carbonates of the Grenville Supergroup (Figure 1.2). The largest of these, the Belmont Iron Deposit, is located about 200 metres from the western contact (Figure

1.2). It has been interpreted by Carter (1980) as a skarn deposit.

Two other smaller deposits of magnetite occur near the eastern contact of the pluton (Figure 1.2). They are also within 200 metres of the Grenville carbonates. Both of these bodies have been excavated by small scale mining operations.

X-ray fluorescence analyses of samples of ore from these deposits are shown in Appendix A.3. Ore from the Belmont deposit and one of the eastern deposits consists of about 87 and 80 percent total Fe_2O_3. The other magnetite deposit near the eastern contact has only 55 percent total Fe_2O_3 with about 6 percent TiO_2, 7.5 percent MgO and 20 percent SiO_2. The high percentage of TiO_2 may indicate the presence of ilmenite in the ore.

Chapter IV

GEOCHEMISTRY OF THE SHEAR ZONES

4.1 INTRODUCTION

X-ray fluorescence analysis for major and trace elements was carried out on samples from six shear zones within the Cordova Gabbro (Figure 4.1). The analysis was made in order to detect elemental variations within the shear zones, especially variations associated with the emplacement of quartz-calcite-pyrite veins.

Samples were taken from the edge of the veins outward to the shear zone margin. Those near the quartz-calcite-pyrite veins were closly spaced, with in some cases virtually continuous sampling for the first .2 metres away from the veins. The spacing of samples was increased away from the veins to a maximum of about 1 metre. Gabbro adjacent to the shear zones was sampled for comparative purposes.

Of the six shear zones, four crossing the northwestern part of the pluton are known to contain gold. Three of these are associated with the Cordova Deposit and one with the Ledyard Deposit. The other two shear zones, not known to contain gold are located in the southeastern portion of the pluton (Table 4.1).

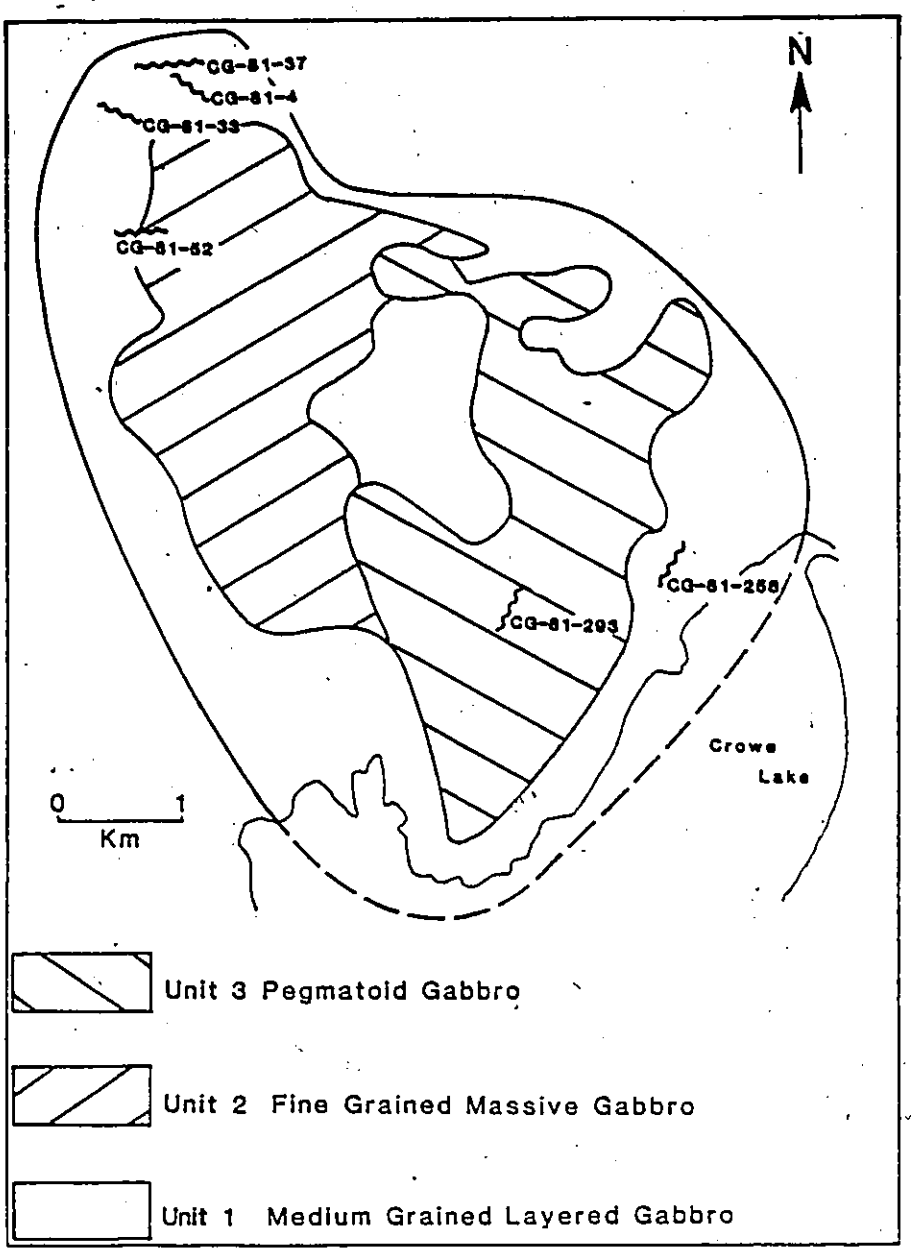

FIGURE 4.1 Location and sample numbers of shear zones sampled for geochemical analyses.

Shear Zone Outcrop Number	Shear Zone Location	Host Rock	Shear Zone Width	Maximum Quartz Vein Width On Surface	Quartz Vein Mineralogy	Number Of Samples Analysed
CG-81-4	Splay Off Shear Zone Hosting Cordova Dep.	Medium Grained Layered Gabbro	3 Metres	.8 Metres	Calcite Ankerite Pyrite	4
CG-81-33	Hosts a Secondary Vein Of The Cordova Dep.	Medium Grained Layered Gabbro	>8 Metres	>1 Metre	Calcite Ankerite Pyrite Au Ag	7
CG-81-37	Hosts The Main Vein, Cordova Dep.	Medium Grained Layered Gabbro	4 Metres	.5 Metres	Calcite Ankerite Pyrite,Au,Ag Chalcopyrite	3
CG-81-52	Hosts The Ledyard Au Deposit	Medium Grained Layered Gabbro	2 Metres	1 Metre	Calcite Ankerite Pyrite Au Ag	5
CG-81-293	South-Eastern Region Of The Pluton	Pegmatoid Gabbro	>2 Metres	.25 Metres	Calcite Ankerite	7
CG-81-258	South-Eastern Region Of The Pluton	Medium Grained Layered Gabbro	5 Metres	.3 Metres	-------	9

TABLE 4.1 CHARACTERISTICS OF QUARTZ VEIN BEARING SHEAR ZONES SAMPLED FOR ANALYSIS OF MAJOR AND TRACE ELEMENT VARIATION.

4.2 RESULTS

The X-Ray fluorescence analyses of the samples from each shear zone may be seen in Appendix A.2.

In order to compare the analyses properly, account must be made for the possibility of volume change in the sheared rocks. Gresens (1967) related compositional and volume changes during alteration, allowing the actual amount of components added or removed from a parent rock during alteration to be known.

The relationship can be expressed as a formula:

The weight of component A transferred from parent to product = gms parent{(vol product/vol parent) x (gms A in product/gms product)x(density product/ density parent) - (gms A in parent/gms parent)}

In order to satisfy this equation the volume of product/volume of parent (called the volume factor) and the density of the products and parents must be known. The density of the samples was determined by measuring the specific gravity of hand samples. The volume factor was calculated by assuming Al_2O_3 was immobile during the alteration process. If it is immobile, differences in weight percent of Al_2O_3 between the parent rock and the shear zone material can be attributed solely to a volume change. Therefore the ratio: (weight% Al_2O_3 product/weight% Al_2O_3 parent) equals the volume factor.

Use of Al_2O_3 as a volume factor has been used with success in a similar exercise by Babcock (1973).

The actual calculation of elemental gains and losses was done by computer with a program supplied by Paul A. Studemeister. The program gives results as gains or losses of components compared with the parent rock. The major oxides are expressed in weight percent and percentage of parent and trace elements are expressed in PPM and percentage of parent.

Comparison of the major and trace element variation of samples on this basis is shown in Figures 4.2 to 4.13.

The most abundant major oxides; SiO_2 , CaO, FeO and MgO, have concentrations which vary widely across the shear zone. Adjacent to the veins these elements usually are highly enriched or depleted. Often in the most densely sampled areas (within about .5 metres of the veins) their concentrations are very erratic, changing from high enrichment to depletion.

In order to check if inhomogeneous samples are responsible for the erratic chemical variation, a moving point average (described by Rivers (1976)) was applied to the data. This involves averaging overlapping groups of data points to estimate the composition over a wider area. Unfortunately the erratic variation, although less pronounced, still was evident across the shear zones.

Figures 4.2-4.13

Comparison of major and trace element variation across shear zones in the Cordova Gabbro hosting quartz veins. All data points represent the calculated gains or losses of individual components in a shear zone sample compared to unsheared parent rock.

The bracketed numbers on the upper right of each component's graph is the oxide wt% or element ppm of the component in the unsheared parent gabbro sampled adjacent to each shear zone.

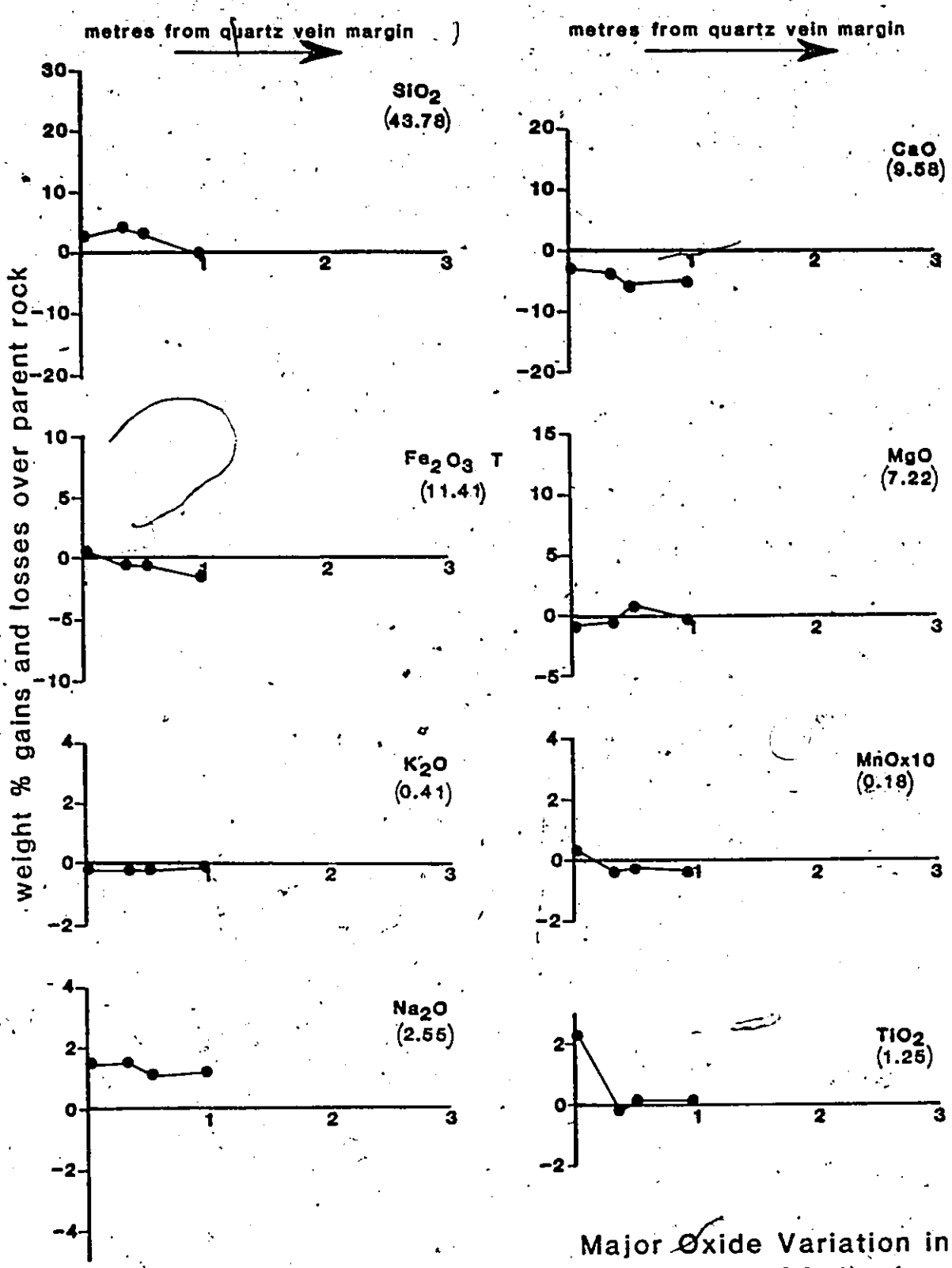

FIGURE 4.2

Major Oxide Variation in Shear Zone CG-81-4

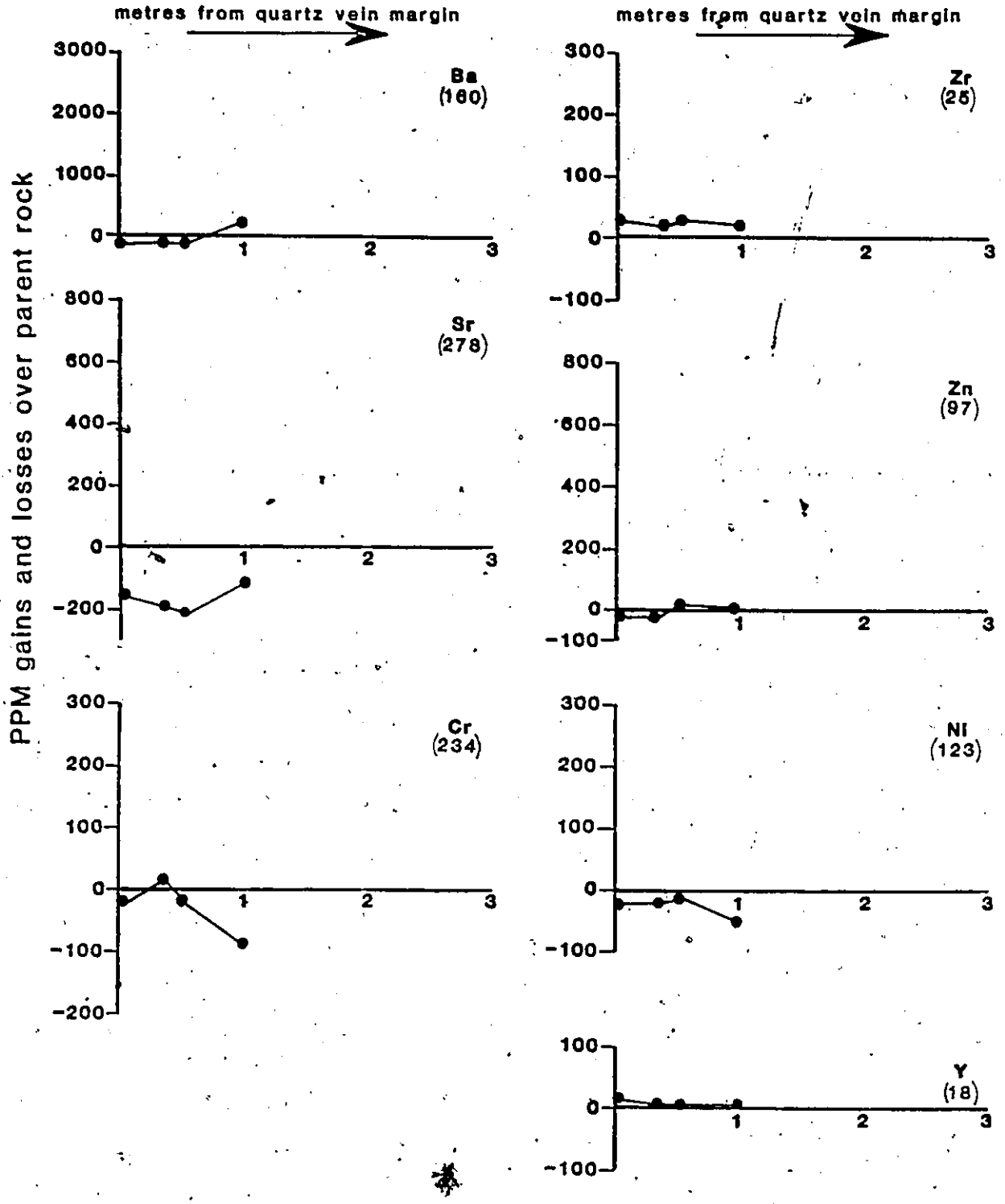

Trace Element Variation in Shear Zone CG-81-4

FIGURE 4.3

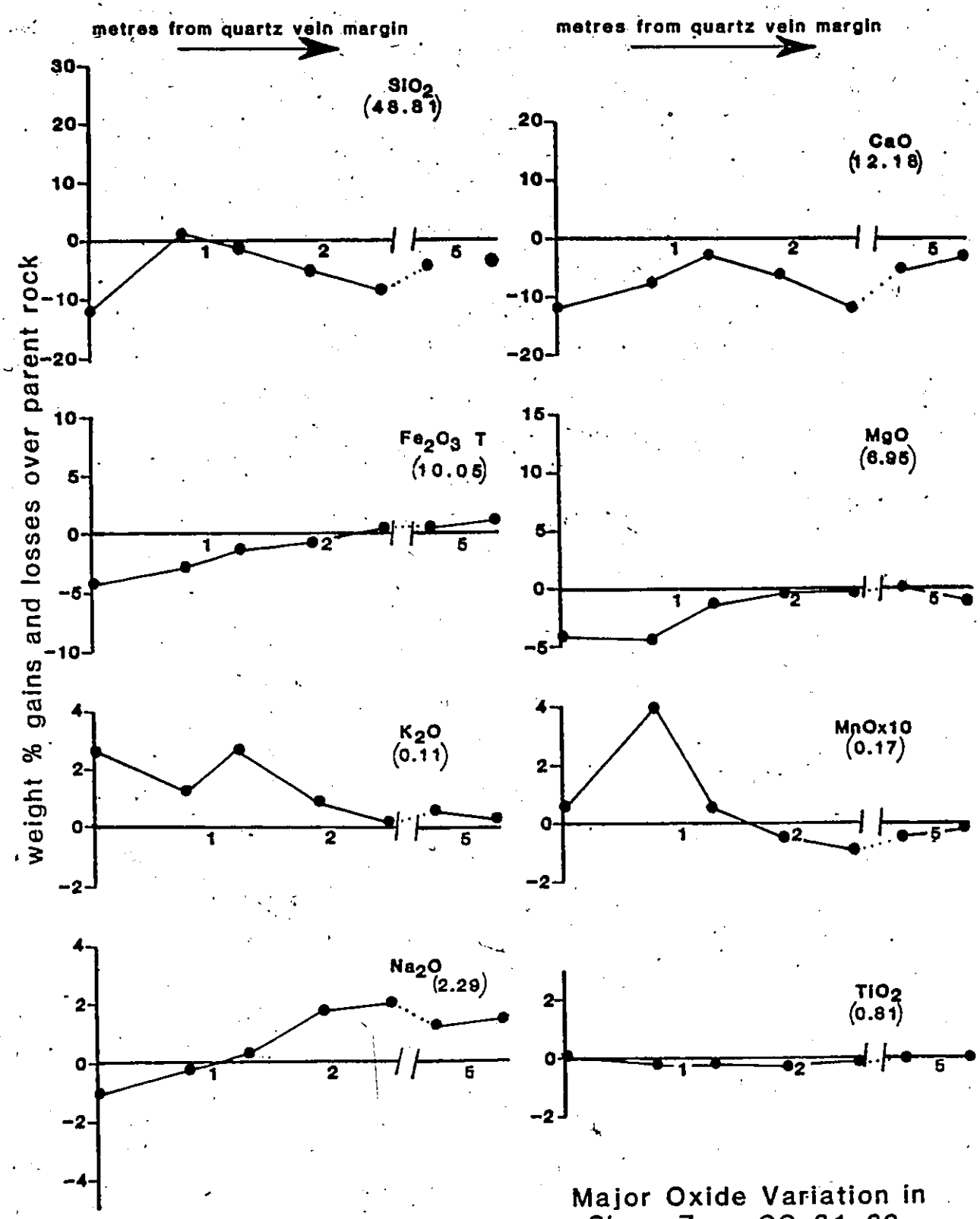

FIGURE 4.4

Major Oxide Variation in Shear Zone CG-81-33

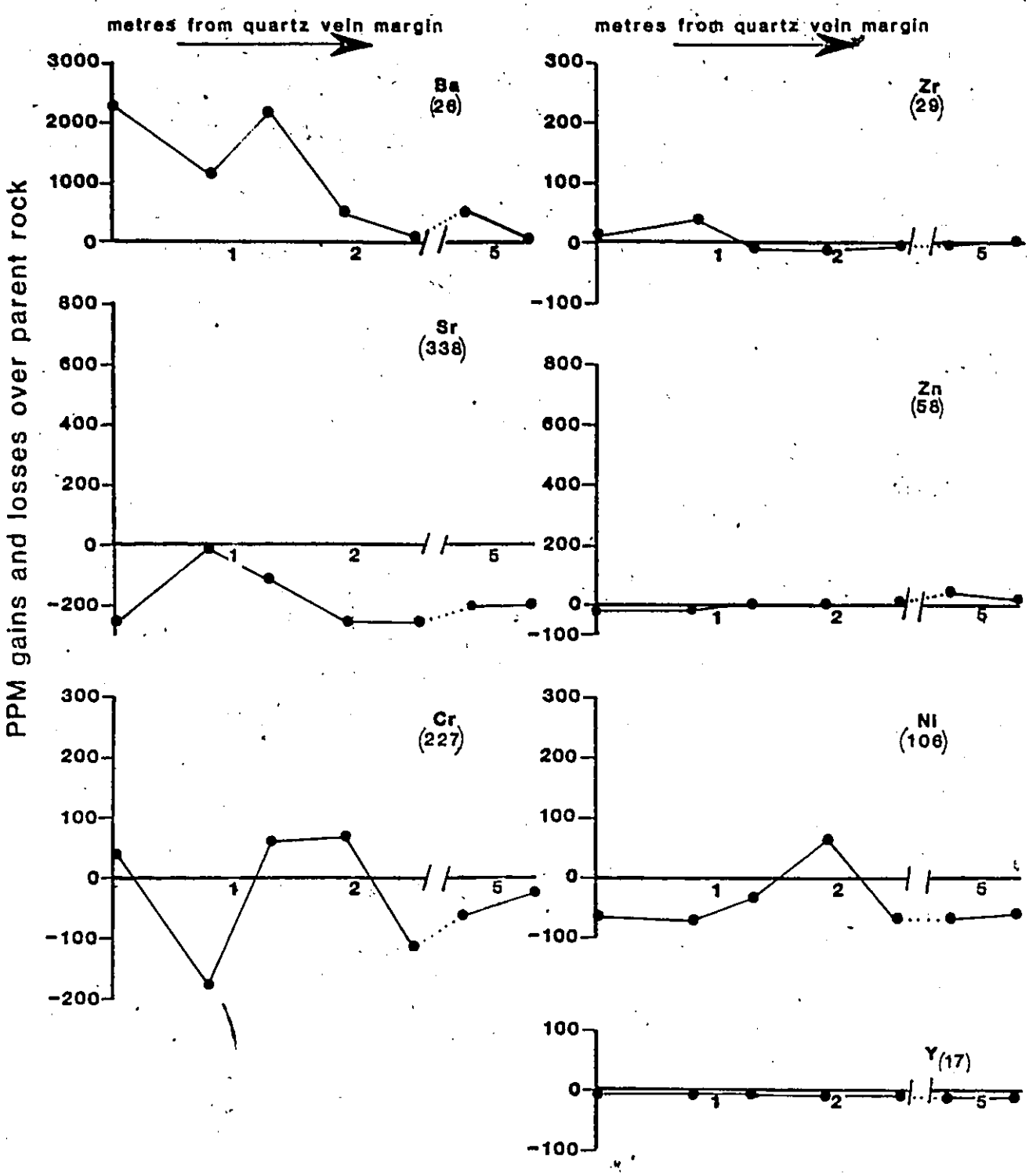

Trace Element Variation in
Shear Zone CG-81-33

FIGURE 4.5

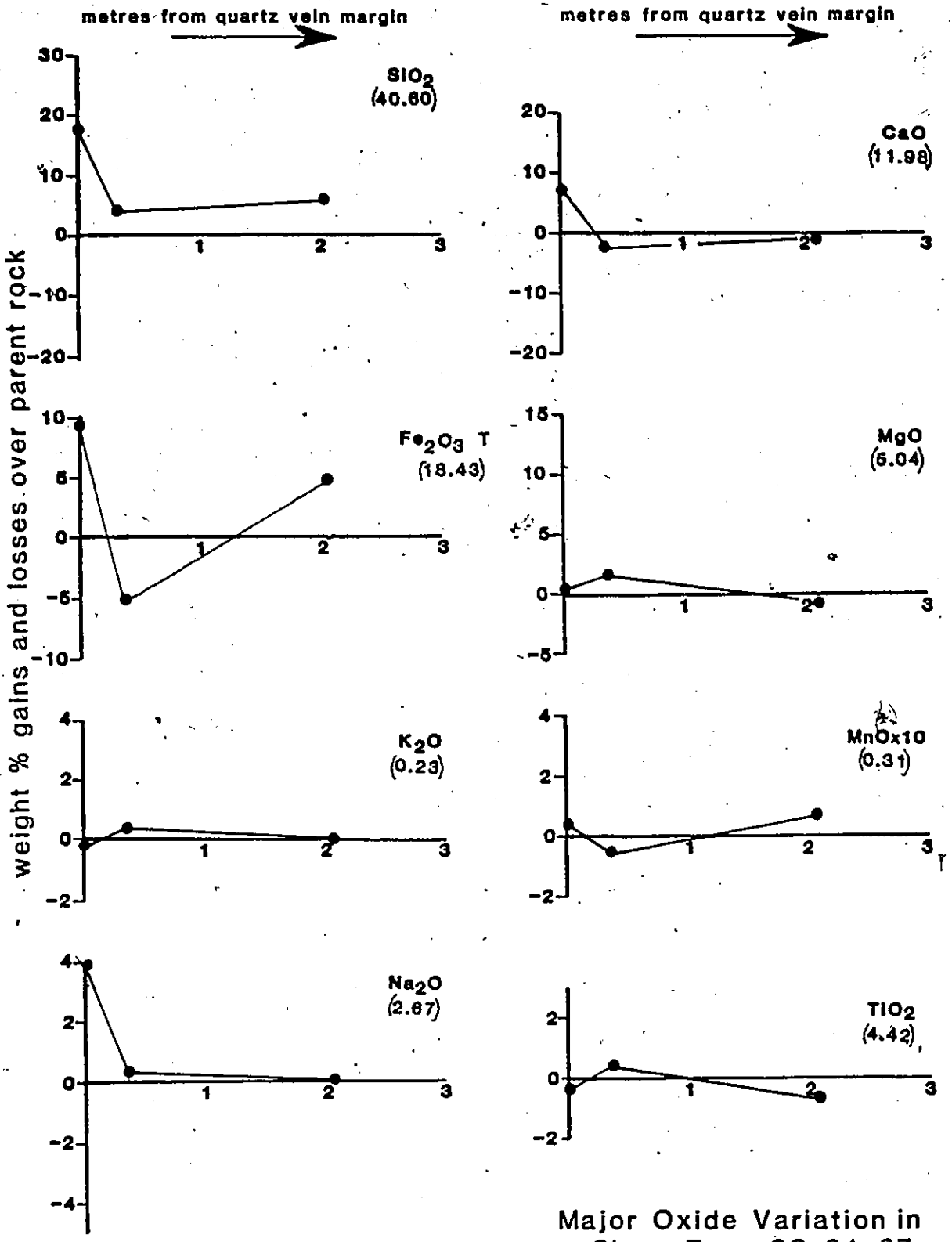

FIGURE 4.6

Major Oxide Variation in Shear Zone CG-81-37

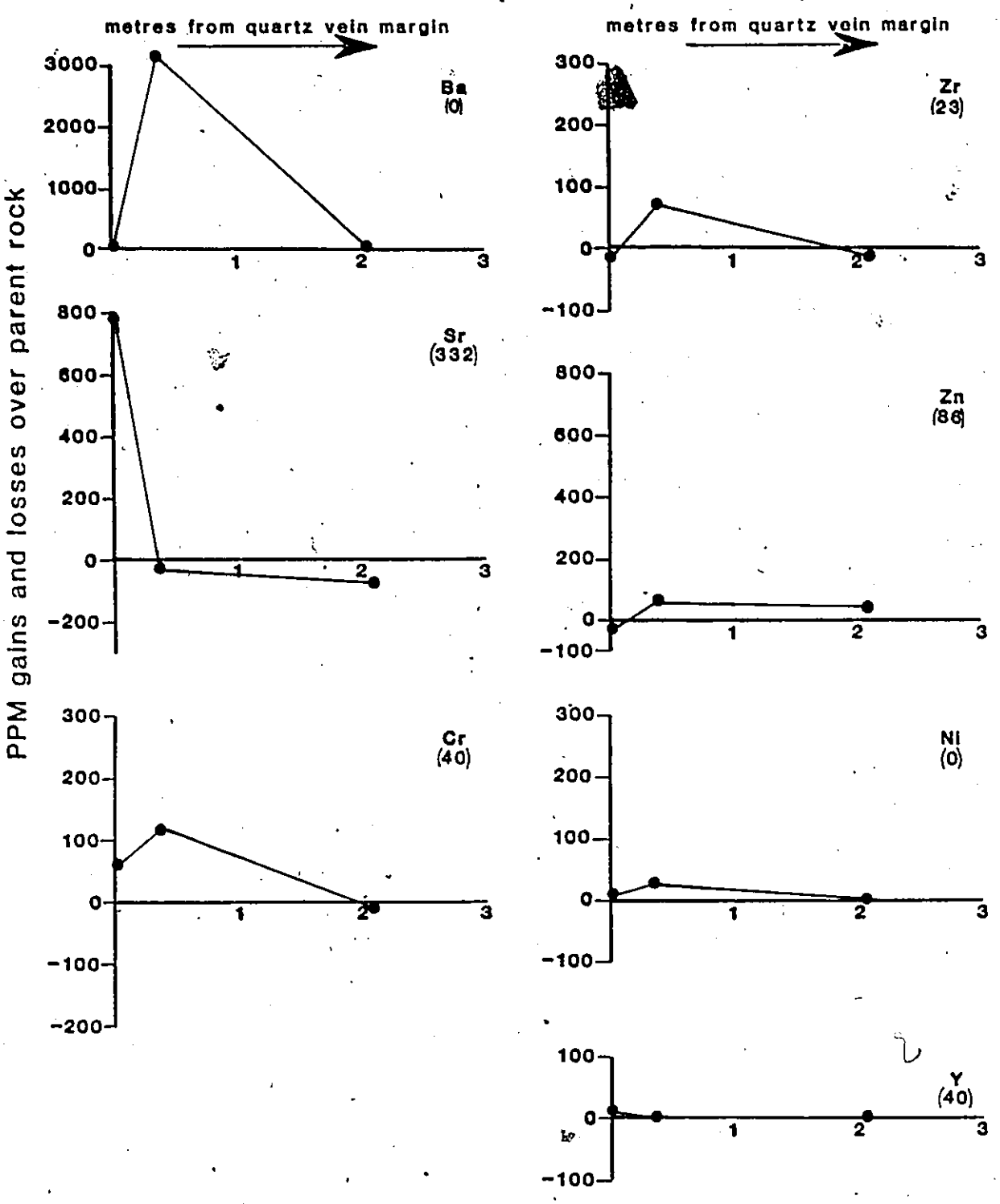

Trace Element Variation in
Shear Zone CG-81-37

FIGURE 4.7

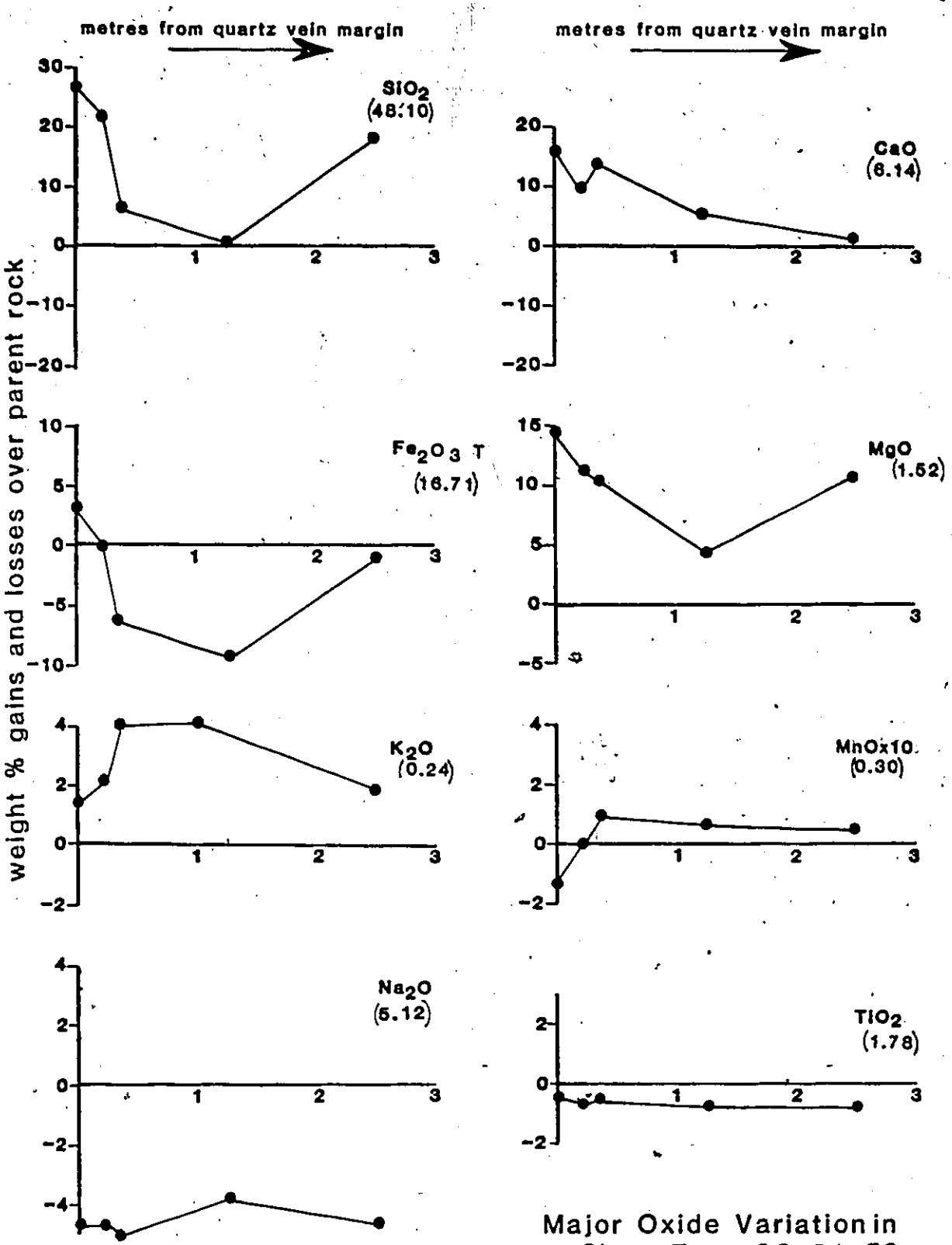

FIGURE 4.8

Major Oxide Variation in Shear Zone CG-81-52

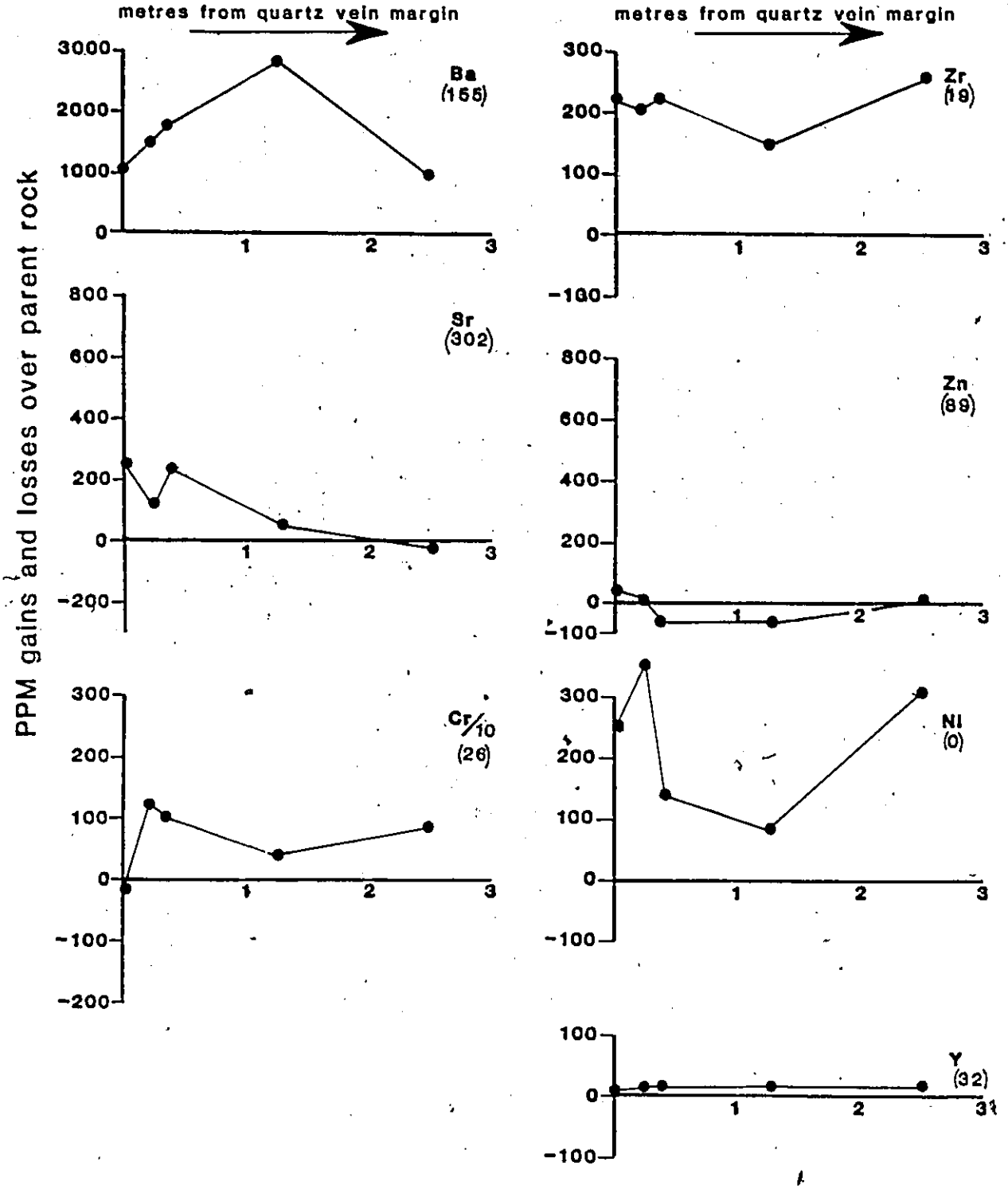

Trace Element Variation in Shear Zone CG-81-52

FIGURE 4.9

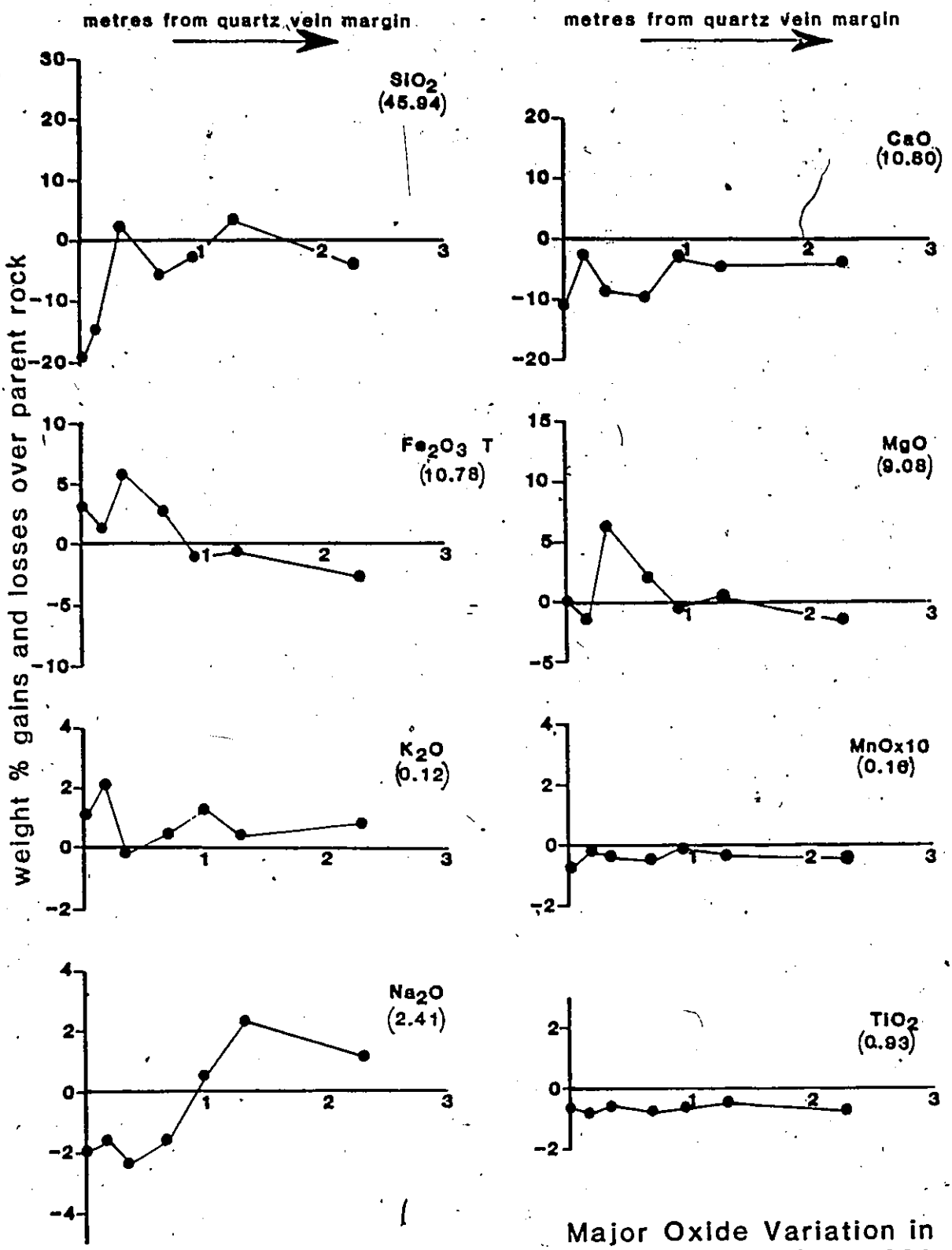

FIGURE 4.10

Major Oxide Variation in Shear Zone CG-81-293

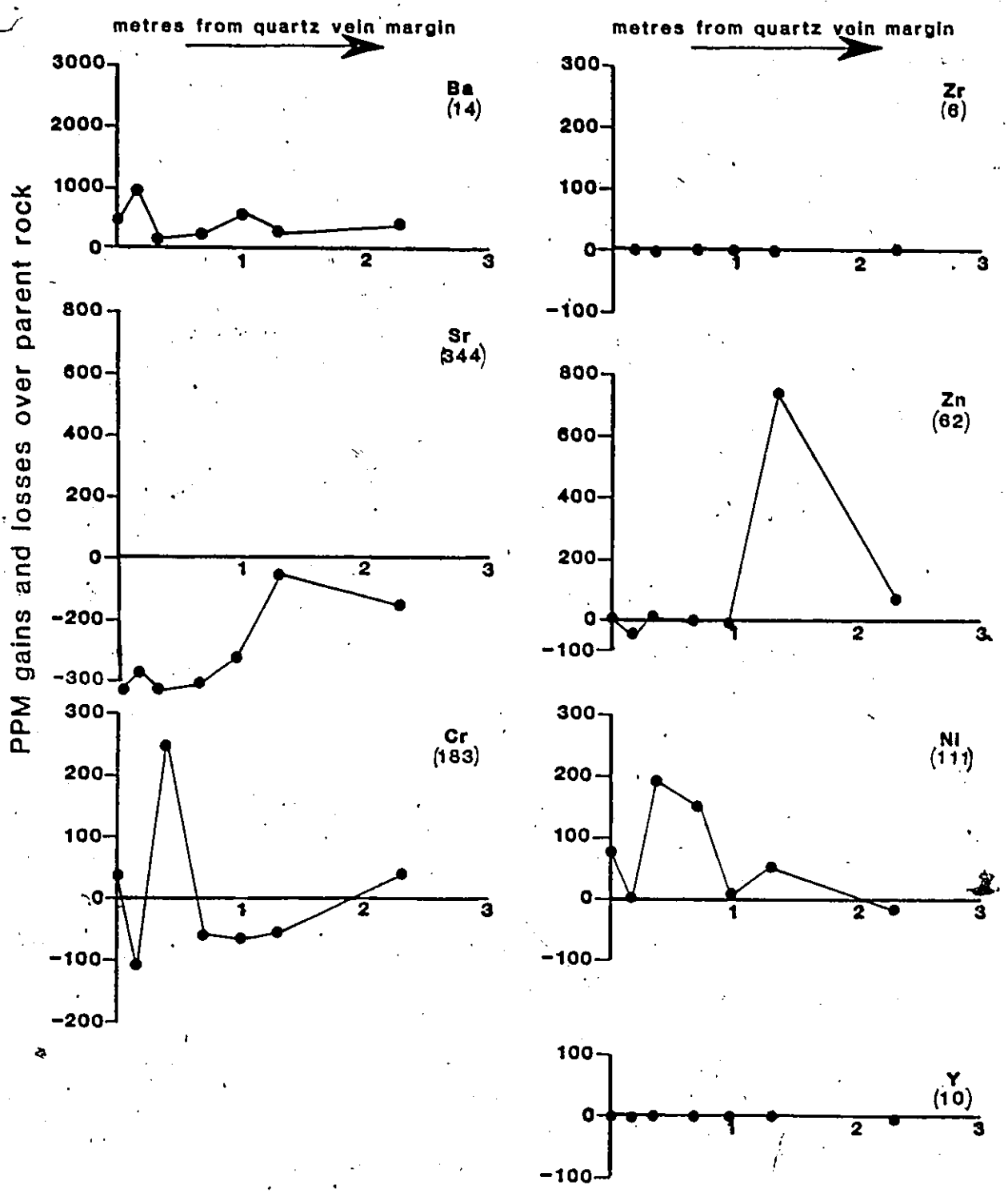

Trace Element Variation in Shear Zone CG-81-293

FIGURE 4.11

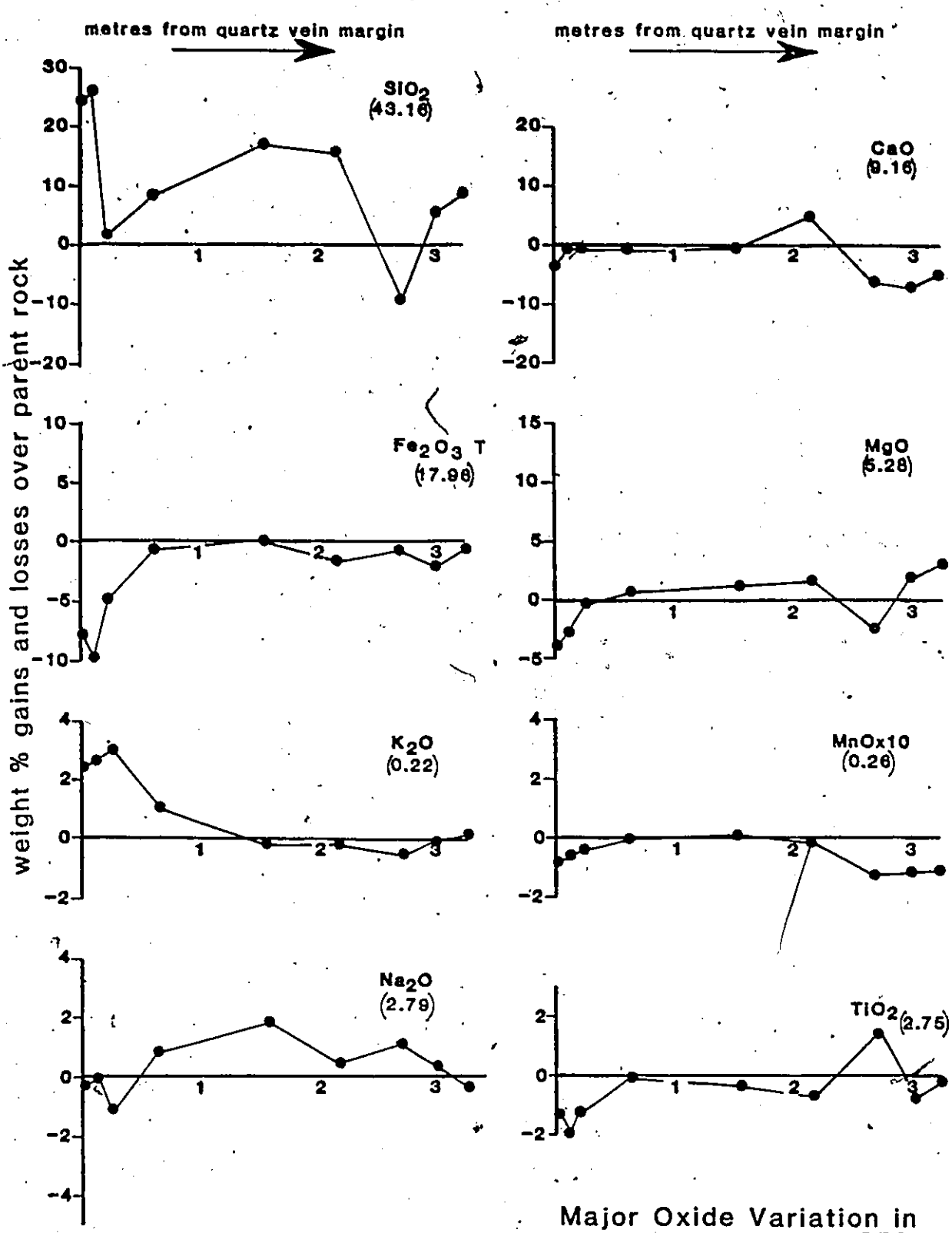

FIGURE 4.12

Major Oxide Variation in Shear Zone CG-81-258

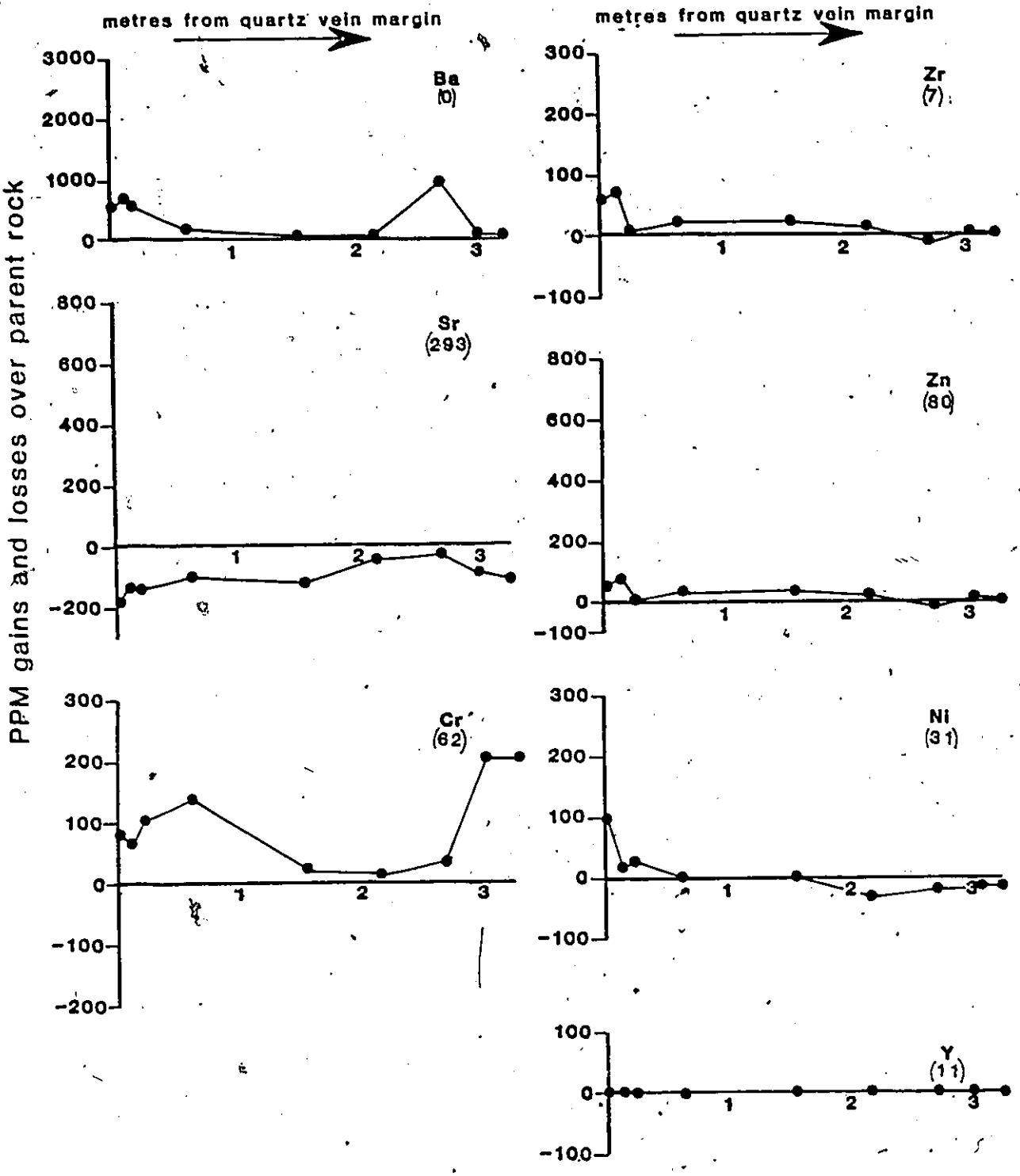

Trace Element Variation in
Shear Zone CG-81-258

FIGURE 4.13

Although concentration of the major oxides is erratic across the shear zones they will often follow identical trends. In three of the shear zones the SiO2 and CaO trends are parallel (Figures 4.4, 4.6, 4.10). In three cases where FeO is depleted overall it has the same trend as MgO (Figures 4.4, 4.8, 4.12).

The variability of concentration over the width of the shear zone makes estimates of the amount added or removed difficult. An overall enrichment or depletion of some components can be recognized. Unfortunately enrichment or depletion of silica could not be determined, but in four shear zones there has been removal of CaO, three shear zones have a definite loss of FeO, and MgO was enriched in three shear zones.

Na2O composes from 2 to 10 percent of most samples. Its concentration may vary markedly across the shear zone. In three shear zones a definite overall enrichment occurred (Figures 4.2, 4.4, 4.12), and in one shear zone it was heavily depleted (Figure 4.8).

In the unsheared gabbro samples analysed, K2O is of a low percentage, usually around .1 to .4 wt%. In three shear zones there has been a high enrichment of K2O and of these three have a high concentration near the veins which tapers to near 0 at the shear zone margins (Figures 4.4, 4.10, 4.12).

Of the trace elements analysed in the study, yttrium varied the least, with virtually identical percentages throughout each shear-zone, indicating little addition or subtraction.

Zirconium, zinc and nickel concentrations are quite low. Within the shear zones they show variable trends which approximately follow the fluctuation of the K2O concentration in some cases (Figures 4.6 and 7, 4.10 and 11, 4.12 and 13).

Barium occurs in high concentration in all the shear zones but is of very low concentration or absent in the unsheared host rocks. In five of the six shear zones the variation in barium concentration matches that of K2O closly (Figures 4.2 and 3, 4.4 and 5, 4.8 and 9, 4.10 and 11, 4.12 and 13).

Cromium occurred in all shear zones. The variation in concentration is erratic but it follows the fluctuation of MgO in a few cases (Figure 4.6 and 7, 4.10 and 11). In three shear zones there is an enrichment of chromium.

Strontium concentration parallels CaO variation in all the shear zones (Figures 4.2-4.13). An overall depletion of strontium occurred in five shear zones (Figures 4.3, 4.5, 4.7, 4.9, 4.11, 4.13).

4.3 DISCUSSION

For most of the samples analysed the results do not show definite trends or evidence of enrichment or depletion. The erratic variation of most of the major elements is reflected in the variation in proportion of the minerals comprising the shear zone. This may be due to inhomogeniaties in the gabbro or a differentiation process active during shearing.

As mentioned above the shear zone consists of domains of parallel chlorite and/or biotite separated by fine granular domains of quartz, calcite, chlorite, plagioclase and minor opaques and microcline. Variation in mineral proportion across the shear zone is probably responsible for the variation of MgO, a major component of chlorite, CaO and Na2O due to their presence in plagioclase, and SiO2 which is a constituent of most of the shear zone minerals and occurs as quartz.

The apparent overall loss of calcium for the shear zone may be due to decomposition of the host gabbro's plagioclase during shearing. The calcium may have gone to form the calcite found in the veins.

The percentage of iron sulfides in the shear zone material is not great. This is confirmed by the low concentration of sulfur and the overall depletion of FeO in some shear zones. In shear zones where FeO is depleted it follows a trend similar to MgO. This suggests that it is occuring mostly in chlorite.

There has been a definite increase in K2O and a less well defined increase in Na2O in some shear zones. The change in K2O concentration from the unsheared to the sheared gabbro is marked. The high K2O and Na2O values adjacent to the veins suggest that the fluids which deposited the vein material were rich in these elements. Some of the K2O was probably used in the formation of biotite, seen in most thin sections of shear zone samples. The remainder of the K2O has probably formed potassic feldspar. Potassic feldspar was only identified in one thin section however it may have been unrecognized in other thin sections due to fine grain size. This conclusion is supported by the enrichment of barium which follows that of K2O and is known to be present in potassium feldspar, (Cox et al 1979).

Other trace elements also vary in concentration in a similar manner to that of the major elements. The strontium concentration follows that of CaO, probably due to the common substitution of strontium into the structure of plagioclase. Likewise the similar variation of MgO and chromium suggest that chromium is present in the chlorite of the shear zone. High chromium percentages in chlorite can cause a lavender or purple interference colour instead of chlorite's usual gray-green, (Kerr 1959). This was not observed in the chlorite of the shear zone samples, but purple chlorite is not an uncommon occurrence in the unsheared gabbro.

Zinc, nickel, and zirconium, which vary in concentration approximately like K2O, may occur in the biotite.

Data from gold-bearing shear zones (CG-81-33, 37, 52) and shear zones not known to contain gold (CG-81-258, 293) are similar. The overall addition or subtraction of elements or variation in concentration seems irrespective of the presence of gold. This is perhaps best shown by the variation of K2O and SiO2. K2O is highly enriched near the quartz veins in both the gold-bearing and barren shear zones (Figures 4.4, 4.12). SiO2 in barren and gold-bearing veins shows overall enrichment in some cases and depletion in others (Figures 4.8 and 8, 4.10 and 12).

4.4 SUMMARY

Evidence for the addition or subtraction of elements during the formation of the quartz veins is generally not clear. Potassium appears to have been introduced and is probably in the form of fine grained potassic feldspar and biotite. Sodium also appears to have been introduced in some cases.

Calcium appears to have been removed from the host gabbro during shearing, probably due to the decomposition of plagioclase feldspar. This calcium may have gone to form the calcite which is associated with the quartz veins.

Evidence of the origin of the SiO2 of the quartz veins is ambigious. From variation in concentration of SiO2 across

the shear zones it cannot be determined if SiO_2 was introduced or was leached from the shear zones.

No geochemical signatures to differentiate between barren and gold-bearing shear zones were found.

Chapter V

FLUID INCLUSIONS IN QUARTZ FROM SHEAR ZONES

5.1 INTRODUCTION

The purpose of this study is to examine fluid inclusions from several shear zones in the Cordova Gabbro and evaluate conditions prevailing during gold mineralization.

The study was carried out using a petrographic microscope with a long focus objective and a Lingham TH 600 heating-cooling stage, (see Appendix 2 - Sample Preparation, Apparatus and Procedure For Fluid Inclusion Study.) Using this apparatus, quartz samples were heated and cooled. The observed temperatures of phase change within the inclusion, coupled with visual estimates of the relative volume of phases suggest the composition, density, and temperature of formation of the ore forming fluids.

In total, quartz from six shear zones was sampled (Figure 5.1). Two shear zones are known to host significant amounts of gold, (one forms the Ledyard Deposit, the other hosts one of the main lodes of the Cordova Deposit), another is associated with the Cordova Deposit but is not known to be mineralized, and three are from shear zones elsewhere in the pluton (Table 5.1).

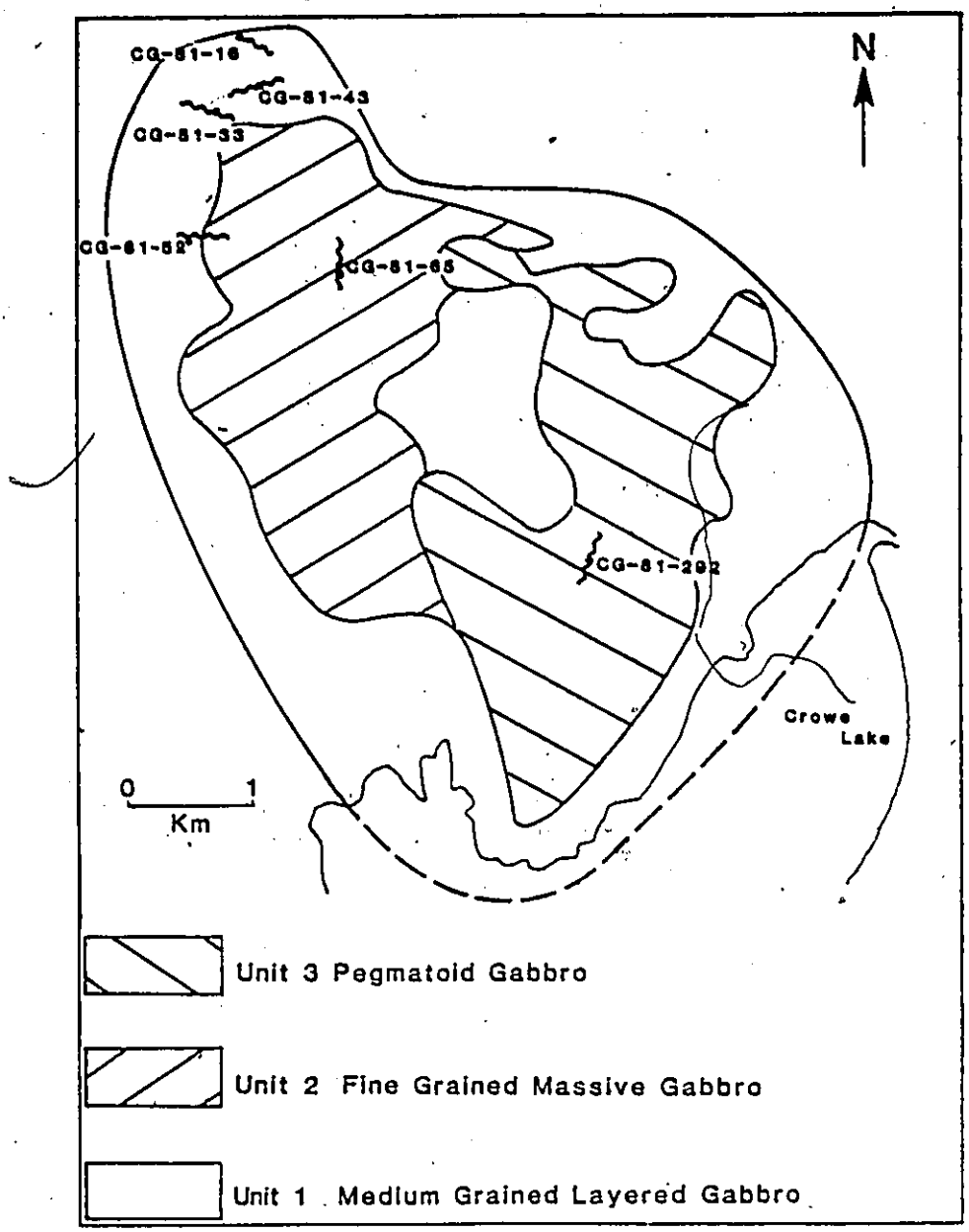

FIGUPE 5.1 Location and outcrop numbers of shear zones sampled for vein quartz for fluid inclusion study.

Quartz Vein Sample Number (See Figure 5.1)	Quartz Vein Location	Host Rock Type	Mineralization	Inclusion Types Present (See Figure 5.2)
CG-81-16	Northern Tip Of The Pluton	Medium Grained Layered Gabbro	Unknown	1 and 2
CG-81-33	Secondary Vein, Cordova Gold Deposit	Medium Grained Layered Gabbro	Au, Ag, Pyrite	1 and 3
CG-81-43	Secondary Vein, Cordova Gold Deposit	Medium Grained Layered Gabbro	Unknown	1 and 3
CG-81-52	Main Vein, Ledyard Gold Deposit	Medium Grained Layered Gabbro	Au, Ag, Pyrite	1 and 3
CG-81-65	Central Region Of The Pluton	Fine Grained Massive Gabbro	Pyrite	1, 2 and 3
CG-81-292	South-Eastern Region Of The Pluton	Pegmatoid Gabbro	Unknown	1, and 2

TABLE 5.1: CHARACTERISTICS OF QUARTZ VEINS SAMPLED FOR FLUID INCLUSION STUDY

5.2 MORPHOLOGY AND TYPE OF FLUID INCLUSIONS STUDIED

Before heating and cooling experiments, the six quartz samples were examined using a petrographic microscope. The purpose of this was to establish what types of inclusions are present, their phase ratios, if there is more than one generation of inclusions and whether or not various inclusion types are primary or secondary.

Three types of fluid inclusions were noted in the samples collected; Type 1, simple liquid-vapor inclusions with liquid as the dominant phase, Type 2, liquid-vapor inclusions with solid phases present, and Type 3, inclusions consisting of two immiscible liquids and a vapour phase (Figure 5.2).

Roedder (1972) suggests Type 1 inclusions usually consist of water with some dissolved salts and a vapour phase, (a near vacuum containing only a few water molecules). The presence of the vapour phase is due to shrinkage of the walls of the inclusion less than the enclosed fluid during cooling from the temperature of formation. Type 2 inclusions are similar to Type 1 except that they contain daughter minerals. The most common is halite, whose presence is an indication that the salinity of the aqueous phase hosting it is over 26 weight percent. This coresponds to the H2O-NaCl eutectic or the maximum percentage of NaCl which can be dissolved in water (at room temperature) before it is saturated (Weast 1970). Type 3 inclusions consist of

COLOURED PICTURES
Images en couleur

10 microns

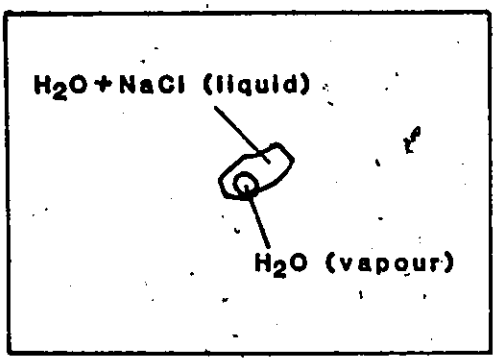

TYPE 1

10 microns

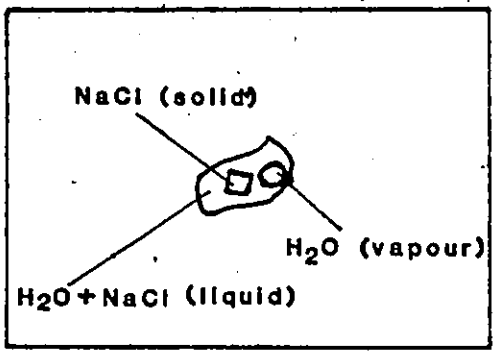

TYPE 2

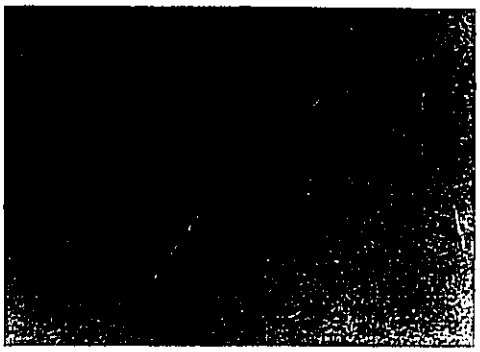

10 microns

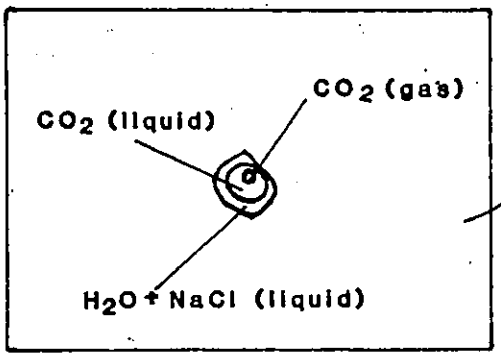

TYPE 3

FIGURE 5.2 Classification scheme for fluid inclusions found in shear zone quartz samples from the Cordova Gabbro.

two liquid phases and a gaseous phase. The liquid phases usually are composed of an outer layer of H_2O (often saline), enclosing liquid CO_2. The gaseous phase is usually CO_2 and is enclosed in the inner liquid phase.

Type 1 fluid inclusions were found in quartz samples from all six shear zones. They occur grouped in planar arrangments and as isolated inclusions. The inclusions vary in shape from elongate and angular to spherical. The latter usually are about 12 microns in diameter. Less commonly the inclusions are elongated up to 25 microns. Visual estimation* of the volume of the vapour phase in inclusions averaged 10 percent.

Type 2 fluid inclusions containing daughter minerals occur in three of the shear zone quartz samples, none of which was associated with Au mineralization (Table 5.1). The inclusions most often form planar groups but occationally they are isolated. These inclusions, like Type 1, range up to 25 microns in length, the larger ones usually being angular. Rare round inclusions, desirable for experimental work (because of their greater chance of being primary), are about 12 microns or less in diameter.

---

* Although visual estimation is the only practical method of volume measurement, serious errors may occur. These are due to the difficulty of estimating the volume of a three dimensional object from a two dimensional view. Roedder (1979) suggests that the error may be reduced if inclusions with regular shapes are measured, especially tabular or disc shaped inclusions.

As for Type 1, the volume of the vapour phase of the Type 2 inclusions averaged about 10 percent. The solid phases consist of small white to colourless daughter minerals 2-3 microns in diameter with a cubic habit. This suggests they are halite.

Type 3 fluid inclusions with 2 liquid and a vapour phase are present in four of the shear zone quartz samples, including the two associated with gold mineralization. The inclusions appear isolated and in planar groups. They are more plentiful than other inclusion types. Overall the rounded inclusions are slightly larger in diameter (10-15 microns) than rounded inclusions of Type 1 or 2.

The central vapour bubble of the vapour phase in these inclusions usually is in constant motion within the enclosing sphere of liquid. This suggests that the inner liquid phase forming the sphere is of low viscosity. Preliminary heating tests caused the inner vapour phase to homogenize with the inner liquid phase at temperatures below 31 degrees C. This indicates that CO2 is the major component of these phases (Roedder 1972). This interpretation is consistent with wetting characteristics of water, CO2 liquid and CO2 gas stated by Roedder (1972), which demand that an inclusion containing these phases has H2O in contact with the inclusion walls and encloses the liquid CO2 which encloses the CO2 gas.

The total CO2 volume averaged 20 percent. Some estimates were as high as 35 percent, however given the inherent inaccuracies of measurment the total CO2 percentage is considered as approximately constant.

The 31 degree critical temperature for CO2 liquid-gas made estimates of the percentage of CO2 gas impractical due to partial absorption of one CO2 phase by the other at room temperature.

Deciding on the primary or secondary nature of these inclusions was very difficult. The main criteria for recognizing primary inclusions in the massive polycrystalline quartz samples of this study is an isolated occurrence (nearest inclusion 5 times its diameter away), (Roedder 1979) and a random distribution throughout the crystal (Roedder and Coombs 1967). Secondary inclusions may be recognized by their occurrence along healed fracture planes or if they have a long thin shape suggestive of streching or necking down (Roedder 1979).

Samples used in this study had inclusions of Type 1, 2 and 3 occuring as both isolated inclusions and in planar arrangements. Using the criteria of Roedder, and Roedder and Coombs, determination of the primary or secondary nature of the inclusion types was not possible. In light of this, tests were carried out on all types of inclusions, but they were restricted to inclusions which were isolated.

5.3 EXPERIMENTAL RESULTS

When a fluid inclusion is cooled until all liquid phases are frozen and then is slowly warmed to high temperatures, several phase transitions will occur.

The range of temperature covered in this study was from -90 to 450 degrees C. Over this temperature range 6 significant phase transitions were: (1) melting of the frozen liquid CO2 phase of Type 3 inclusions, (2) melting of the frozen aqueous phase of Type 1 inclusions, (3) melting of frozen CO2 hydrate compounds in the aqueous phase of Type 3 inclusions, (4) dissolution of daughter minerals within the aqueous phase of Type 2 inclusions, (5) homogenization of CO2 liquid and CO2 gas in Type 3 inclusions and (6) homogenization to a single phase of Type 1, 2 and 3 inclusions.

From the temperatures of the above phase changes inferences may be made of the purity of the CO2 phase of Type 3 inclusions, the salinity of the aqueous phases of all inclusion types, the density of the CO2 phase in Type 3 inclusions and the minimum temperature of formation of all inclusion types.

The following sections describe each of the above topics. They are roughly in order of the occurrence of the associated phase change as inclusions with all liquid phases frozen are heated.

5.3.1 Purity Of The CO2 Phases Of Type 3 Inclusions

If a Type 3 fluid inclusion is cooled to a temperature below[5] -56.6 degrees C the liquid CO2 will freeze and co-exist with the CO2 gas phase. When the inclusion is slowly warmed it will reach a temperature at which the solid will begin to melt and solid, liquid and gaseous CO2 will coexist. This is known as the triple point. For pure CO2 it should occur at -56.6 degrees C (Weast 1970). Variance of the triple point temperature from this value indicates impurities are present.

In this study Type 3 inclusions were cooled to approximately -90 degrees C at which time the liquid CO2 phase took on a rough grainy appearance and the CO2 gas bubble lost its spherical shape. This is interpreted as the freezing point of the liquid CO2 phase.

As the sample was slowly heated and the triple point temperature was achieved the melting of the CO2 solid could be recognized by the return of the CO2 gas phase to its spherical shape, followed quickly by the loss of the rough texture of the CO2 liquid phase. The transformation took place over a very small temperature range, usually within .1 degree C. The triple point temperature was recorded at the

[5] Often there may be a large difference between the freezing point (<-80 degrees C) of liquid CO2 and its melting point (-56.6 degrees C). This is due the meta-stable conditions of the cooling fluid. Roedder (1972) suggests that this condition occurs when a fluid is free of particulate matter which often act as nuclei for crystallizing liquid. Meta-stability occurred in all the fluid phases cooled in this study.

time the CO2 gas bubble resumed its spherical shape.

There was difficulty in seeing the transformation of the CO2 solid to liquid due to the small area of the phases involved. This was often compounded by condensation of water vapour on the viewing windows of the sample chamber. Flushing of the chamber with dry nitrogen gas reduced the problem, however the CO2 solid to liquid phase change could only be seen clearly in seven cases. In one case the solid to liquid phase change occurred at 54.2 degrees, all others occurred within one degree of 56.6. If the error from the limits of reproducibility of data for this temperature range is considered (Appendix 2) the measured triple point temperatures indicate that the CO2 phase is pure.

Touret (1977) suggests that this method of testing CO2 purity may not always be accurate. If the CO2 phase contains methane as an impurity it is possible that upon cooling the methane will separate from the CO2 liquid into tiny, almost invisible bubbles. When the inclusion is reheated the CO2 will melt at -56.6 degrees C giving a false indication of purity.

Unfortunately the only way to avoid the possibility of errors from this phenomenon is to check the CO2 purity using gas chromatography, a difficult operation not possible in this study.

5.3.2 Salinity Of The Aqueous Phases

For simple two phase inclusions (Type 1 of this study), salinity is estimated by measuring the freezing temperature of the aqueous phase. The resulting salinity is given in weight percent NaCl equivalent to allow for the presence of other salts (commonly KCl),(Roedder 1972).

The salinity of the aqueous phase in Type 1 inclusions was measured several times. Due to supercooling of the liquid the point of last melting of the frozen phase is taken as the point of freezing. Freezing of the aqueous phase could be recognized by the textural change of the aqueous phase from smooth with low relief to a grainy rough texture, caused by the formation of ice crystals. The point of last melting was taken to be the point when the smooth texture returned. Normally this occurred over a range of 1 or 2 degrees. In a few cases the ice crystals could be seen to shrink and move about, until finally fading from view. This gave an unambiguous temperature of last melting.

The temperature of last melting of the H2O solid ranged from -10 to -4 degrees C (Figure 5.3). Potter et al (1978) measured the freezing point depression of aqueous NaCl solutions and report that a freezing point depression of 6 to 7 degrees C corresponds to an aqueous solution containing 10 weight percent NaCl.

As previously mentioned, Type 2 inclusions are those having a dominant liquid phase, a gas phase and a solid

Histogram of ice fusion temperatures

in Type 1 fluid inclusions.

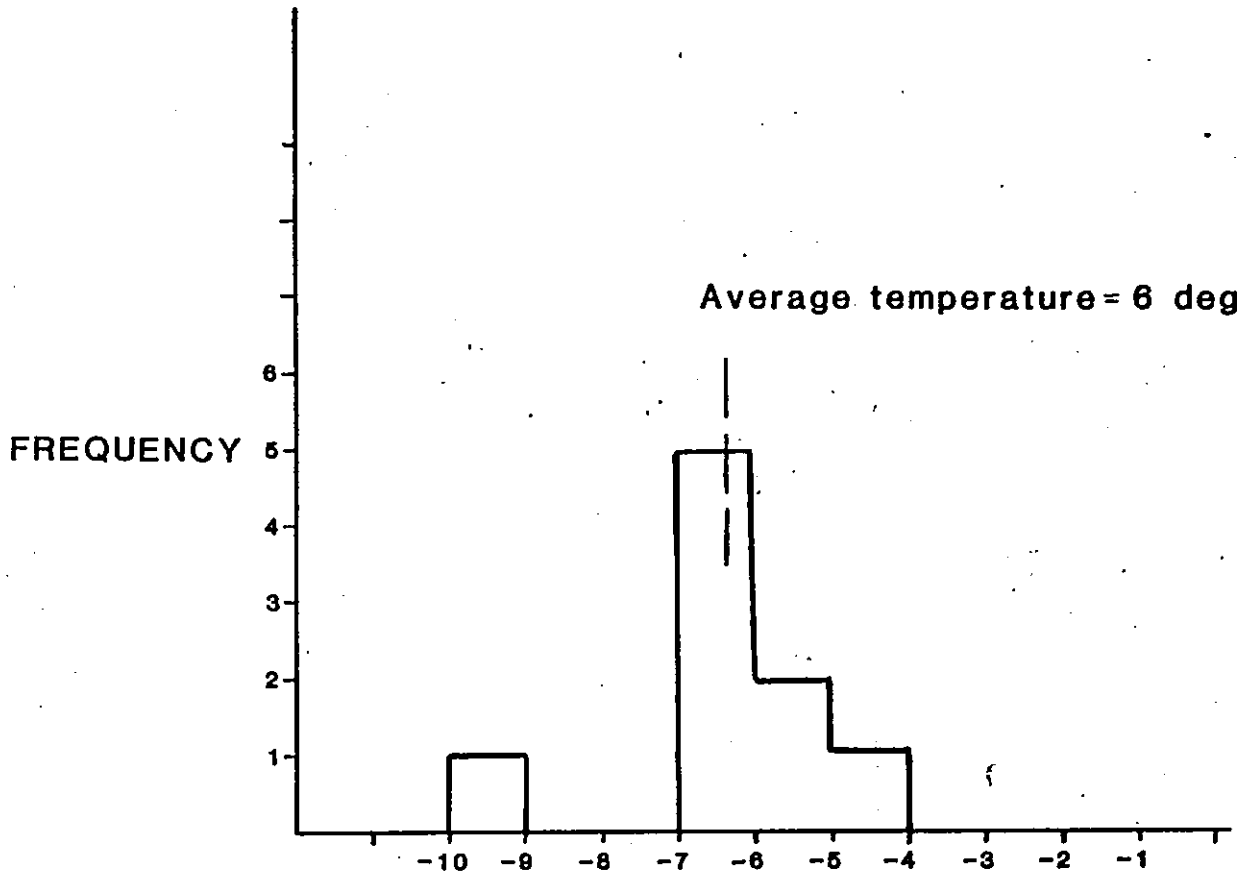

FIGURE 5.3

phase or daughter mineral, which in this study seems to be halite.

To provide a satisfactory estimate of salinity, Type 2 inclusions are heated until the daughter mineral dissolves. The temperature of dissolution can be compared to that of known solutions and a salinity estimate made.

Suitable Type 2 inclusions for this test were difficult to find, and upon heating, some of these were unsatisfactory; the inclusions often became indistinct and the daughter minerals often moved to places where it was impossible to see them dissolve.

In all, only six inclusions clearly showed the solution of daughter minerals. In all cases the NaCl dissolved before the gas bubble began to shrink. Of the six, three had temperatures of dissolution between 180 and 185 degrees C two had temperatures between 230 and 235 degrees and one had a temperature of 285 degrees. Although these temperatures differ substantially they correspond to 26, 29 and 30 weight percent NaCl equivalent (Roedder 1972) indicating a high but constant salinity for the Type 2 inclusions.

When CO2 bearing inclusions (Type 3) are cooled a carbon-dioxide hydrate with the formula (CO2 5.75 H2O) freezes out prior to the formation of ice from the H2O phase (Collins 1979). When CO2 hydrate crystals form, no NaCl is taken into their structure. As CO2 hydrate freezes out of

solution the remaining aqueous phase becomes more saline and freezing point depression measurments of ice will be inaccurate.

If the presence of CO2 hydrate can be determined and its melting point observed, the salinity of the aqueous phase may be estimated.

Due to the small size of inclusions under study and the unfortunate fact that CO2 hydrate has a refractive index close to that of water (Roedder 1972), its observation was difficult. In this study the presence of CO2 hydrate became apparent when upon cooling a jagged interface developed between the aqueous phase and the liquid CO2. Collins (1979) noted a similar feature and attributed it to the presence of CO2 hydrate crystals in the aqueous phase.

Melting of the CO2 hydrate was first seen when the jagged boundary between the CO2 liquid and the aqueous phase became smooth again. This was followed in almost all cases by a resumption of the bouncing or vibrating motion of the CO2 gas bubble which in all cases had remained motionless after the inclusion was cooled. It is probable that the CO2 hydrate crystals extended into the liquid CO2 phase, effectivly restricting the CO2 gas bubble up to that point. The temperature of final melting of the CO2 hydrate was taken when the CO2 gas bubble began to move again.

Using this technique, the melting point of CO2 hydrate and hence the salinity of the aqueous phase of 37 Type 3

inclusions could be measured with certainty. The results can be seen graphically in Figure 5.4. The observed temperatures of CO2 hydrate fusion have a range of 11 degrees C, from -3.5 to 7.5 C. These values correspond to 5 and 19 weight percent NaCl equivalent.

This range is rather wide, however some of the spread of values may be attributed to the difficulty in observing final fusion of the CO2 hydrate. An average of all the temperatures of fusion is 3.2 degrees which corresponds to a salinity of 12 weight percent.

5.3.3 Density Of The CO2 Phases Of Type 3 Inclusions

In a Type 3 inclusion the liquid and gaseous CO2 may be considered pure members of the system CO2, due to the low solubility of H2O in liquid CO2 (Roedder 1965). In the pure system CO2, 31.0 degrees C is considered the critical temperature, i.e. the maximum temperature at which CO2 liquid and gas can coexist. Corresponding to the critical temperature is a critical density of .468 gms/cc. If coexisting CO2 liquid and gas have a total density that differs from .468 gms/cc the temperature of homogenization will be less than 31.0 degrees C. Roedder (1965) noted in CO2 bearing inclusions that CO2 liquid and gas homogenized to gas if the CO2 total density was less than .468 gms/cc, and to liquid if the density was over .468 gm/cc (Figure 5.5).

Histogram of CO_2 hydrate fusion temperature in Type 3 fluid inclusions.

FIGURE 5.4

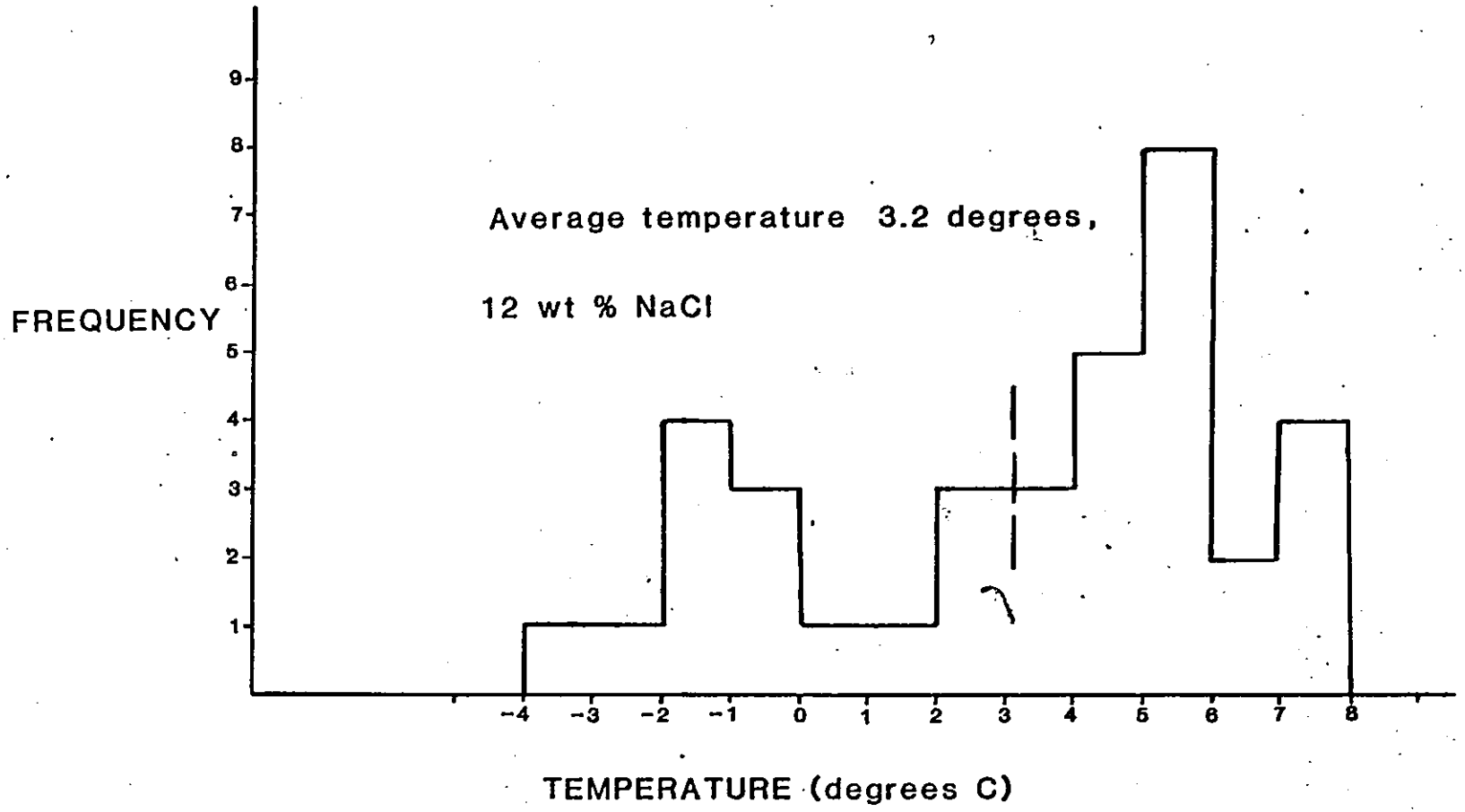

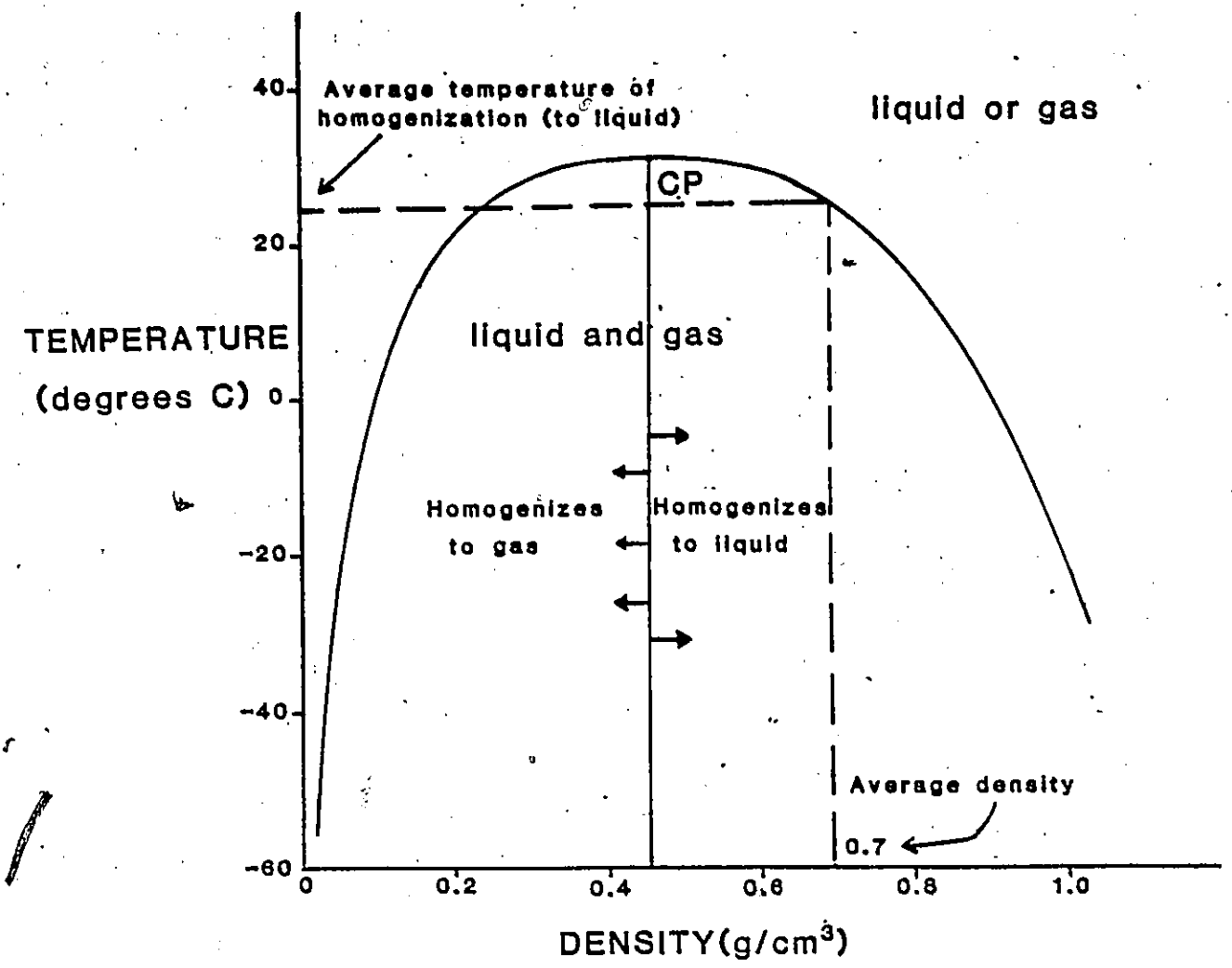

FIGURE 5.5

The 2 phase fluid in the system CO_2 (after Poedder 1972). This curve relates the temperature of CO_2 liquid and gas homogenization to the total CO_2 density. The vertical line originating at .468 gm/cm^3 (critical density) and terminating at the CP (critical point) divides mixtures which homogenize to gas or to liquid. Shown is the average density, found by using the average temperature of CO_2 gas and liquid homogenization in Type 3 inclusions (see figure 5.6).

In this study 70 CO2 liquid-gas homogenizations were observed. In all cases the central CO2 gas bubble shrank and disappeared, indicating homogenization to liquid and a total density of greater than .468 gms/cc.

The actual CO2 liquid-gas homogenization temperature varied from 17.4 to 30.1 degrees C (Figure 5.6). A majority of inclusions homogenized between 20 and 28 degrees corresponding to a density of .63 and .75 gms/cc respectivly. An average of all CO2 liquid-gas homogenization temperatures gives a value of 24 degrees C, indicating an average density of .70 gms/cc for the CO2 phases in the inclusions.

5.3.4 Minimum Temperature Of Formation Of Type 1,2 and 3 Inclusions

The consistancy of phase ratios shown by each of the inclusion types of this study is an indication that at the time of inclusion formation the fluid was under pressure and temperature conditions high enough that boiling or immisibility of components could not occur.

As inclusions cool from the temperature of trapping, the enclosed liquids follow a temperature-pressure path or isochore unique to that fluid's composition. The slope of an isochore in a pressure versus temperature field is dependent on the composition and density and hence the coefficent of thermal expansion of the fluid it represents.

Histogram of CO_2 gas to liquid homogenization temperature in Type 3 fluid inclusions.

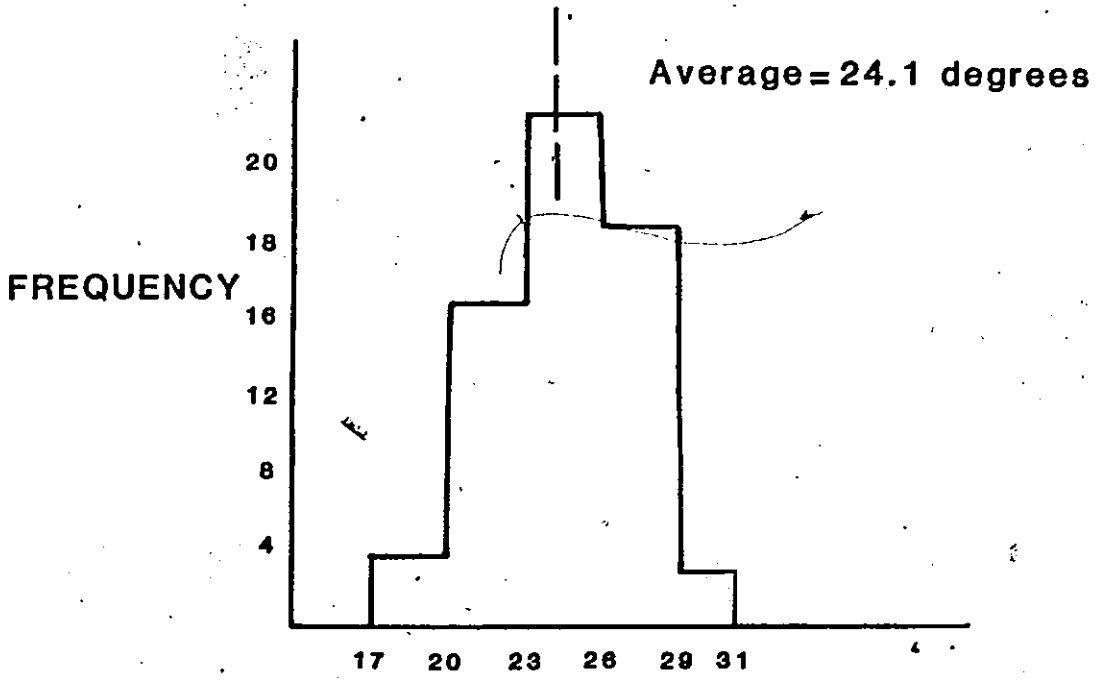

FIGURE 5.6

The coefficent of thermal expansion of the fluid phase of inclusions is much greater then that of the enclosing mineral. As an inclusion cools the liquid phase shrinks more than the enclosing mineral causing a pressure drop in the inclusion.

In inclusions containing members of the H2O-NaCl system (Types 1 and 2 of this study), a temperature and pressure will be reached during cooling which corresponds to the vapor pressure (or boiling) point of that liquid. At this point a vapor phase will form.

In a similar way the CO2 phase of Type 3 inclusions form. In this case the drop in temperature and pressure along the isochoric path for the fluid's composition reaches a point when the CO2 dissolved in the H2O becomes immisible and forms another liquid phase. This point represents the boiling point for that fluid's composition in the H2O-CO2-NaCl system.

If inclusions which have liquid and gas phases at room temperature are reheated, they should homogenize to a single phase at elevated temperatures. The temperature at which this occurs, (called the homogenization temperature) represents the intersection of the isochore of that fluid with the boiling curve of that system, and can be used as the minimum temperature of trapping of the inclusion.

Of this study's samples, the Type 1 inclusions had the lowest average temperature of homogenization. Temperatures

ranged from 145 degrees C to 219 degrees C. with an average temperature of homogenization of 176 degrees (Figure 5.7).

Type 2 inclusions had very erratic temperatures of homogenization ranging from 88 to 470 degrees C. When plotted on a histogram (Figure 5.7) temperatures in the range 88 degrees to 205 degrees C are most common.

For the Type 1 and 2 inclusions the homogenization of liquid and gas was relatively easy to observe. In most cases the small gas bubble could be seen to slowly shrink to a point and then disappear. In a few cases the gas bubble would move about, occasionally into a position where it was no longer visible.

The homogenization of the aqueous phase and the liquid CO2 phase in Type 3 inclusions took place at the expense of the liquid CO2. Unfortuneatly the shrinkage and final disappearance of the liquid CO2 was only seen in about one-sixth of the Type 3 inclusions. In the other cases the liquid CO2 phase expanded very quickly at some temperature, and the inclusion became very dark or opaque. Upon cooling these inclusions did not regain their original form. It is likely that this behavior is due to cracking of the inclusion. The cracking (and subsequent leakage of inclusion fluid) is caused by high internal pressure developed during heating. This is not an uncommon occurrence, Burruss (1981) noted inclusions containing CO2-H2O often have high internal pressures and crack before

Histogram of Type 1 and 2 fluid inclusions'

temperature of final homogenization

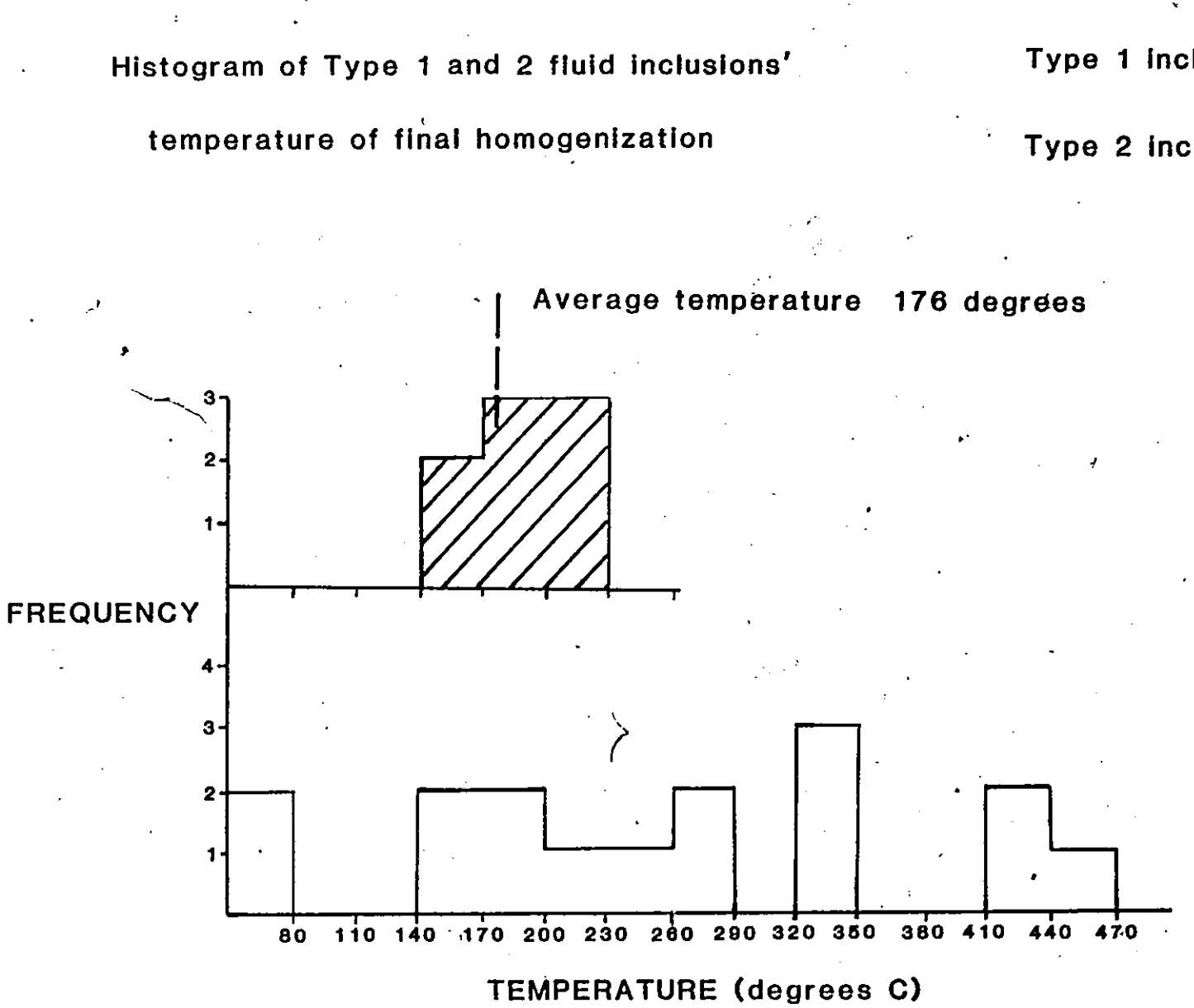

FIGURE 5.7

final homogenization, especially those with CO2 density much greater than the critical density.

If both the temperatures at which the inclusions became opaque and the successful H2O-CO2 homogenization temperatures are plotted on a histogram, the homogenization temperatures form a peak between 280 and 370 degrees C and the temperatures at which the inclusions became opaque form a large peak up to 60 degrees lower (Figure 5.8). This is good evidence that cracking occurred before homogenization. As a result of this, an average temperature of homogenization of 320 degrees C was calculated from temperatures associated with the CO2-H2O homogenization.

5.4 DISCUSSION

Using the results from the previous sections in combination allows further insights into the conditions prevailing at the time of trapping of the fluid inclusions.

Important conditions which can be determined are the density, salinity and the temperature of inclusion fluid at the time of trapping.

5.4.1 Density Of Inclusions

If the composition and relative volume of the various phases present in an inclusion are known then an estimate of the overall density of the inclusion can be made.

FIGURE 5.8

Histogram of homogenization and failure temperature of Type 3 fluid inclusions

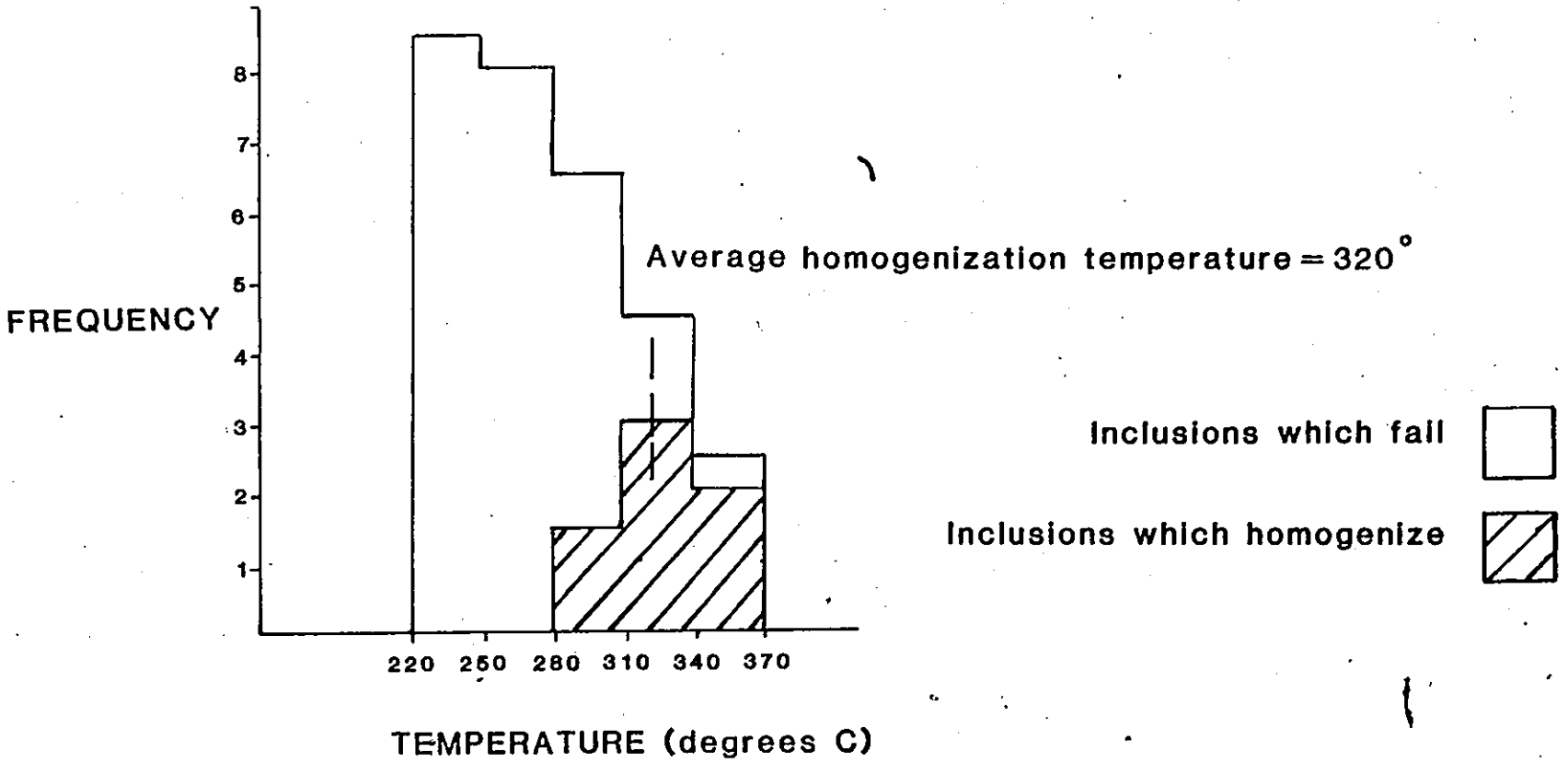

For simple inclusions such as Type 1 and 2 of this study, density can be easily estimated if the inclusion is considered to contain the components: water, NaCl and vapor and their relative volumes are known. Freezing tests of Type 1 inclusions indicated a salinity of about 10 weight percent for the aqueous phase. At low temperature the average Type 1 inclusion was about 10 volume percent vapor. Water may be assumed to be relatively incompressible at room temperature and hence has a density of 1 gm/cc. The density of the vapor phase can be considered 0.

Using these values the total density of Type 1 inclusions (and hence the density at trapping) is .95 gms/cc (Figure 5.9).

A similar operation can be carried out for Type 2 inclusions whose salinity has been determined to average 29 weight percent. It is difficult to measure the density of a solution containing solid NaCl (ie. over 26 wt %) due to the necessity of a volume estimation. For this reason the density of a saturated solution was used in the calculation of total density. The volume of the vapour phase averaged 10 percent of the inclusion. Using these values the total density for Type 2 inclusions was determined to equal 1.1 gm/cc (Figure 5.9).

In the same manner the density of Type 3 inclusions was estimated. It is known that total density of the CO2 phases at near room temperature averages .70 gms/cc. The average

TYPE 1 INCLUSIONS

Salinity of the aqueous phase = 10 wt %, (1.07 g/cc)
Volume of the aqueous phase = .9 cc
Volume of the vapour phase = .1 cc
Density of the vapour phase = 0 g/cc

weight of the aqueous phase = (.9cc x 1.07g/cc) = .95 g
weight of the vapour phase = (.1cc x 0 g/cc) = 0 g
Total weight = .95 g

TOTAL DENSITY = .95 g/cc

TYPE 2 INCLUSIONS

Salinity of the aqueous phase = 29 wt %, (1.20 g/cc)
Volume of the aqueous phase = .9 cc
Volume of the vapour phase = .1 cc
Density of the vapour phase = 0 g/cc

weight of the aqueous phase = (.9cc x 1.20g/cc) = 1.08 g
weight of the vapour phase = (.1cc x 0 g/cc) = 0 g
Total weight 1.08 g

TOTAL DENSITY = 1.1 g/cc

TYPE 3 INCLUSIONS

Salinity of the aqueous phase = 12 wt %, (1.09 g/cc)
Volume of the aqueous phase = .8 cc
Volume of the CO_2 phase = .2 cc
Density of the CO_2 phase = .70 g/cc

weight of the aqueous phase = (.8cc x 1.09g/cc) = .87 g
weight of the CO_2 phase = (.2cc x .70g/cc) = .14 g
Total weight = 1.01 g

TOTAL DENSITY = 1.0 g/cc

FIGURE 5.9 Calculation of the total density for Type 1, 2 and 3 fluid inclusions of this study. Salinites and volumes quoted represent the average of observed values for each inclusion type. The density of the vapour phase in Type 1 and 2 inclusions is assumed to be 0. Densities quoted for the saline fluids are from the Handbook of Chemistry and Physics 1970. All calculations are based on a hypothetical inclusion with a volume of 1 cc.

salinity of the aqueous phase is 12 weight percent and the average volume of CO2 present was estimated to be 20 percent.

Using these variables the total density of the Type 3 inclusions and the fluid at the time of trapping was calculated to be 1.0 gm/cc (Figure 5.9).

It is interesting to note that all inclusion types have densities close to 1.0 gm/cc even though their compositions vary.

An ore forming fluid with a density of close to 1.0 gm/cc is not unusual. Roedder (1979) states that most hydrothermal ore deposits form from fluids having densities from .5 to slightly over 1.0 gm/cc.

5.4.2 Total Salinity Of Inclusions

The weight percent salinities determined for the aqueous phases of the Type 1 and 2 fluid inclusions can be assumed to represent the overall salinity for the inclusions due to the near vacuum conditions in the vapour phase. For Type 3 inclusions the salinity of the aqueous phase must be adjusted for the presence of the CO2 phase. The salinity of the aqueous phase ranges from 5 to 20 wt %, an average value of 12 % was used for these calculations. The aqueous phase volume was 80% of the inclusion and its density averaged 1.1 gm/cc. The CO2 phase occupied the remaining 20% of the volume and had a density of .70 gms/cc.

In a hypothetical inclusion having a volume of 1 cc, 0.8 ccs would be aqueous fluid with a total mass (0.8 x 1.1)= 0.88 gms. Of this 0.88 gms, 12 wt percent or 0.11 gms are NaCl. The CO2 phase of the inclusion has a mass of 0.14 gms. The total mass of the inclusion is therefore (0.88 + 0.14)= 1.02 gms of which 0.11 gms are NaCl. This equals an average total salinity of 11 weight percent.

5.4.3 Metastability

The metastable behavior of inclusion phases during cooling experiments was interpreted by Roedder (1972) as an indication that the inclusion was trapped from a very slow moving solution with very little suspended material. The lack of suspended material inhibits the nucleation of solid phases.

The common occurrence of metastability in inclusions of this study suggests that the same conditions existed in the inclusion forming fluid.

5.4.4 Temperature And Pressure During Fluid Inclusion Formation

A temperature of formation for fluid inclusions may be obtained by applying a correction to the temperature at which the inclusion homogenizes. The correction adjusts for the portion of the cooling path (isochore) in the pressure-temperature field which is above the boiling curve (the point where separation of phases occurs).

If the correct pressure during formation and the isochore of the inclusion fluid is known, a correction can be easily made to the homogenization temperature to give the actual temperature of formation. In the same way, if the temperature of trapping is known the pressure at formation can be determined. Unfortunately, these corrections are difficult for inclusions formed from homogeneous solutions. The main problems are: the trapping pressure or temperature is not known and except in unusual cases must be estimated from outside sources, and isochores for a particular fluid composition are rarely available due to the scarcity of P,V,T,X data for the systems found in fluid inclusions.

In this study the pressure or temperature of formation could not be determined directly from the inclusions. Limits to the temperature of formation can be applied using outside sources.

Temperatures of formation for the fluid inclusions can be restricted to below 450 degrees C (the upper limit of the greenschist facies) due to the lack of a higher grade metamorphic aureole in the gabbroic rock hosting the shear zone.

Working within the framework of temperatures less than 450 degrees estimates of the formation pressure are possible.

For Type 1 and 2 fluid inclusions of this study isochores may be extrapolated from data presented by Roedder and

Bodnar (1980), (Figure 5.10). Using the isochore for the Type 1 inclusions (that is an isochore corresponding to an aqueous solution containing 10% NaCl and with a density of .95 gms/cc) and the assumed maximum temperature of formation of 450 degrees C indicates the pressure during inclusion formation was 2.75 kilobars or less.

For Type 2 inclusions an approximate isochore corresponding to 29% salinity and a density of 1.1 gms/cc can be constructed (Figure 5.10). Using this isochore and the above constraints gives similar results, that is a pressure of formation of 2.75 kilobars or less if the temperature of formation is 450 degrees C or less.

There are no experimentally derived isochores available corresponding to the composition and density of the Type 3 inclusions of this study. Touret (1977) describes a method by which a linear isochore can be produced. It is called the two point method and requires the plotting of the pressure versus temperature of the CO2 liquid and gas homogenization point and the point of intersection of the homogenization temperature and the boiling curve for the particular inclusion fluid. The boiling curve of the Type 3 inclusions of this study can be approximated using data of Takenouchi and Kennedy (1965), (Figure 5.11).

Using the resulting isochore and a maximum temperature of formation of 450 degrees C gives a maximum pressure of formation of 1.25 kilobars.

FIGURE 5.10 Estimated isochores for Type 1 and 2 fluid inclusions. The position of the isochore for Type 1 inclusions (10 wt% NaCl .95 gm/cc) and Type 2 inclusions (29 wt% NaCl 1.1 gm/cc) were extrapolated from the isochores for pure water and water with 10 and 25 wt percent NaCl.

———— water

— — — — — 10 wt% NaCl

—— — —— — —— 25 wt% NaCl

Use of the estimated isochores for Type 1 and 2 inclusions and a maximum formation temperature of 450 degrees indicates a maximum pressure of formation of 2750 bars for both inclusion types.

Pure water, 10% NaCl and 25% NaCl isochores are from Roedder and Bodnar (1980) who used data from Sourirajan and Kennedy (1976).

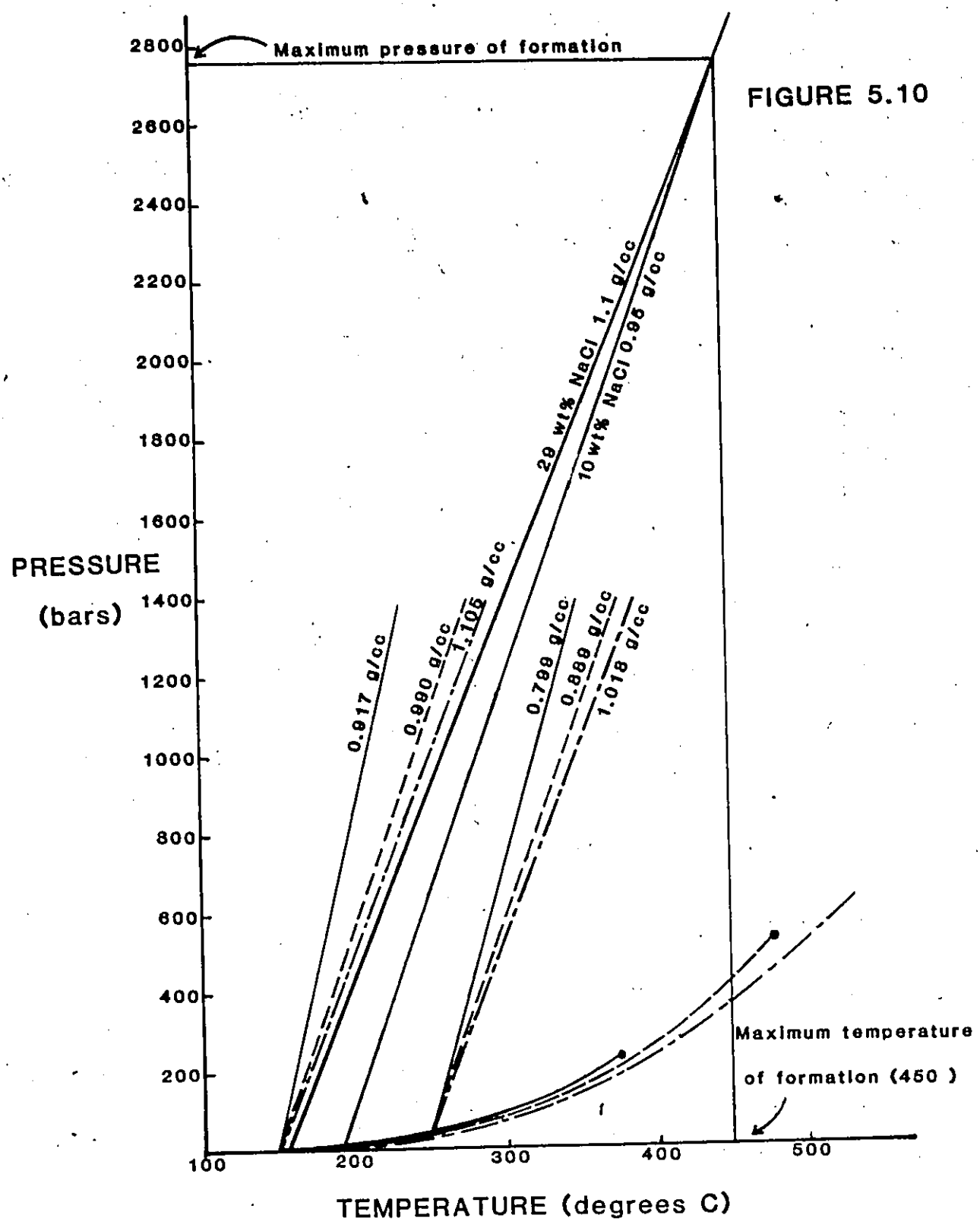
Maximum pressure of formation
2800
2600
2400
2200
2000
1800
1600
1400
1200
1000
800
600
400
200
PRESSURE
(bars)
20 wt% NaCl 1.1 g/cc
10 wt% NaCl 0.95 g/cc
0.917 g/cc
0.990 g/cc
1.105 g/cc
0.798 g/cc
0.888 g/cc
1.018 g/cc
Maximum temperature
of formation (450)
100
200
300
400
500
TEMPERATURE (degrees C)

FIGURE 5.10

FIGURE 5.11 Estimated isochore for Type 3 inclusions. Type 3 inclusions average 14 wt% CO_2 and 11 wt% NaCl. Using the method described by Touret (1977) the isochore is defined by points A and B. Point A is defined by the temperature and pressure of the CO_2 gas to liquid homogenization (24 degrees and approximately 30 bars (Touret 1977 Fig.4)). Point B is defined by the intersection of the boiling curve of the inclusion fluid and the homogenization temperature. Using data from Takenouchi and Kennedy (1965) boiling curves for 20 and 6 wt% NaCl in the 14 wt% CO_2 field can be estimated (solid curves). With these curves an estimate of the position of the of the boiling curve for 11 wt% NaCl (dashed curve) can be made and point B established. The resulting isochore and a maximum formation pressure of 450 degrees indicates a maximum formation pressure of 1.25 kilobars.

FIGURE 5.11

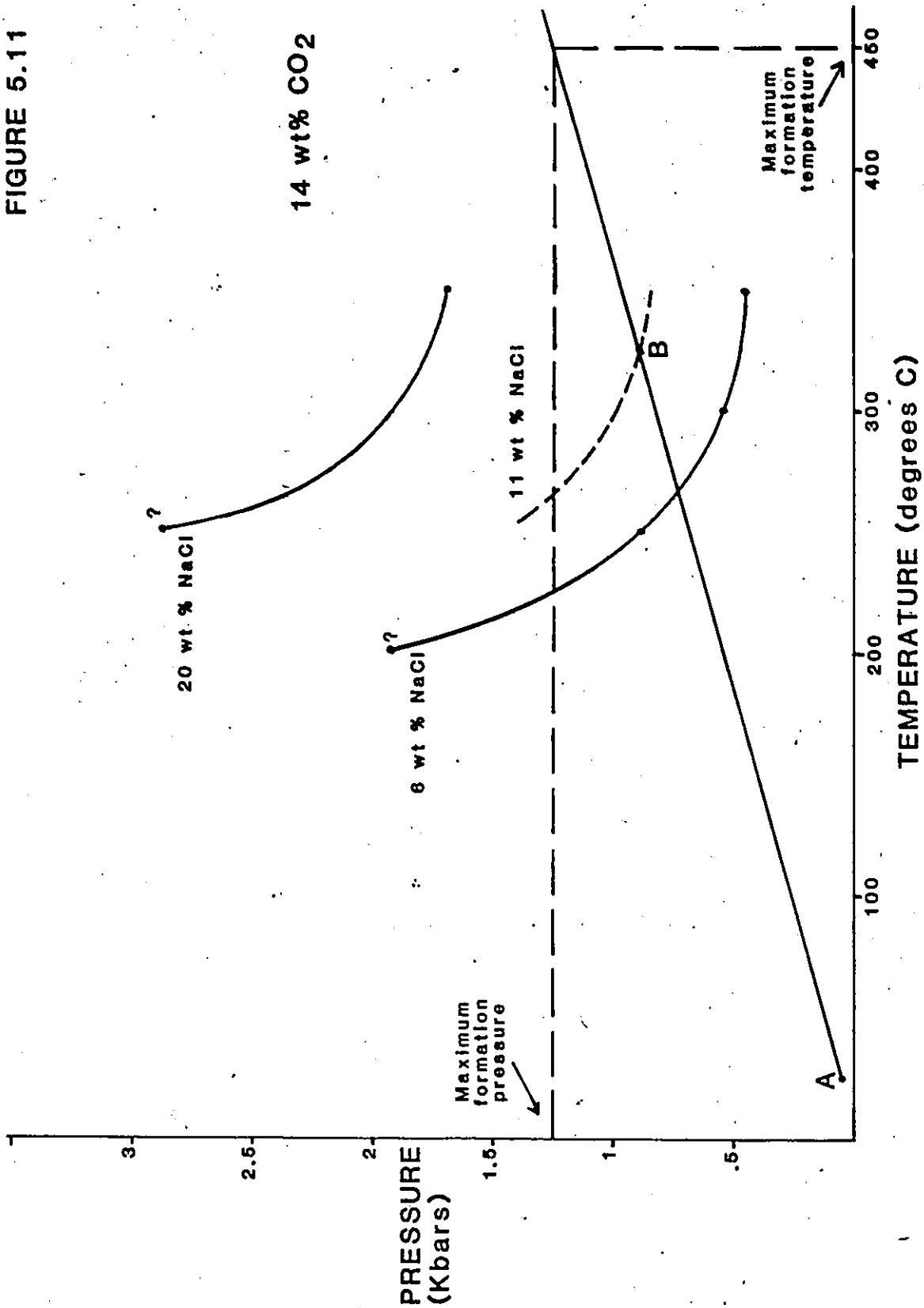
14 wt% CO_2
20 wt % NaCl
?
6 wt % NaCl
?
11 wt % NaCl
B
A
Maximum formation pressure
Maximum formation temperature
PRESSURE (Kbars)
TEMPERATURE (degrees C)
3
2.5
2
1.5
1
.5
100
200
300
400
460

The flatness of the isochore for Type 3 inclusions (Figure 5.11) indicates that the value of 1.25 kilobars at 450 degrees C is close to the pressure of formation since the corresponding temperature must be between 320 degrees C (the average homogenization temperature) and 450 degrees C. These extremes correspond to .85 and 1.25 kilobars, a difference of only 400 bars.

5.4.5 Conclusions

As mentioned above it is impossible to tell which of the inclusion types are primary on the basis of inclusion shape and occurrence alone. Unfortunately experimental results do not provide the answer to this question.

Although the primary or secondary nature of inclusion types cannot be determined it can be concluded that Type 1 and 2 inclusions are of a different generation than Type 3 inclusions. This is shown by the contrast in compositions, specifically the presence of a consistent 20 volume percent of CO2 in Type 3 inclusions. It is possible to form Type 1,2 and 3 inclusions at the same time. This however, requires the presence of an immisible CO2 phase at the time of trapping. If this occurs, inclusions containing 0-100 percent CO2 would be trapped. The consistent phase ratio of 20 volume percent CO2 in Type 3 inclusions is strong evidence of an independent generation.

The independent generation of the Type 3 inclusions may be linked to the deposition of the gold. Three of the four CO2 bearing quartz samples are from the Ledyard and the Cordova Mine areas and of these two are from shear zones known to contain gold. The samples taken from the southeast and extreme north of the pluton do not have CO2 bearing inclusions. On this basis it is concluded that the fluid which carried and deposited the gold is likely the one which was trapped to form the Type 3 inclusions of this study.

This corresponds to a homogeneous, aqueous solution, rich in dissolved CO2 and NaCl. It had a density of about 1 gm/cc and at the time of trapping was at a temperature between 320 and 450 degrees C and a pressure of between .85 and 1.25 kilobars.

Chapter VI

SUMMARY AND CONCLUSIONS

6.1 SUMMARY

In the previous chapters several conclusions were drawn regarding the Cordova Gabbro, the shear zones which cut it, and the mineralizing fluids which passed through them.

1. The Cordova Gabbro may be divided into three rock units: Unit 1, a medium grained gabbro with a primary layering, Unit 2, a fine-grained massive gabbro and Unit 3, a pegmatoid gabbro.
2. All the rock units have been metamorphosed resulting in variable alteration of plagioclase to epidote group minerals and complete alteration of pyroxene to amphibole. The amphibole has been altered to chlorite, calcite and quartz.
3. The rock units are similar geochemically, indicating the main differences are textural and differentiation was not an important process during crystallization. In addition, the geochemical analyses of the rock units closely match estimates of the average composition of gabbros worldwide, suggesting the metamorphism has been essentially isochemical.

4. The pluton is cut by many shear zones which are host to quartz veins. Some of these veins host pyrite and gold minerals.
5. The sheared gabbro has been altered to a schistose mass consisting of chlorite, calcite, plagioclase, quartz, biotite, and minor oxides and potassic feldspar.
6. Elemental variance across the shear zones is erratic, paralleling an erratic variation in mineral proportions. There appears however, to be a definite increase in potassium and a less well defined increase in sodium in the sheared gabbro as the quartz veins are approached. This indicates that the fluid associated with the deposition of the quartz veins was enriched in sodium and potassium.
7. An overall depletion of calcium from the shear zones occurred. It could not be concluded whether the SiO_2 forming the quartz veins was leached from the wall rock or whether it is from another source.
8. At room temperature three types of fluid inclusions were identified in the shear zone quartz: Type 1, consisting of a vapour phase and saline H_2O, Type 2, consisting of H_2O saturated with salts, a solid phase (probably NaCl), and a vapour phase, and Type 3, consisting of saline H_2O, liquid CO_2 and gaseous CO_2.

9. The fluid from which the gold minerals precipitated is thought to be represented by the fluid trapped in the CO2 rich inclusions. This corresponds to a saline fluid, rich in CO2, which was trapped at a temperature between 320 and 450 degrees C and a pressure between .85 and 1.25 kilobars.

6.2 CONCLUSIONS

6.2.1 Evolution Of Gabbro

The Cordova Gabbro can be described as a small funnel or bowl shaped body (areal extent 30 sq km), the shape being suggested by the steep dip of the lowermost layered unit (1) toward the centre. The small size of the pluton may be the reason for its lack of chemical differentiation.

The variation between rock units, which is mostly textural, is probably due to a variation in the cooling rate of the pluton. Rapid cooling of the pluton due to the proximity of cold country rocks could produce layering (Unit 1) in the manner described by McBirney and Noyes (1979). The pegmatoid unit (3) represents a later, slower cooling stage. The massive finer grained rocks of Unit 2 probably formed by rapid cooling although they seem to be isolated from the country rock by Unit 1.

The evolution of the Cordova Gabbro to its present state fits well into models proposed by many workers for the formation of the Grenville Province in this part of the Canadian Shield (Lumbers 1967, Moore and Thompson 1980).

The intrusion of the Biotite-Diorite Series of Lumbers (1967) before the Ottawan episode of regional metamorphism and deformation (Moore and Thompson 1980) explains many features of the Cordova Gabbro. The most obvious of these is the heavy alteration of plagioclase and pyroxene. In addition, the shear zones cutting the pluton may be interpreted as the response of the gabbro to deformational stresses accompanying metamorphism. The deflection of the regional fabric in the Grenville Supergroup around the Cordova Gabbro suggests it did not deform as plastically as the country rocks.

6.2.2 Genesis Of The Gold Deposits

Genesis of the gold deposits within the Cordova Gabbro is also attributed to the regional metamorphism and deformation.

Three factors which affect the gesesis of gold deposits are discussed below. These are the source of gold, its transportation, and its deposition.

The source of gold for most hydrothermal deposits is largely conjectural due to the presence of gold in most rock types and by the suggestion of Tilling et al (1973) that the concentration of gold in possible source rocks is unimportant. More important is the attendant transport and deposition mechanism. They point out that since a thousand-fold increase in concentration of gold is necessary to

produce ore, the comparatively small variance in average gold concentration for most rock types is unimportant. It may be said, therefore, that a suitable source of gold is available for the deposits.

The removal of gold from source rocks and its transfer to a site of gold deposition is dependent upon the presence of a fluid containing chemical species capable of combining with gold to form soluble complexes.

The most obvious process for producing fluid for transporting the gold in the Cordova Pluton is metamorphism. As previously stated, the Cordova Gabbro was emplaced before the onset of the main episode of Grenville Metamorphism. Greenschist metamorphism of the gabbro and adjoining basalt would not release much water. In fact, the widespread change of pyroxene to amphibole requires addition of water. However if mafic rocks exist at deeper levels they probably experienced a higher grade of metamorphism. Elevation of mafic rocks from greenschist to amphibole grade of metamorphism liberates water through the change of chlorite and epidote to new, less hydrous phases. Fyfe and Henly (1973) have proposed this process for the supply of transporting fluids for the shear zone hosted Morro Velho gold deposit of Brazil.

The geochemical and fluid inclusion study indicates that the fluid which deposited the quartz-pyrite-gold veins was rich in Na, Cl, Au, K and CO2. The association of gold with

pyrite, suggests that the solution contained sulfur and possibly iron (the iron may have been derived from the wall rocks).

The presence of these ions in the transporting fluid makes the formation of several gold-bearing complexes possible. Two complexes of gold most often thought to be present in hydrothermal solutions are sulphide and chloride complexes. Opinions differ on which of these complexes is dominant in the transport of gold, but it seems that the importance of these complexes varies with changing physio-chemical conditions such as pH, oxidation state, temperature, etc. The most striking of these factors seems to be the pH of the gold carrying solution. Chloride complexes are more soluble in solutions which are acidic (Helgeson and Garrels 1968; Boyle 1979). Conversly, sulphide complexes are more soluble in alkaline to neutral solutions (Seward 1973).

The pH of solutions forming the ore of the Cordova Gabbro's deposits is not known. A low pH coupled with the high percentage of NaCl in the ore fluids would fovour the formation of chloride complexes. The precipitation of gold could have been caused by the leaching of $CaCO_3$ which produced more alkaline conditions and a reduction of chloride complex stability. The depletion of $CaCO_3$ in the shear zone is supportive of this possibility.

A neutral to slightly alkaline pH solution at the formation temperatures of 320 to 450 degrees C would provide conditions allowing a high solubility of certain sulphide complexes (Seward 1973). Precipitation of gold could be caused by a shift in pH to more acid conditions. One way to lower the pH and cause gold to precipitate is by the dissociation of H_2SO_4 due to mixing with meteoric water. Evidence for mixing was absent from fluid inclusions studied. More evidence is needed before drawing conclusions about chloride or sulphide complexes being the important transporters of gold.

In summary, the gold deposits largely owe their formation to the metamorphism and deformation associated with the Ottawan Orogeny. The metamorphism probably produced the fluids which leached gold from the source rocks and transported it. In addition, the shear zones which host the gold deposits resulted from the regional deformation.

6.3 SUGGESTIONS FOR FURTHER WORK

Future work on this pluton and its mineral deposits could take many interesting forms. Oxygen isotope analysis of the shear zone quartz may indicate more definitely the source of the mineralizing fluids. The mode of occurrence of the gold metal is uncertain, microprobe analyses may link it to pyrite mineralization.

A sense of shear for the shear zones could not be determined. Detailed study of the sheared gabbbro in thin section may give an answer from C and S structures. In addition a study of the zoned amphiboles to try to explain the reversals in compositional variation from core to rim may prove interesting.

Appendix A

GEOCHEMICAL ANALYSES

This appendix contains all geochemical analyses referred to in chapters 1 through 6 of this thesis. It is divided into 5 sections:

A.1 - X-Ray fluorescence analyses of rock samples from the Cordova Gabbro.

A.2 - X-Ray fluorescence analyses of shear zone and unsheared gabbro samples.

A.3 - X-Ray fluorescence analyses of iron ore samples.

A.4 - Atomic absorption and optical emission analyses for trace metals in quartz samples.

A.5 - Microprobe analyses of plagioclase, amphibole and chlorite in samples from the Cordova Gabbro.

Sample locations for all analyses and outcrops listed in this appendix with the prefix CG-81 may be found on Figure 3.1a (in pocket).

Low totals for analyses of sheared gabbro samples are common. This is attributable to a high percentage of $CaCO_3$ and hydrous mineral phases. Water and $CaCO_3$ are lost when samples are fused for XRF analysis.

Sample Number	CG- 81-30	CG-81-67	CG-81-94	CG-81-126	CG-81-146	CG-81-189	CG-81-194
Rock Unit	Unit 1	Unit 1	Unit 1	Unit 1	Unit 1	Unit 1	Unit 1
(wt.%)							
SiO_2	48.81	44.85	41.27	45.79	45.26	44.39	47.52
Al_2O_3	15.28	12.99	12.24	17.81	14.85	14.05	17.28
Fe_2O_3T	10.91	17.07	18.56	8.14	15.17	17.95	9.59
MgO	4.18	6.08	5.58	10.23	5.21	4.11	8.42
CaO	10.12	8.47	7.60	10.08	8.00	9.29	11.19
Na_2O	4.01	3.04	1.74	2.29	3.74	3.26	2.40
K_2O	0.29	0.76	0.21	0.12	0.70	0.44	0.38
TiO_2	3.37	3.90	2.69	0.28	4.80	2.76	0.87
P_2O_5	0.0	0.01	3.24	0.0	0.05	1.99	0.0
MnO	0.15	0.24	0.23	0.13	0.19	0.22	0.15
S	0.04	0.04	0.02	0.00	0.01	0.03	0.02
(ppm)							
Ba	93	143	0	43	0	38	97
Cr	44	70	33	408	48	36	272
Zr	33	74	14	3	52	88	44
Sr	382	202	197	267	251	202	283
Rb	0	11	4	0	6	0	4
Y	21	33	27	10	19	51	20
Nb	0	3	0	0	0	4	0
Zn	38	129	99	57	91	107	92
Ni	0	42	0	138	10	0	88
Total	97.22	97.56	93.43	94.99	98.04	98.57	97.94

APPENDIX A.1 X-Ray fluoresence analyses of rock samples from the Cordova Gabbro.

Sample Number	CG-81-290	CG-81-28	CG-81-50	CG-81-64	CG-81-84	CG-81-162	CG-81-184	CG-81-114
Rock Unit	Unit 1	Unit 2	Unit 2	Unit 2	Unit 2	Unit 2	Unit 2	Unit 3
(wt.%)								
SiO_2	46.34	47.80	46.19	42.82	45.52	46.73	48.90	48.05
Al_2O_3	14.59	14.08	16.88	13.41	16.42	18.09	15.57	16.28
Fe_2O_3T	13.53	13.42	9.95	10.25	12.82	9.20	17.05	9.71
MgO	9.48	5.95	9.09	5.62	8.29	9.10	2.19	8.66
CaO	7.77	10.76	9.22	5.14	10.19	9.40	8.00	10.57
Na_2O	2.85	2.29	2.07	3.38	2.01	2.33	3.69	1.22
K_2O	0.19	0.35	0.66	0.18	0.43	0.66	0.54	0.13
TiO_2	0.95	1.97	0.80	1.07	1.27	0.76	1.76	0.34
P_2O_5	0.08	0.69	0.00	0.10	0.00	0.00	0.92	0.00
MnO	0.27	0.22	0.15	0.10	0.21	0.15	0.28	0.20
S	0.01	0.04	0.01	0.02	0.09	0.01	[illegible]	0.00
(ppm)								
Ba	89	64	227	120	80	112	33	63
Cr	214	169	401	203	280	275	31	491
Zr	12	49	102	75	81	35	66	74
Sr	192	297	304	180	313	292	279	345
Rb	0	5	24	0	21	7	9	12
Y	17	45	25	21	12	20	53	8
Nb	1	0	0	0	0	0	9	0
Zn	97	94	92	66	82	92	231	46
Ni	77	51	145	34	88	171	0	102
Total	96.16	97.67	95.19	82.18	97.38	96.58	99.02	95.30

Sample Number	CG-81-197	CG-81-222	CG-81-229	CG-81-263	CG-81-307	CG-81-320	CG-81-343
Rock Unit	Unit 3	Unit 3	Unit 3	Unit 3	Unit 3	Unit 3	Unit 3
(wt.%)							
SiO_2	46.02	45.19	50.83	48.51	44.24	46.57	40.31
Al_2O_3	14.62	18.30	20.48	21.26	18.60	17.06	14.23
Fe_2O_3T	12.32	9.35	6.72	8.44	12.21	8.20	19.68
MgO	8.17	10.51	3.30	4.05	5.78	9.83	9.12
CaO	10.88	10.27	10.53	9.88	11.24	13.11	6.46
Na_2O	2.62	2.25	3.75	3.97	2.50	1.26	1.34
K_2O	0.18	0.08	0.63	0.21	0.21	0.24	1.20
TiO_2	1.22	0.61	1.07	0.84	1.77	0.34	1.75
P_2O_5	0.00	0.00	0.00	0.00	0.00	0.00	1.01
MnO	0.20	0.13	0.12	0.11	0.17	0.14	0.32
S	0.04	0.02	0.00	0.01	0.02	0.03	0.05
(ppm)							
Ba	21	57	56	65	0	81	401
Cr	347	313	36	205	288	343	356
Zr	7	13	3	0	0	1	23
Sr	302	335	475	414	378	323	164
Rb	0	0	1	0	1	4	18
Y	12	12	9	7	8	12	28
Nb	0	1	0	0	0	0	0
Zn	71	64	31	48	51	49	94
Ni	91	167	13	34	81	110	169
Total	96.37	96.83	97.50	97.39	96.85	96.91	95.62

APPENDIX A.1 ...concluded.

APPENDIX A.2 X-Ray fluoresence analyses of shear zone and gabbro (unsheared) samples used to calculate elemental gains and losses due to shearing and quartz vein emplacement.

Shear Zone Outcrop CG-81-4							Shear Zone Outcrop CG-81-33				
Sample No.	419	420	421	422	423 *		434	432	431	429	
Metres from qtz. vein	.05	.3	.5	1	2		.05	.8	1.3	1.9	
SiO_2 (wt.%)	43.41	48.15	48.28	47.09	43.78		49.94	53.01	44.69	45.75	
Al_2O_3	14.35	15.55	15.74	16.64	15.45		21.54	16.82	14.99	17.01	
Fe_2O_3T	11.20	10.83	11.21	11.33	11.41		8.03	4.94	8.32	9.86	
MgO	6.01	6.78	8.17	7.36	7.22		3.79	2.52	5.26	7.56	
CaO	7.13	5.02	2.98	4.12	9.56		1.53	5.37	8.64	5.08	
Na_2O	3.95	4.30	3.76	4.01	2.55		3.93	6.87	2.19	4.28	
K_2O	0.36	0.17	0.14	0.57	0.41		3.86	1.49	3.22	0.94	
TiO_2	3.19	1.03	1.36	1.34	1.25		1.14	0.47	0.47	0.49	
P_2O_5	0.00	0.07	0.12	0.69	0.00		0.11	0.04	0.00	0.00	
MnO	0.21	0.13	0.14	0.13	0.18		0.13	0.14	0.17	0.13	
S	0.03	0.03	0.01	0.02	0.01		0.07	0.05	0.03	0.01	
(ppm)											
Ba	66	83	30	369	160		3288	1194	2054	480	
Cr	60	245	211	148	234		367	53	272	317	
Zr	50	38	47	35	25		43	63	14	13	
Sr	125	96	56	181	278		100	218	187	73	
Rb	7	4	0	12	6		64	23	54	11	
Y	20	16	13	28	18		10	16	16	12	
Nb	1	0	0	0	0		1	0	0	0	
Zn	79	91	104	101	97		62	45	63	78	
Ni	36	95	114	60	123		64	30	59	180	
Total	89.80	92.14	91.99	93.42	91.97		94.52	91.91	88.29	91.27	
Spec. Grav.	2.42	2.76	2.61	2.67	2.90		2.55	2.54	2.84	2.67	

* Unsheared gabbro

Shear Zone Outcrop CG-81-33 ..con't					Shear Zone Outcrop CG-81-37			
Sample No.	428	426	425	424 *	409	410	411	36 *
Metres from qtz. vein	2.4	4.7	5.3	10	.05	.4	2	10
(wt.%)								
SiO_2	49.36	46.05	44.56	48.81	34.45	43.64	40.41	40.60
Al_2O_3	19.20	16.36	15.58	15.91	7.56	12.45	11.24	12.95
Fe_2O_3T	12.44	10.54	10.97	10.05	16.41	12.46	20.06	18.34
MgO	6.63	6.00	6.21	6.95	3.14	6.20	3.38	5.04
CaO	0.43	6.39	7.78	12.18	11.46	9.06	8.84	11.98
Na_2O	5.37	3.72	3.78	2.29	4.10	2.97	2.76	2.87
K_2O	0.33	0.76	0.19	0.11	0.08	0.49	0.03	0.23
TiO_2	0.63	0.89	0.94	0.81	2.78	1.51	3.35	4.42
P_2O_5	0.08	0.00	0.00	0.00	2.21	0.05	2.09	3.02
MnO	0.08	0.11	0.12	0.17	0.42	0.24	0.40	0.31
S	0.00	0.02	0.01	0.01	0.10	0.01	0.02	0.03
(ppm)								
Ba	78	498	97	26	0	314	0	0
Cr	125	180	195	227	59	156	31	40
Zr	29	28	26	29	10	77	9	23
Sr	95	124	137	338	657	284	216	332
Rb	0	8	0	0	1	15	0	0
Y	11	16	15	17	31	30	29	40
Nb	0	2	0	0	0	0	0	0
Zn	85	94	71	58	50	135	113	86
Ni	44	29	38	106	10	29	0	0
Total	94.61	90.97	90.21	97.40	82.81	89.23	92.36	99.86
Spec. Grav.	2.57	2.74	2.77	3.06	3.12	2.76	2.90	3.15

* Unsheared gabbro

APPENDIX A.2 ...continued

Shear zone Outcrop CG-81-52							Shear zone Outcrop CG-81-293			
Sample No.	442	443	444	445	446	51 *	461	462	463	464
Metres from qtz. vein	.05	.2	.4	1.3	2.5	45	.05	.1	.3	.6
(wt.%)										
SiO_2	39.50	42.34	35.57	42.54	45.99	48.10	36.79	35.58	44.13	44.36
Al_2O_3	8.02	9.25	9.98	13.37	10.95	15.36	22.27	18.79	15.14	18.03
Fe_2O_3T	10.45	10.23	6.77	6.39	11.07	16.71	18.77	9.49	14.91	14.81
MgO	8.38	7.74	7.67	4.99	8.79	1.52	12.49	8.74	14.37	12.54
CaO	12.07	10.09	13.33	9.92	5.74	6.14	0.09	9.60	2.39	1.03
Na_2O	0.22	0.29	0.18	1.27	0.51	5.19	0.68	0.99	0.08	0.89
K_2O	0.95	1.42	2.85	3.84	1.59	0.24	1.68	2.68	0.02	0.69
TiO_2	0.71	0.73	0.82	0.94	0.79	1.78	0.51	0.22	0.30	0.23
P_2O_5	0.33	0.38	0.76	0.89	0.77	0.52	0.01	0.00	0.00	0.01
MnO	0.23	0.19	0.27	0.20	0.17	0.31	0.12	0.16	0.14	0.13
S	0.00	0.00	0.00	0.01	0.02	0.02	0.00	0.00	0.00	0.00
(ppm)										
Ba	621	1007	1893	2707	836	155	716	1046	43	307
Cr	1011	784	740	395	663	26	300	90	401	120
Zr	131	144	158	187	199	19	0	0	0	0
Sr	290	262	391	308	194	302	19	67	10	20
Rb	12	16	41	62	34	0	27	48	0	8
Y	21	25	28	29	28	32	6	7	7	7
Nb	3	2	1	6	4	0	0	1	0	0
Zn	66	59	15	19	69	89	90	35	62	58
Ni	288	356	146	74	314	0	259	130	287	305
Total	81.15	83.00	78.62	84.82	86.68	95.97	93.59	86.41	91.58	92.81
Spec. Grav.	2.73	2.76	2.82	2.76	2.82	2.80	2.68	2.53	2.66	2.70

* Unsheared gabbro

Shear Zone Outcrop CG-81-293 ..con't					Shear Zone Outcrop CG-81-258					
Sample No.	465	466	467	292 *	448	449	450	451	452	453
Metres from qtz. vein	1	1.3	2.3	10	.05	.1	.2	.6	1.6	2.2
(wt.%)										
SiO_2	41.85	42.62	41.30	45.94	57.72	55.14	41.91	40.92	45.91	44.19
Al_2O_3	15.86	17.67	16.05	16.46	13.74	12.77	14.85	12.90	12.27	12.18
Fe_2O_3T	9.01	8.83	7.72	10.78	8.38	6.54	12.01	13.61	13.46	12.09
MgO	8.45	8.26	7.40	9.08	1.29	2.02	4.64	4.99	4.90	5.34
CaO	7.98	5.44	7.50	10.80	4.37	6.48	7.64	7.92	6.69	10.41
Na_2O	1.48	3.99	3.36	2.42	2.06	2.10	0.91	2.90	3.49	2.32
K_2O	1.41	0.54	1.03	0.12	2.40	2.45	2.90	1.10	0.12	0.07
TiO_2	0.35	0.32	0.28	0.93	1.20	1.20	1.24	2.21	1.84	1.05
P_2O_5	0.00	0.00	0.00	0.00	0.00	0.00	0.00	0.00	0.00	0.00
MnO	0.14	0.10	0.11	0.16	0.16	0.15	0.21	0.20	0.24	0.18
S	0.00	0.01	0.00	0.02	0.01	0.00	0.00	0.00	0.02	0.00
(ppm)										
Ba	603	204	402	14	671	678	786	191	0	33
Cr	327	92	220	183	132	101	156	155	58	53
Zr	0	0	0	6	58	60	7	26	23	8
Sr	88	259	164	349	102	132	146	161	140	200
Rb	23	8	16	0	41	38	45	13	0	0
Y	9	8	8	10	11	16	14	17	11	16
Nb	0	0	0	0	1	3	0	0	0	0
Zn	48	705	150	62	16	3	45	52	46	90
Ni	120	149	95	111	38	31	42	20	26	0
Total	86.69	87.94	84.87	96.80	91.46	88.97	86.46	86.84	88.98	87.87
Spec. Grav.	2.65	2.72	2.72	3.01	2.59	2.72	2.80	2.86	2.76	2.74

* Unsheared gabbro

Shear Zone Outcrop CG-81-258 ..con't

Sample No.	454	455	456	458 *
Metres from qtz. vein	2.7	3	3.3	3.6
SiO_2 (wt.%)	40.70	49.23	46.96	43.16
Al_2O_3	19.08	15.98	14.49	16.20
Fe_2O_3T	19.81	15.61	15.83	17.96
MgO	3.25	7.14	6.92	5.28
CaO	2.76	1.55	2.72	9.16
Na_2O	4.53	2.90	2.15	2.79
K_2O	1.42	0.19	0.49	0.22
TiO_2	4.21	1.98	2.22	2.75
P_2O_5	0.00	0.05	0.06	0.00
MnO	0.13	0.14	0.14	0.26
S	0.00	0.01	0.02	0.02
(ppm)				
Ba	940	17	32	0
Cr	110	264	240	62
Zr	4	7	6	7
Sr	321	196	150	293
Rb	12	8	23	0
Y	4	9	9	11
Nb	0	0	1	0
Zn	84	130	124	80
Ni	19	49	16	31
Total	96.06	94.87	92.09	97.86
Spec. Grav.	3.03	2.61	2.72	3.11

* Unsheared gabbro

Sample Number		Belmont Fe	CG-81-79	CG-81-89
Rock Unit		Unit 1	Unit 1	Unit 1
SiO_2	(wt.%)	0.08	2.22	4.86
Al_2O_3		2.16	4.52	3.60
Fe_2O_3T		86.88	76.16	55.40
MgO		0.40	2.56	7.40
CaO		6.32	4.44	1.28
Na_2O		1.24	0.92	1.76
K_2O		0.52	0.24	0.28
TiO_2		0.20	0.28	5.76
P_2O_5		0.00	0.88	0.16
MnO		0.12	0.56	0.48
S		0.04	0.08	0.16
Ba	(ppm)	262	344	60
Cr		124	108	132
Zr		204	220	204
Sr		172	116	88
Rb		0	0	0
Y		32	36	28
Nb		24	12	16
Zn		144	476	204
Ni		28	0	96
Total		98.10	99.73	95.92

APPENDIX A.3 X-Ray fluoresence analyses of iron ore samples from the Belmont Iron Deposit and two small pits near the eastern contact of the Cordova Gabbro.

APPENDIX A.4 Atomic absorption and optical emission analyses for trace metals in quartz samples.

Sample Number	Shear Zone Outcrop No.	As	Au	B	Ba	Co	Cr	Cu	Hg	Li	Ni	Pb	Sb	Zn	Mo	W
400	CG-81-15	20	-2	2700	60	-5	10	-5	-20	8	-5	-10	2	9	-3	-50
408	CG-81-37	40	2450	46	50	23	6	745	-20	3	23	-10	2	250	-3	-50
412	CG-81-37	-10	-2	240	70	-5	5	-5	-20	-3	-5	-10	-1	-5	-3	-50
415	CG-81-4	20	16	39	60	-5	-5	-5	-20	-3	-5	-10	1	5	-3	-50
416	CG-81-4	30	-2	24	40	-5	-5	-5	-20	-3	-5	-10	2	6	-3	-50
417	CG-81-4	60	14	22	40	20	-5	52	-20	-3	55	-10	3	32	-3	-50
44b	CG-81-44	-10	-2	2800	30	-5	-5	-5	-20	-3	-5	-10	-1	-5	-3	-50
65b	CG-81-65	20	-2	260	80	-5	13	5	-20	-3	15	-10	1	8	-3	-50
54b	CG-81-54	10	-2	540	60	-5	8	-5	-20	-3	-5	-10	1	6	-3	-50
43b	CG-81-43	30	-2	45	430	-5	27	-5	-20	-3	5	-10	1	7	-3	-50
435	CG-81-33	20	-2	20	80	-5	-5	7	-20	-3	6	-10	1	7	-3	-50
436	CG-81-33	30	-2	19	220	-5	30	6	-20	-3	8	-10	1	18	-3	-50
437	CG-81-33	30	-2	16	110	-5	14	-5	-20	-3	-5	-10	1	9	-3	-50
438	CG-81-33	40	-2	16	80	-5	-5	-5	-20	-3	-5	-10	1	6	-3	-50
439	CG-81-52	20	-2	115	80	-5	29	6	-20	-3	23	-10	1	6	-3	-50
440	CG-81-52	120	-2	30	50	-5	-5	-5	-20	-3	-5	-10	2	-5	-3	-50
441	CG-81-52	20	-2	220	70	-5	10	5	-20	-3	13	-10	1	5	-3	-50
447	CG-81-258	60	-2	280	70	10	9	44	-20	-3	26	-10	2	10	-3	-50
459	CG-81-293	40	-2	21	30	-5	-5	-5	-20	-3	-5	-10	2	5	-3	-50
234b	CG-81-234	20	-2	18	30	-5	-5	-5	-20	-3	-5	-10	-1	-5	-3	-50
244	CG-81-244	20	-2	47	100	-5	-5	-5	-20	-3	-5	-10	1	5	-3	-50
Values in -		pptm	ppb	ppm	ppm	ppm	ppm	ppm	ppb	ppm	ppm	ppm	pptm	ppm	ppm	ppm
Method* -		A	A	E	A	A	A	A	A	E	A	A	A	A	A	E

Neg. values = below detection limit. *A = atomic absorption, E = optical emission

APPENDIX A.5 Microprobe analyses of amphibole, plagioclase and chlorite in rock samples from the Cordova Gabbro.

Sample Number	CG-81-343		CG-81-343		CG-81-162		CG-81-162	
Rock Unit	Unit 3		Unit 3		Unit 2		Unit 2	
Mineral	amphibole (rim)		amphibole (core)		amphibole (rim)		amphibole (core)	
	moles	ox. wt%	moles	ox. wt%	moles	ox. wt%	moles	ox. wt%
Fe	1.89	15.17	1.66	13.97	1.46	12.17	1.28	10.54
Mg	2.64	11.85	3.56	16.77	3.54	16.50	3.89	17.88
Mn	.04	.37	.04	.35	.03	.29	.04	.40
Si	6.40	42.82	7.68	53.91	7.28	50.55	7.66	52.48
Ti	.26	2.31	.02	.26	.01	.09	.02	.23
Al	1.94	11.04	.21	1.30	.89	5.30	.25	1.49
Ca	1.88	11.76	1.95	12.79	1.94	12.61	1.95	12.46
Na	.38	1.34	.04	.18	.15	.54	.09	.32
K	.16	.86	.00	.01	.01	.08	.00	.02
Cl	.10	.40	.00	.02	.00	.04	.02	.08
F	.01	.03	.10	.24	.02	.05	.04	.10
Total	23.00	97.95	23.00	99.79	23.00	98.20	23.00	96.02

APPENDIX A.5 ...concluded.

Sample Number	CG-81-30		CG-81-30		CG-81-343		CG-81-162		CG-81-162	
Rock Unit	Unit 1		Unit 1		Unit 3		Unit 2		Unit 2	
Mineral	amphibole (rim)		amphibole (core)		chlorite		plagioclase		plagioclase	
	moles	ox. wt%	moles	ox. wt%	moles	ox.wt%	moles	ox.wt%	moles	ox.wt%
Fe	1.60	13.38	2.32	18.42	3.80	25.92				
Mg	3.40	15.86	2.16	9.63	4.13	15.92				
Mn	.04	.34	.05	.41	.05	.39				
Si	7.81	54.36	6.60	43.78	4.37	24.97	9.60	52.79	9.89	54.30
Ti	.00	.01	.34	3.05	.02	.19				
Al	.16	.97	1.60	9.05	4.12	19.94	6.32	29.52	6.00	27.96
Ca	2.01	13.06	1.91	11.87	.00	.04	2.54	13.06	2.34	12.03
Na	.09	.32	.36	1.24	.02	.07	1.51	4.29	1.69	4.79
K	.00	.05	.11	.61	.00	.02	.01	.07	.00	.02
Cl	.00	.02	.07	.29	.01	.03				
F	.00	.00	.00	.00	.03	.07				
Total	23.00	98.36	23.00	98.35	23.00	87.48	32.00	99.73	32.00	99.10

Appendix B

APPARATUS, SAMPLE PREPARATION AND PROCEDURE FOR FLUID INCLUSION STUDY

B.1 APPARATUS

Fluid inclusion studies for this thesis were carried out using a Linkam TH 600 programable heating-cooling stage. The apparatus basically consists of a disc shaped chamber in which a sample rests upon a silver plated thermal block. Other important features include a platinum resistance thermocouple, a heating element within the thermal block, and intake and exhaust ports to allow passage of: water to cool the chamber walls, cold nitrogen gas to cool the sample, and dry nitrogen gas to flush the interior of the chamber. The bottom and top of the chamber and the thermal block have windows to permit light to pass through the cell and the sample. The entire assembly fits on a standard microscope stage.

Heating and cooling rates within the sample chamber are controlled by a programmable apparatus wired to it. This apparatus provides a continuous digital readout of the thermal block temperature.

Other materials required are dry nitrogen gas and liquid nitrogen. The design of this stage and its operation are described by Shepard (1981).

B.2 SAMPLE PREPARATION

Of prime importance when choosing a sample for fluid inclusion study is that there is neither too few or too many inclusions. The common milky appearance of quartz is due to an extremely high density of fluid inclusions. Usually the density is too high allow easy observation of single inclusions. For this reason the most clear quartz present was chosen for this study, in hopes of seeing plentiful yet isolated inclusions.

Quartz samples chosen were slabbed and doubly polished to a thickness of about 100 microns, about 3 to 4 times the normal thickness of a thin section. It is desirable to have the slab thin enough to transmit light easily but thick enough to have inclusions intact on several levels.

B.3 PROCEDURE

B.3.1 Calibration

Prior to experimental use calibration of the heating-cooling stage is necessary. A good description of the calibration of this type of apparatus including standards used, rates of heating and cooling, and construction of calibration curves is given in Macdonald and Spooner (1981). Their methods were followed and 15 of the recommended standards for calibration were used. The deviation of the standards from their expected temperature of melting can be seen in Table B.1.

Table B.1

Standards used for calibration of the Lingham TH 600.

	Expected Melting Temperature (C)	Observed Melting Temperature (C)	Temperature Difference
chloroform	-63.5	-61.1	2.4
chlorobenzene	-45	-43.1	1.9
toluene	-25	-22.7	2.3
carbon tetrachloride	-22.8	-20.8	2.0
distilled water	0	2.0	2.0
Signothem Std. 70	70	71.8	1.8
napthalene	80.25	82.0	2.0
Signothem Std. 100	100	101.3	1.3
adipic acid	151.4	154.5	3.1
Signothem Std. 200	200	198.	-2.0
Signothem Std. 247	247	249.	2
sodium nitrate	306.8	305	-2
Signothem Std. 398	398	400	2
potassium dicromate	398	400	2

Using these values a calibration curve was constructed (Figure B.1). Use of the curve allows corrections to the observed temperatures to be quickly made.

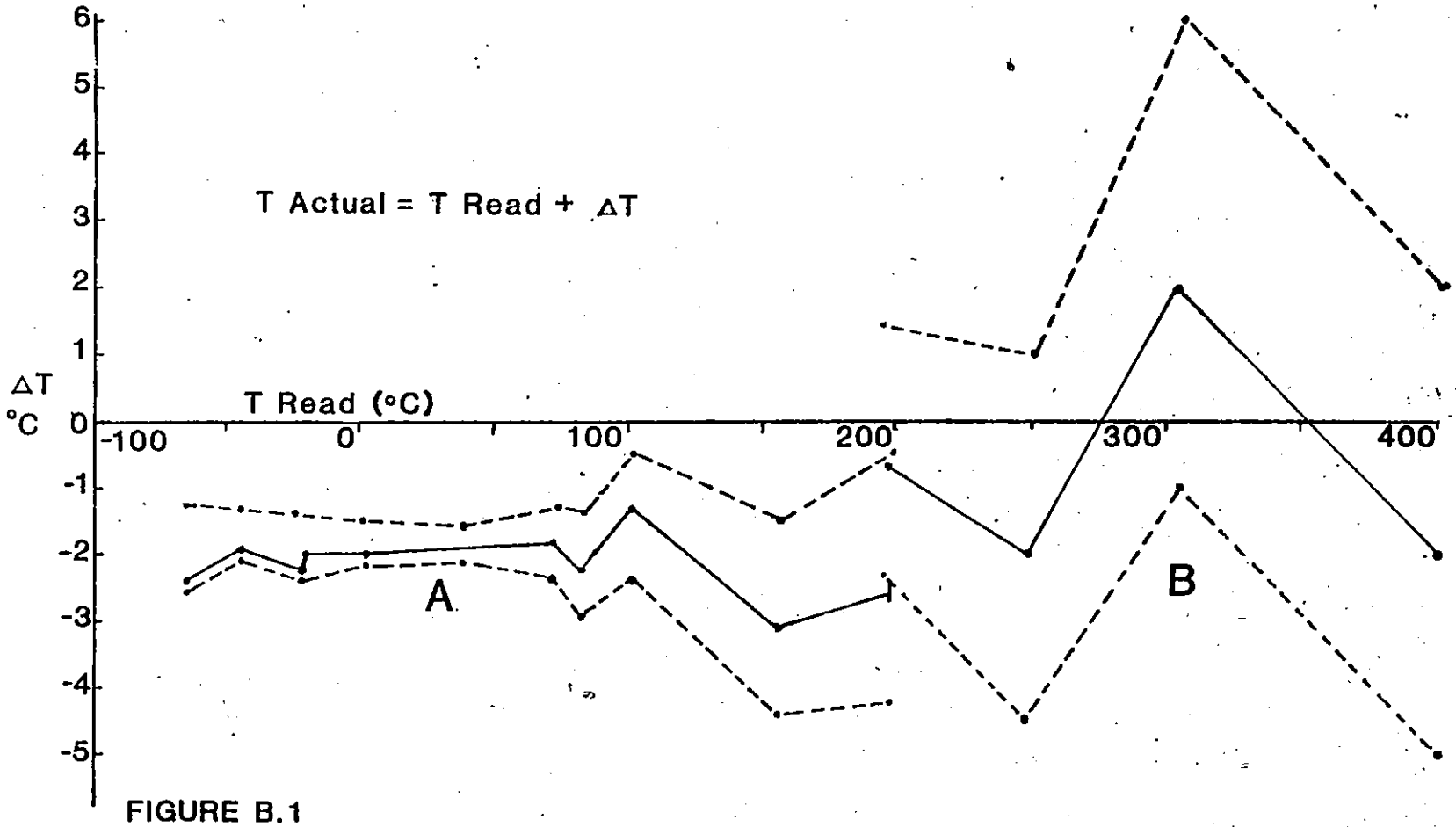

FIGURE B.1

Calibration curve for the Lingham TH-600 heating-cooling stage used in this study. Dashed lines enclose an uncertainty envelope constructed using data from MacDonald and Spooner (1981). Curve A represents the low temperature setting (-90°to 200° C). Curve B represents the high temperature setting (198°to 600°C).

Time constraints did not allow detailed tests for reproducibility of data to be made. Average reproducibilities of measurements by Macdonald and Spooner (1981), have been added to the calibration curve to represent a minimum limit of reproducibility for the results of this study.

B.3.2 Technique

Before heating and cooling experiments can be undertaken a suitable group of inclusions must be located in the sample. To do this, a small (3x3 mm) chip of the sample is broken off and placed on the thermal block of the chamber. Suitable inclusions can usually be found by moving the slab about with a pencil point or toothpick while observing it through the microscope.

Care must be taken to centre inclusions of interest under the cross hairs or slightly to the viewers left of them. This placement is necessary because during cooling experiments the thermal block tends to move to the viewers right, often causing the inclusion to leave the field of view. The movement is thought to be due to contraction of the metal tubes supporting the thermal block.

When a suitable inclusion has been located and centred the chamber is sealed. For this study the normal procedure was to cool the sample until all the liquid phases were frozen and then increase the temperature slowly and observe the phase changes.

When cooling the inclusions the rate was not considered critical, 25 to 30 degrees C per minute was used. During the warming the heating rate must be much slower. Generally the inclusions were warmed at a rate of about 10 degrees per minute until the temperature was within 5 degrees of the expected phase change temperature. At this point the temperature was held for 5 minutes to allow equilibration within the chamber. A rate of .5 degrees per minute was then set until the phase change was observed.

REFERENCES

Abbey, S., 1977, Studies in standard samples for use in the general analysis of silicate rocks and minerals. Geological Survey of Canada Paper 77-34.

Babcock, R.S., 1973, Computerized models of metasomatic processes. Lithos, vol. 6, pp. 279-290.

Bartlett, J.R., 1983, Stratigraphy, physical volcanology and geochemistry of the Belmont Lake Metavolcanic Complex, Southern Ontario. Unpublished MSc thesis, Department of Geology, Carleton University, Ottawa.

Bartlett, J.R., and Moore, J.M., Jr., 1983 Precambrian geology of Marmora Township, southern part, Hastings County. Ontario Geological Survey Map P. 2613, Geol. series preliminary map, scale 1:15,840, Geology 1981.

Bartlett, J.R., Moore, J.M., Jr. and Murray, M.J., 1982 Precambrian geology of Belmont and southern Meuthen Township, Southern Ontario. O.G.S. Preliminary Map P. 2488. Geol. Series, scale 1:15,840, Geology 1980.

Bell, L.V., and Bell, A. M., 1935, Structural features of gold deposits in certain intrusives of Western Quebec Economic Geology, vol. 30, pp.347-369.

Bell, K., 1981, Will the real Grenville orogeny please stand up? Nature, vol 290, pg. 89

Berthe', D., Choukroune, P. and Jegouzo, P., 1979, Orthogneiss, mylonite and non-coaxial deformation of granites: the example of the South Armorican shear zone. Journal of Structural Geology, vol. 1, pp. 31-41.

Boyle, R.W., 1969, Hydrothermal transport and deposition of gold (a discussion). Economic Geology, vol. 64, pp. 112-115.

Boyle, R.W., 1979, The geochemistry of gold and its deposits. Geological Survey of Canada Bulletin No. 280, 584 pages.

Brown, P.H., and Thivierge, R.H., 1976a, Notes on the Tudor Gabbro. Unpublished report - Atomic Energy of Canada Ltd.

Brown, P.H., and Thivierge, R.H., 1976b Notes on the Lingham Lake Complex Unpublished report - Atomic Energy of Canada Limited.

Burruss, R.C., 1981, Analysis of fluid inclusions: Phase equilibra at constant volume. American Journal of Science, vol. 281, pp. 1104-1126.

Carmichael, D.M., Moore, J.M., Jr. and Skippen, G.B., 1978, Isograds around the Hastings Metamorphic Low. 'Toronto 78' Field trips guidebook, ed. A.L. Currie and W.O. Mackasey. Joint Annual Meeting G.S.A.-G.A.C.-M.A.C., Toronto 1978.

Carter, T.R., 1980, Metallic mineral deposits of the Grenville Province Southern Ontario. pp. 169-174 in Summary of Field Work, 1980 by the Ontario Geological Survey, ed. V.G. Milne, O.L. White, R.B. Barlow, J.A. Robertson and A.C. Colvine, O.G.S. Miscellaneous paper 96, 201p.

Collins, P.L.F., 1979, Gas hydrates in CO2 bearing fluid inclusions and the use of freezing data for estimation of salinity. Economic Geology, vol. 74, pp. 1435-1444.

Cox, K.G., Bell, J.D. and Pankhurst, R.J., 1979, The intrepretation of igneous rocks. George Allen and Unwin Ltd. London.

Davidson, A., Britton, J.M., Bell, K., and Blinkinsop, J., 1969 Regional synthesis of the Grenville Province of Ontario and Western Quebec. Current Research, Geological Survey of Canada Paper 79-1b.

Deer, W.A., Howie, R.A. and Zussman, J., 1979, An introduction to the rock forming minerals. Longman Group Ltd., London.

De Jongh, W.K., 1973, XRF analysis applying theoretical matrix correction, (Stainless). X-Ray Spectrometry, vol. 2, pp. 151-158.

Dunlop, D.J., York, D., Berger, G.W., Buchan, K.C. and Stirling J.R., 1980, The Grenville Province, a paleomagnetic case study of Precambrian continental drift. In; The Continental Crust and its Mineral Deposits, ed. D.W. Strangway, Geological Association of Canada Special Paper No. 20, pp. 487-502.

Freeman, E.B., ed., 1979, Geological highway map of southern Ontario. Ontario Geological Survey Map No. 2241.

Fyfe, W.S. and Henley, R.W., 1973, Some thoughts on chemical transport processes with particular reference to gold. Minerals Science and Engineering, vol. 5, p. 295.

Gresens, R.I., 1967, Composition-volume relationships of metasomatism. Chemical Geology, vol. 2, pp. 47-65.

Helgeson, H.C. and Garrels, R.M., 1968, Hydrothermal transport and deposition of gold. Economic Geology, vol. 63, pp. 622-635.

Hewitt, D.F. and Satterly, J., 1957, Haliburton-Bancroft Area. Ontario Dept. of Mines Map 1957b, scale 1:126,720.

Haas, J.L., Jr., 1971, The effect of salinity on the maximun thermal gradient of a hydrothermal system at hydrostatic pressure. Economic Geology, vol. 66, pp. 940-946.

Irvine, T.N. and Baragar, W.R.A., 1971, A guide to chemical classification of the common volcanic rocks. Canadian Journal of Earth Science, vol. 8, p.523.

Jaffey, A.H., Flynn, K.F., Glendenin, L.E., Bently, W.C., and Essling, A.M., 1971 Precision measurement of half lives and specific activities of U 235 and U 238 Physical Reviews, Series C, vol. 4, pp.1889-1906.

Kerr, P.F., 1977, Optical Mineralogy, McGraw-Hill, New York.

Laakso, R.K., 1968, Geology of Lake Township, Hastings County. Ontario Dept. of Mines Report 54, 36 p.

Leake, B.E., 1978, Nomenclature of amphiboles. Canadian Mineralogist, vol. 16, pp. 501-520.

Lopez-Martinez, M., and York, D., 1983, Further thermochronometric unravelling of the age and paleomagnetic record of the southwest Grenville Province. Canadian Journal of Earth Sciences, vol. 20, pp. 953-960.

Lumbers, S.B., 1964, Preliminary report on the relationship of mineral deposits to intrusive rocks and metamorphism in part of the Grenville Province of southeastern Ontario. Ontario Dept. of Mines Report 1964-4.

Lumbers, S.B., 1967, Stratigraphy, plutonism and metamorphism in the Ottawa River Remnant in the Bancroft-Madoc area of the Grenville Province of southeastern Ontario, Canada. Unpublished PhD. thesis, Dept. of Geology, Princeton University.

Lumbers, S.B., 1969, Geology of Limerick and Tudor Townships. Ontario Dept. of Mines Report 67, 110 p.

MacDonald, A.J. and Spooner E.T.C., 1981, Calibration of a Lingham Th 600 programmable heating-cooling stage for microthermometric examination of fluid inclusions. Scentific Communications, vol. 76, pp. 1248-1258.

McBirney A.R. and Noyes B., 1979, Crystallization and layering of the Skaergaard Intrusion. Journal of Petrology , vol. 20, pp. 487-554.

Miyashiro, A., 1973, Metamorphism and Metamorphic Belts. George, Allen and Unwin, London.

Miller, W.G., and Knight, C.W., 1914, Belmont Lake Sheet, Map 22a. accompanies Report of the Canadian Bureau of Mines, vol 22, Part 2. scale 1: 15,840.

Moore, J.M., Jr., and Thompson, P.H., 1972, The Flinton group, Grenville Province, Eastern Ontario. 24th Internation Geological Congress Montreal P.Q., Proceedinds of Section 1.

Moore, J.M., Jr., and Thompson, P.H., 1980, The Flinton group, a late Precambrian succession in the Grenville Province of eastern Canada. Canadian Journal of Earth Science, vol. 17, pp. 1685-1707.

Nockolds, S.R., 1954, Average chemical compositions of some igneous rocks. Bulletin of the United States Geological Survey, vol. 65, pp.1007-1032.

Potter, R.W., Chynne, M.A. and Brown, D.L., 1978, Freezing point depression of aqueous sodium chloride solutions. Economic Geology, vol. 73, pp. 284-285.

Rivers, T., 1976, Textures and structures of metamorphic rocks, Ompah area Grenville Province Ontario. unpublished PhD. thesis, Department of Geology, University of Ottawa.

Roedder, E., 1965, Liquid CO2 inclusions in olivine bearing nodules and phenocrysts from basalts. American Mineralogist, vol. 50, pp. 1746-1786.

Roedder, E., 1972, The composition of fluid inclusions Chapter JJ, In; Data of Geochemistry, ed. M. Fleischer, 6th edition, United States Geological Survey Profesional Paper 440JJ, 164 p.

Roedder, E., 1979, Fluid inclusions as samples of ore fluids. In; Geochemistry of Hydrothermal Ore Deposits, pp. 684-737, ed. H.L.Barnes, Wiley, New York.

Roedder, E, and Bodnar, R.J., 1980, Geologic pressure determinations from fluid inclusion studies. Annual Review of Earth and Planitary Science Letters, vol. 8, pp. 263-301.

Roedder, E., and Coombs, D.S., 1967, Immiscibility in granitic melts, indicated by fluid inclusions in ejected granitic blocks from Ascention Island. Journal of Petrology, vol. 8, pp. 417-451.

Rucklidge, J. and Gasparini, E.L., 1969, Specifications of a computer program for processing electron microprobe analytical data, E.M.P.A.D.R. 7. Department of Geology, University of Toronto, Toronto, Ontario.

Seward, T.M., 1973, Thio-complexes of gold and the transport of gold in hydrothermal solutions. Geochimica et Cosmochimica Acta, vol. 37, pp. 370-390.

Shepherd, T., 1981, Temperature programmable, heating-freezing stage for microthermometric analysis of fluid inclusions. Economic Geology, vol. 76, pp. 1244-1247.

Silver, L.T. and Lumbers, S.B., 1966, Geochronologic studies in the Bancroft-Madoc area of the Grenville Province of Ontario, Canada, (abstract). Geological Society of America Special Publication Number 87 p. 156.

Sourirajan, S. and Kennedy, G.C., 1962, The system H2O-NaCl at elevated temperatures and pressures. American Journal of Science, vol. 260, pp. 115-141.

Springer, J.S., 1982, Gold and base metal vein deposits in Eastern Ontario: Structural inferences and the significance of vein mineralogy, pp. 210-217 in; Summary of Field Work 1982, by the Ontario Geological Survey, ed. J. Wood, O.L. White, R.B. Barlow and A.C. Colvine. O.G.S. Misc. Paper 106.

Takenouchi, S. and Kennedy, G.C., 1965, Carbon dioxide in NaCl solutions at high temperatures and pressures. American Journal of Science, vol.263, pp. 445-454.

Thomas, P.B. and Cherry, M.E., 1981, The geology of the Cordova Gabbro and its associated gold deposits. pp. 251-253 in; Summary of Field Work 1981, by the Ontario Geological Survey, ed. J. Wood, O.L. White, R.B. Barlow, and A.C. Colvine, O.G.S. Misc. Paper 100.

Tilling, R.I., Gottfried, D. and Rowe, J.J., 1973, Gold abundances in igneous rocks, bearing on gold mineralization. Economic Geology, vol. 68, pp. 168-186.

Touret, J., 1977 The significance of fluid inclusions in metamorphic rocks. In; Thermodynamics in Geology, ed. D.G. Fraser, Reidel Publishing Company, Dordrecht, Holland, pp. 203-227.

Wager, L.R., and Brown, G.M., 1967, Layered Igneous Rocks. Freeman, San Fransisco.

Weast, R.C. (ed), 1970, Handbook of Chemistry and Physics. Chemical Rubber Company Press Inc., Boca Raton, Florida.

Weissberg, B.G., 1970, Solubility of gold in hydrothermal alkaline sulphide solutions. Economic Geology, vol. 65, pp. 551-556.

Wilson, M.E., 1940, Geology of Marmora Township, Ontario. Geological Survey of Canada Map 560a, Scale 1: 63,360, Geology 1920-1925.

Wynne-Edwards, H.R., 1972, The Grenville Province. In; Variations in Tectonic Styles in Canada, eds. R.A. Price and R.J.W. Douglas, Geological Association of Canada Special Paper 11.

Appendix C

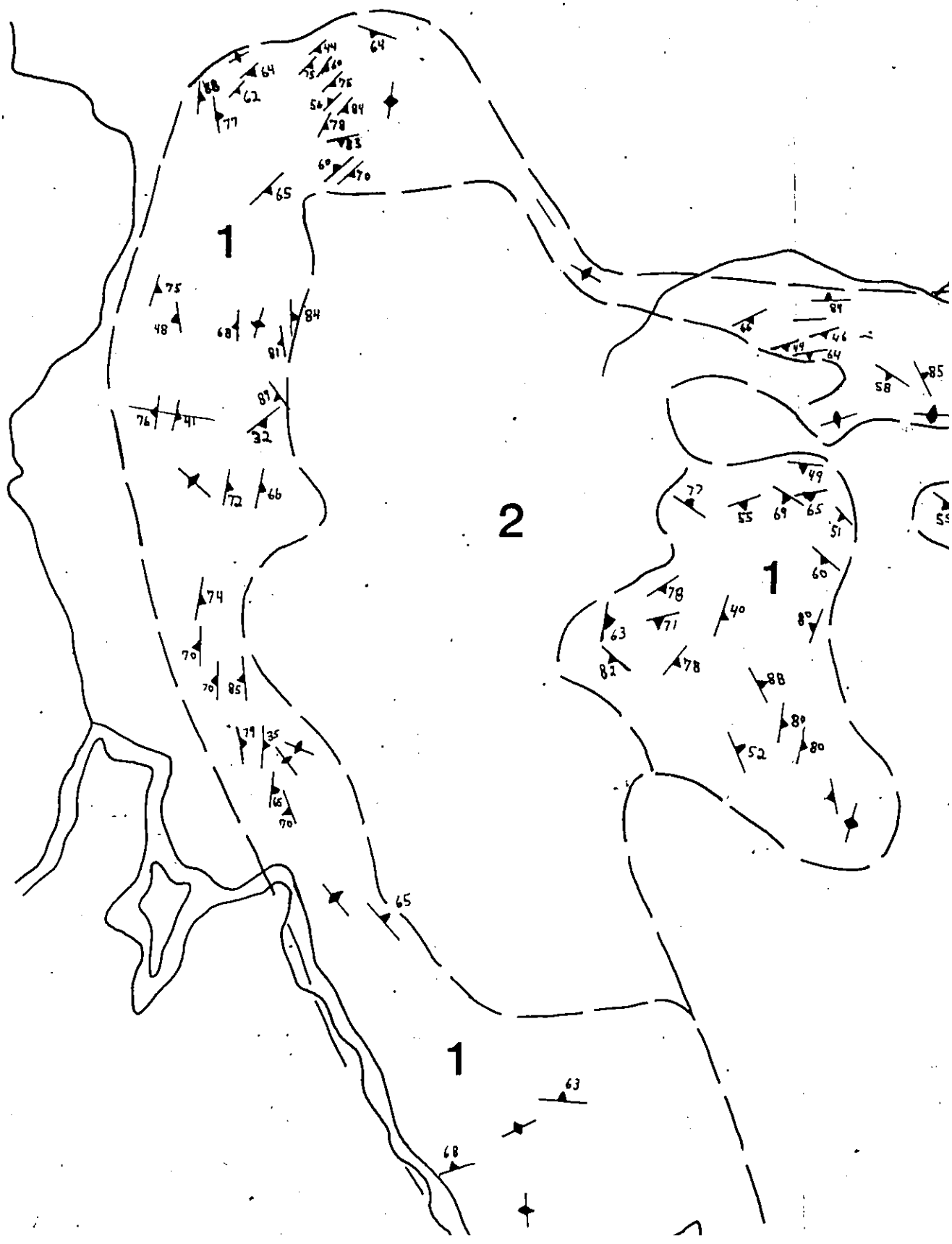

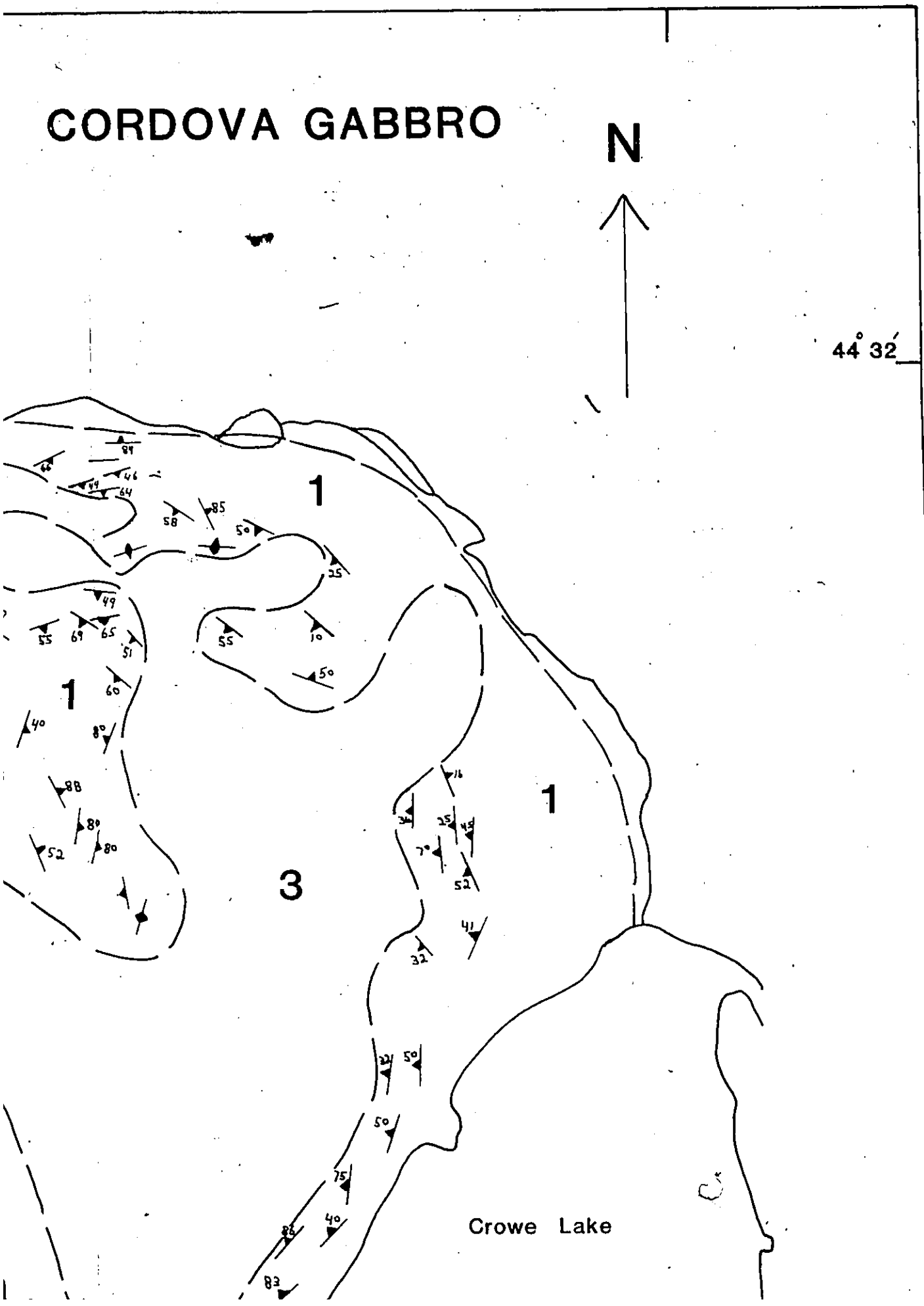
CORDOVA GABBRO
N
44° 32'
1
1
1
3
Crowe Lake

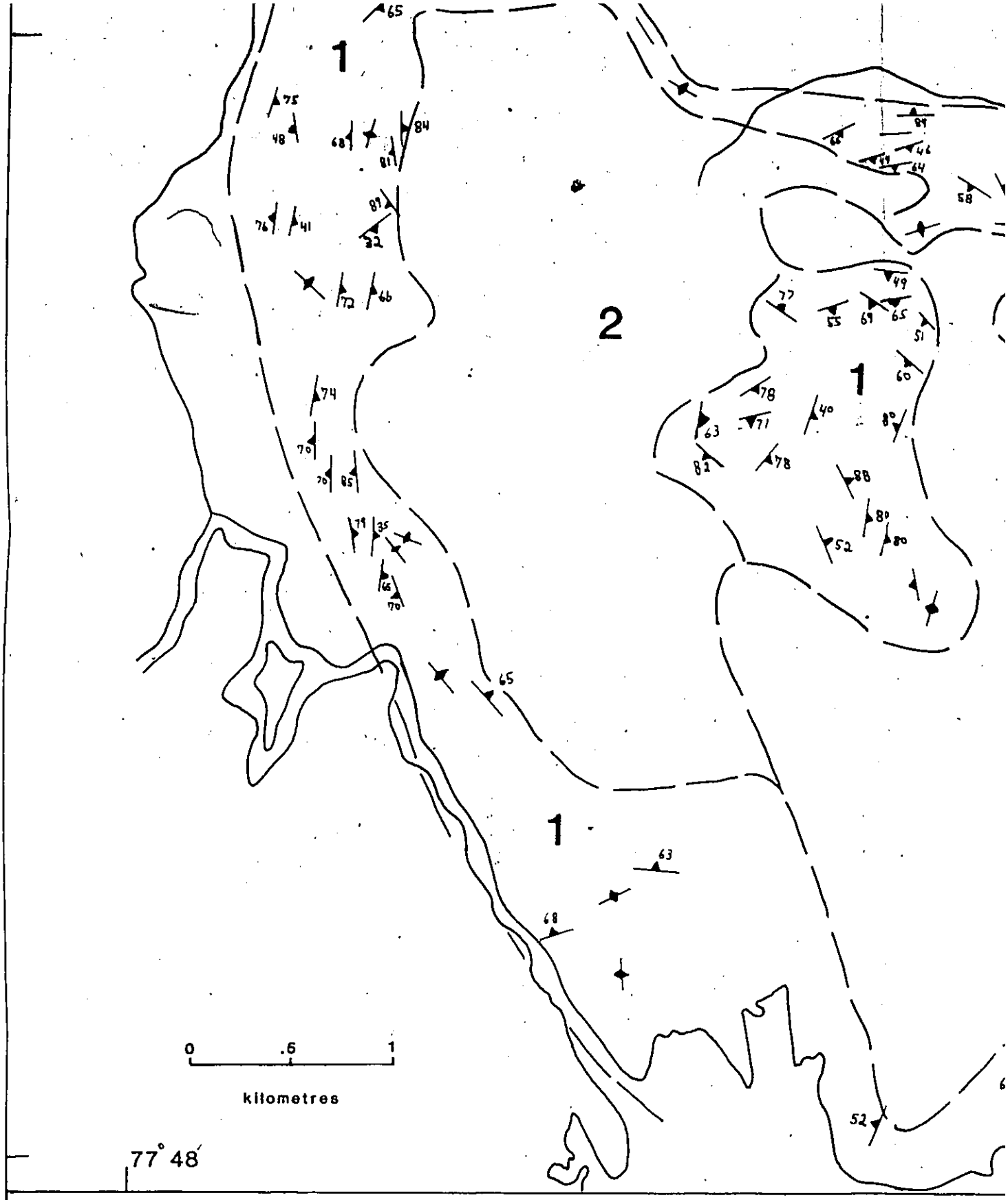

APPENDIX C

Orientation of primary layering in

Unit 1 – Medium Grained Layered Gabbro

1 Medium Grai

2 Fine Grained

3 Pegmatoid G

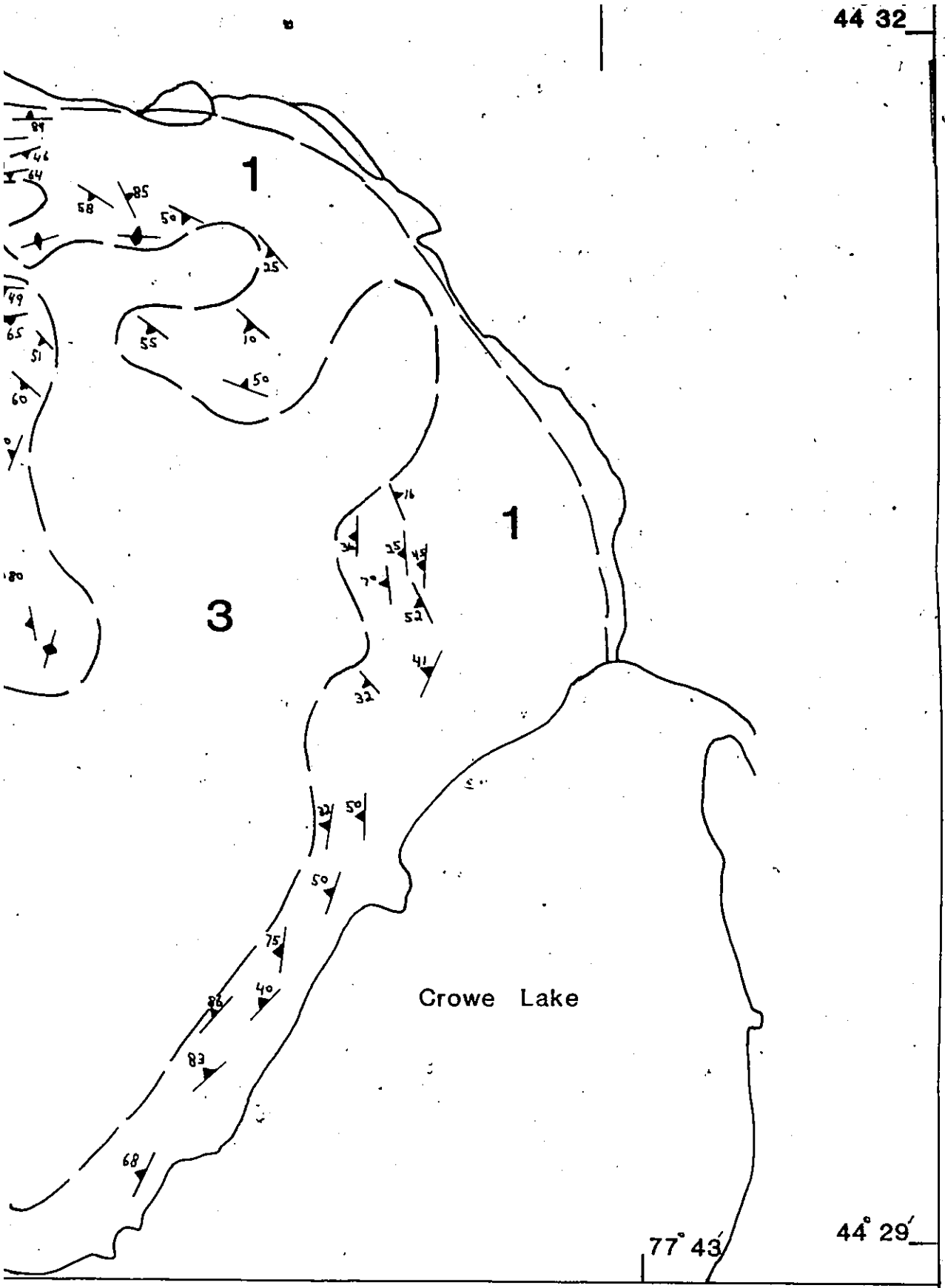

lium Grained Layered Gabbro

Grained Massive Gabbro

matoid Gabbro

60

Strike and dip of primary layering

Geologic boundary

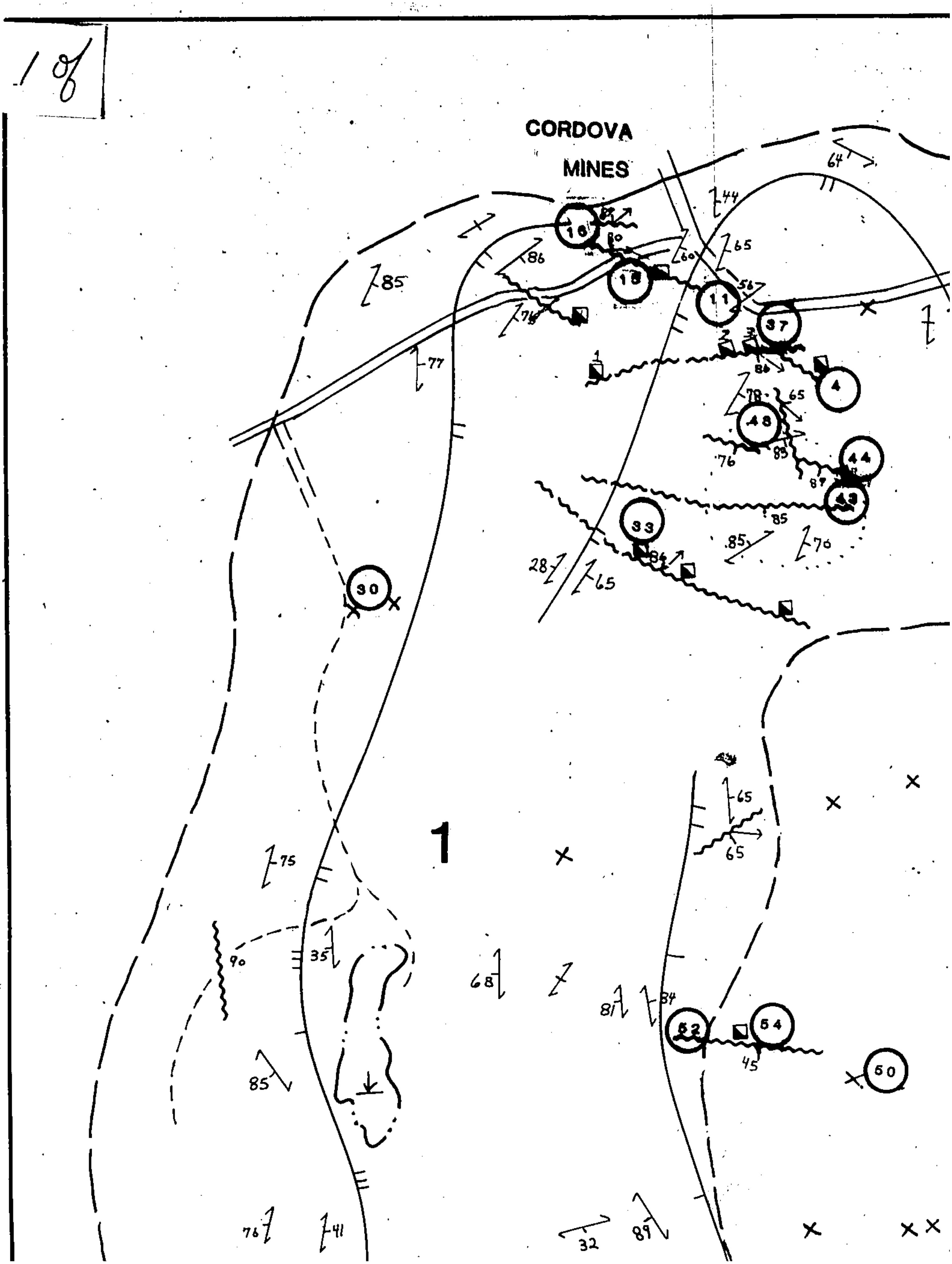
1 of
CORDOVA
MINES
16
18
11
37
4
48
44
43
33
30
1
52
54
50

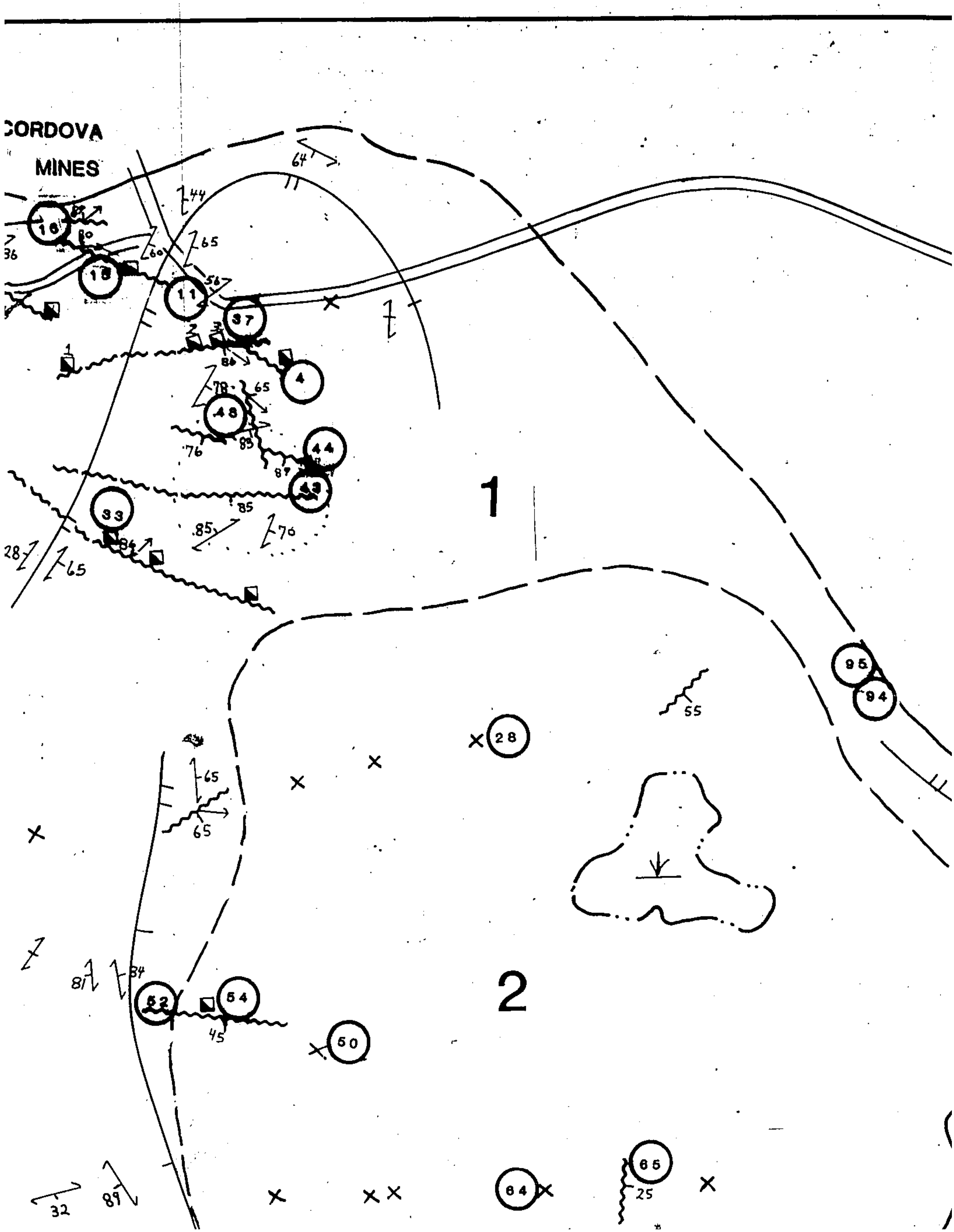

CORDOVA
MINES
1
2

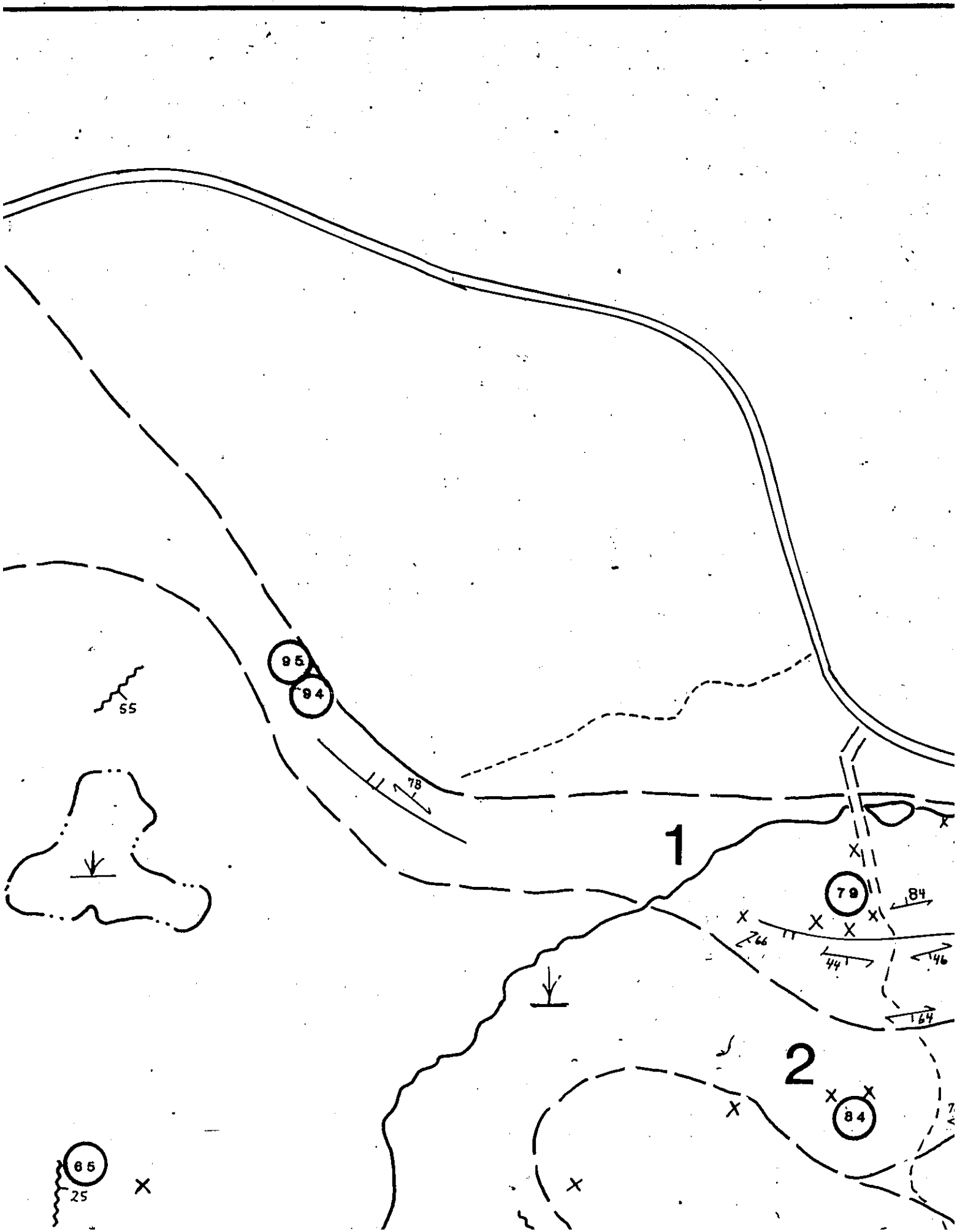
95
94
55
78
1
79
84
66
44
46
164
2
84
66
25

FIG

GE

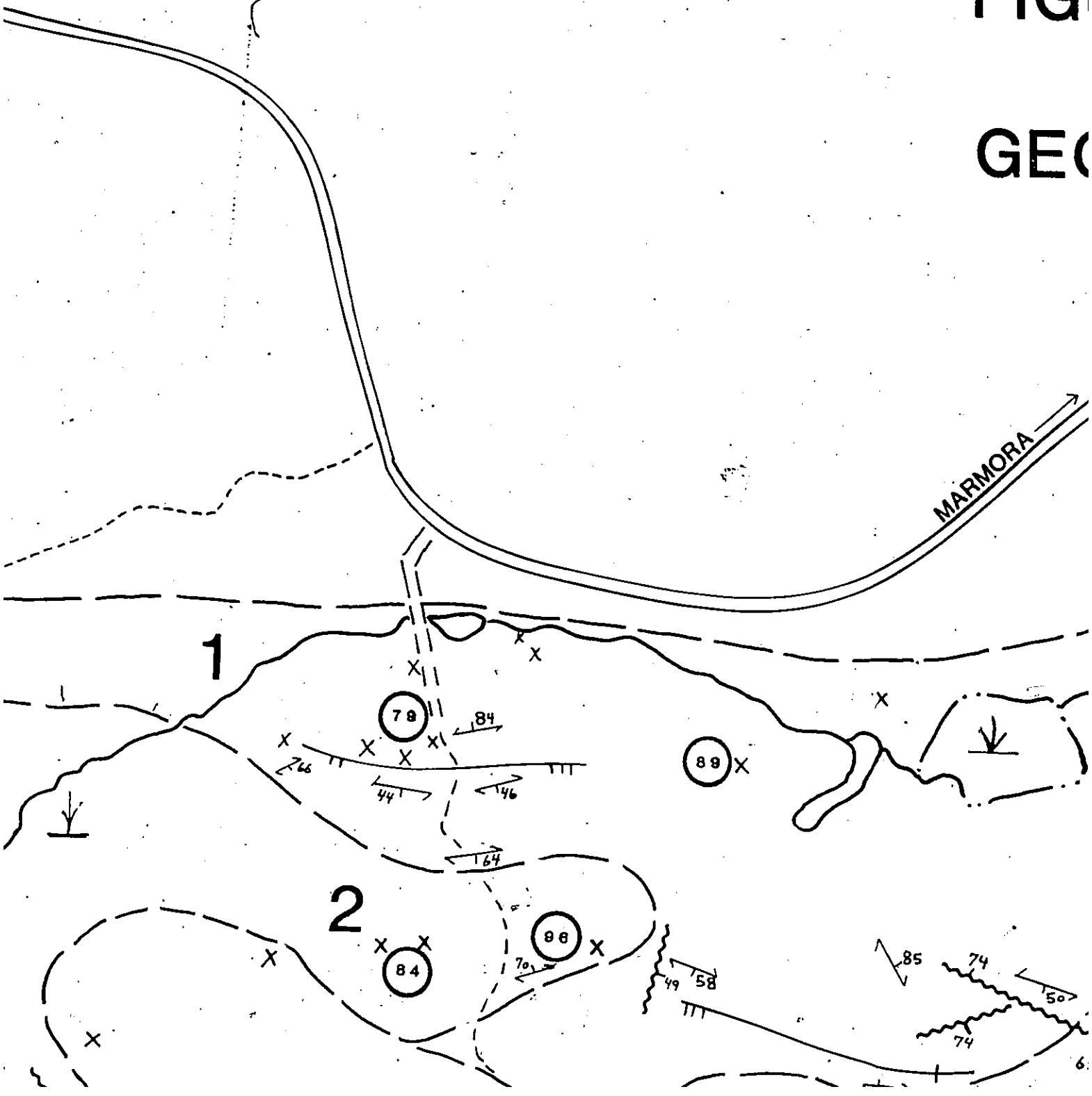

FIGURE 3.1A

GEOLOGY OF THE CO

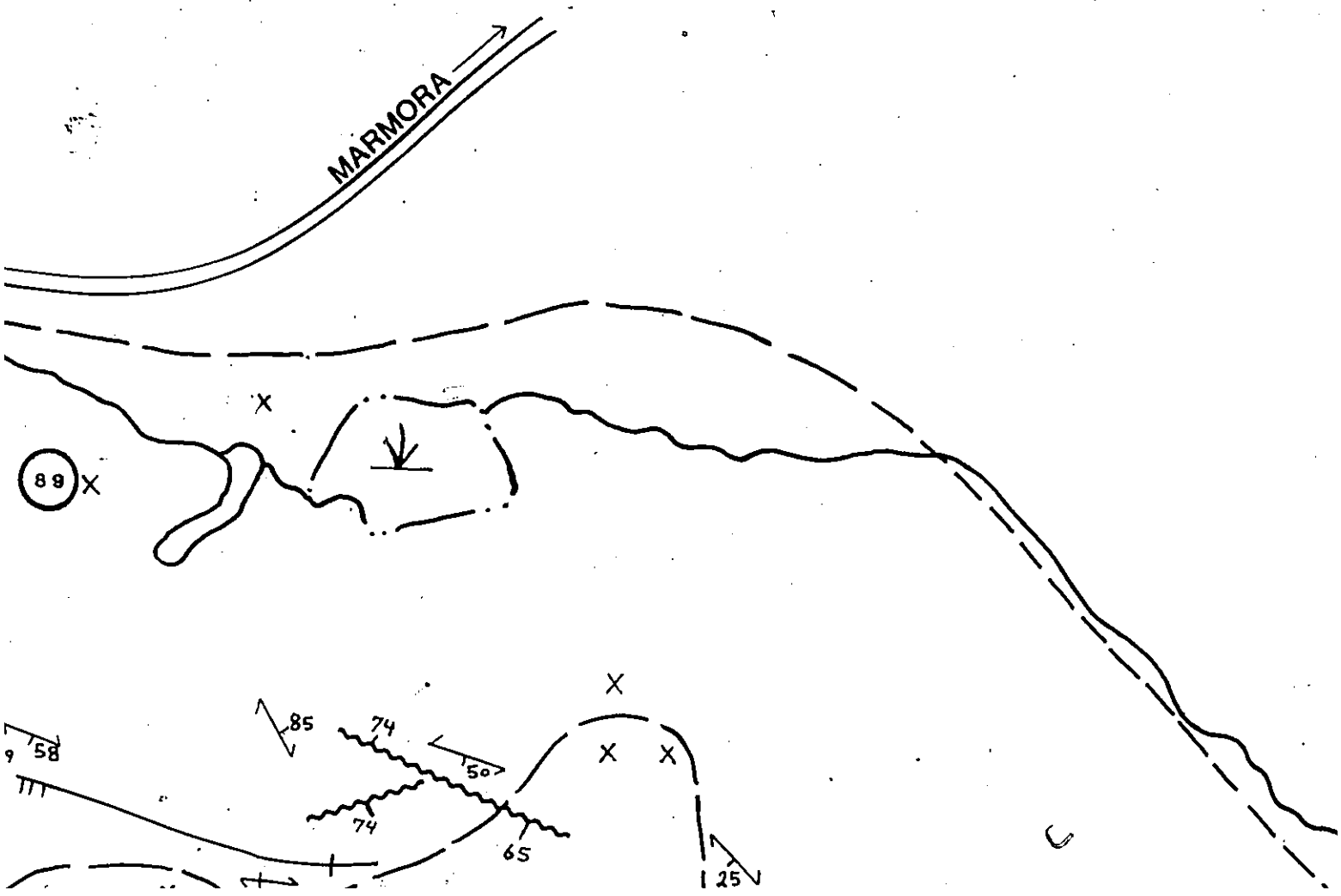

A

OF THE CORDOVA GABBRO

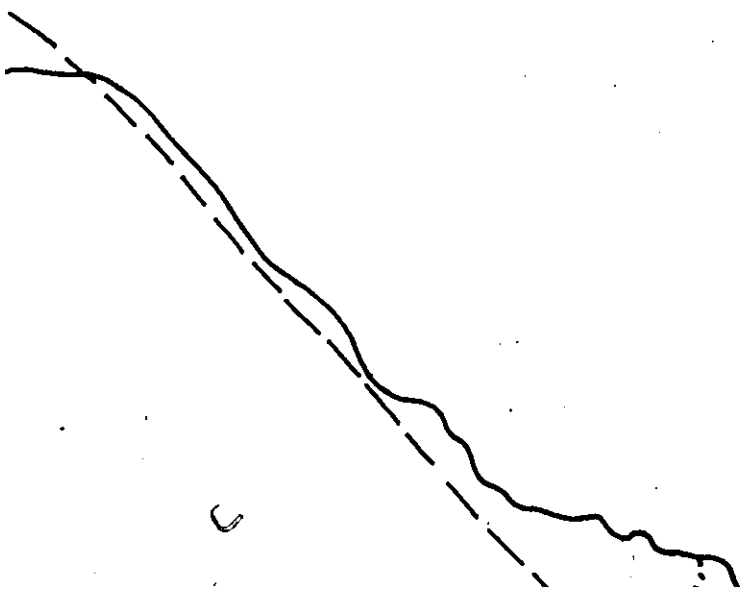

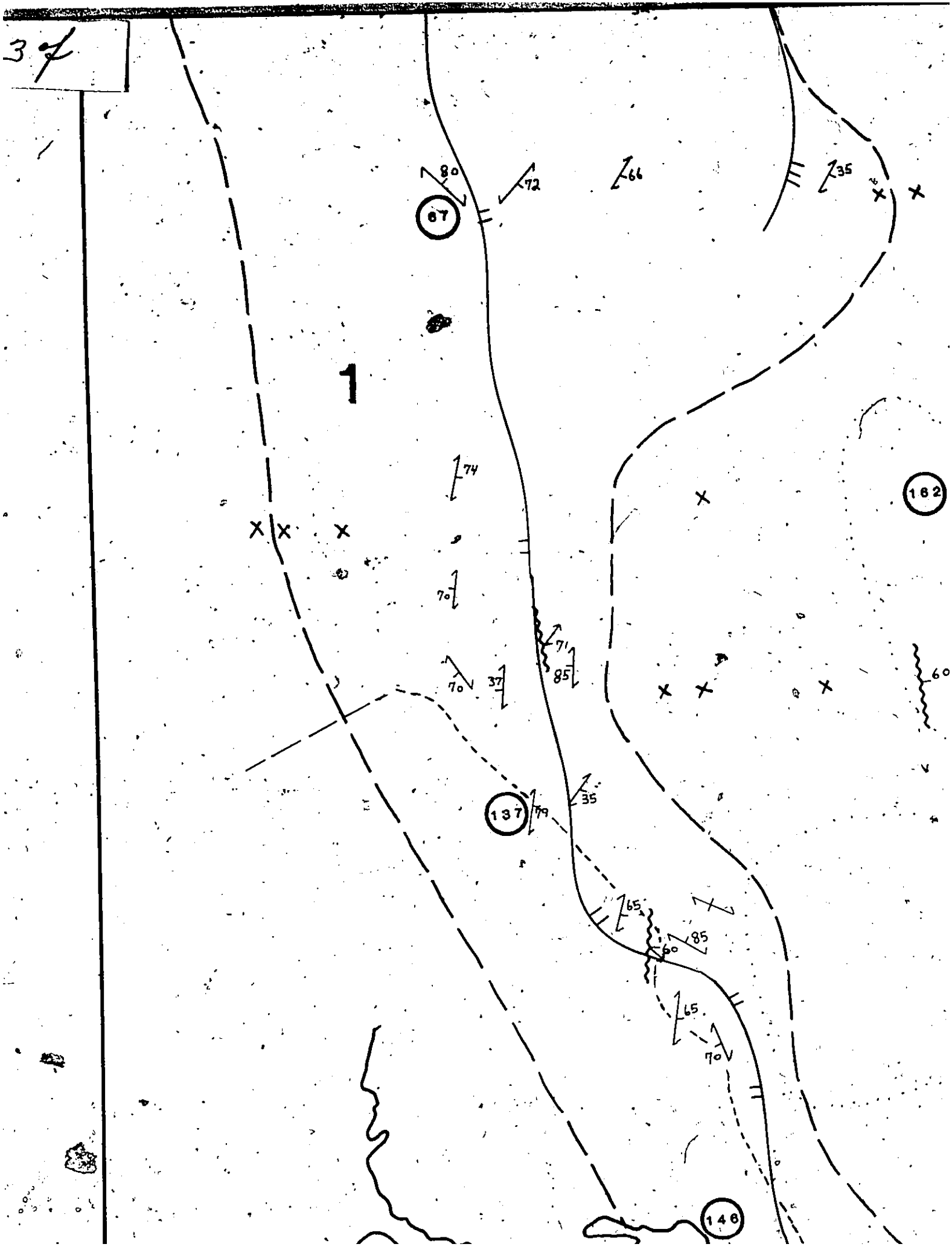
3 2
80
72
66
35
67
1
74
162
70
71
85
70
37
60
137
79
35
65
85
60
65
70
146

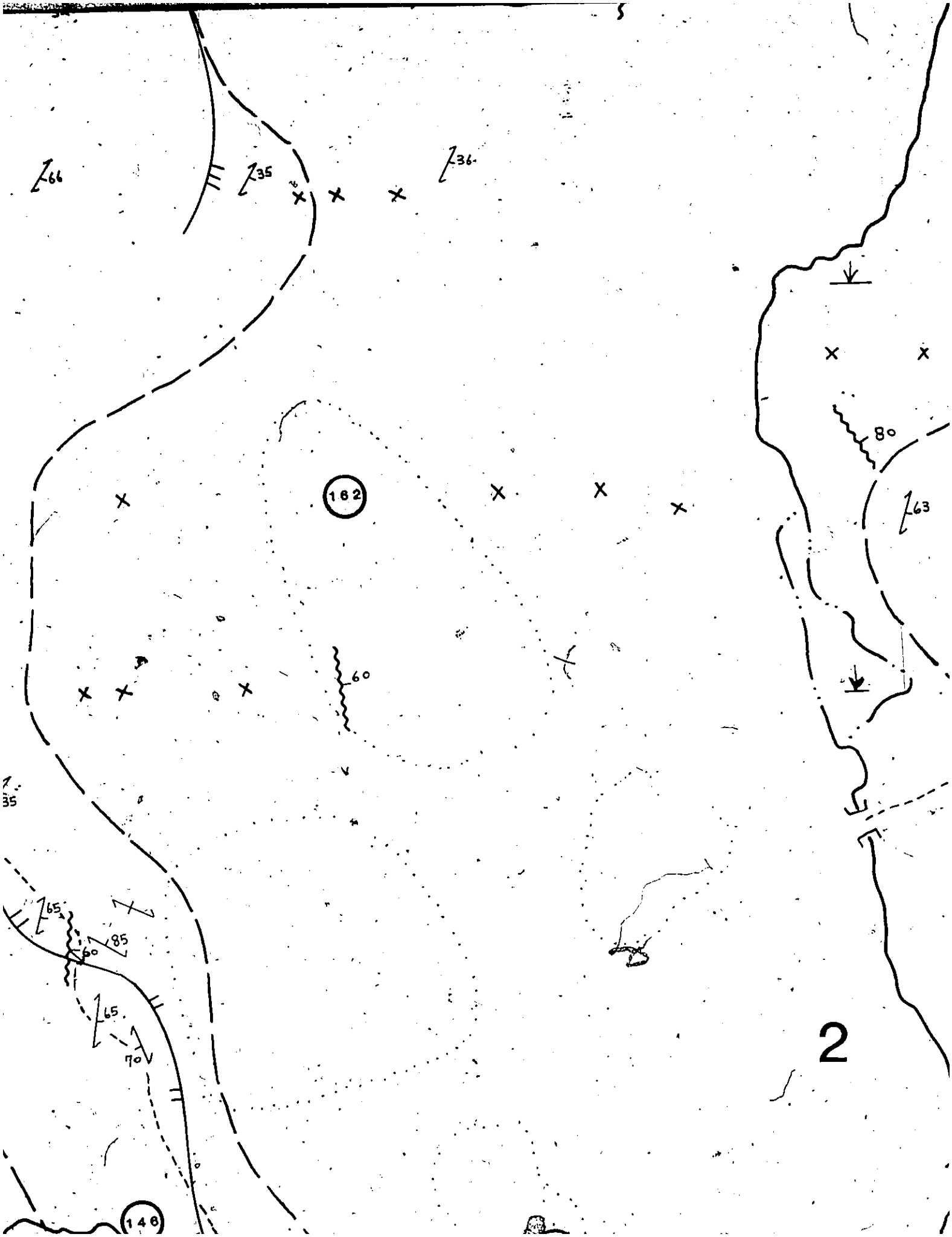
66
35
36
162
80
63
60
35
65
60
85
65
70
146
2

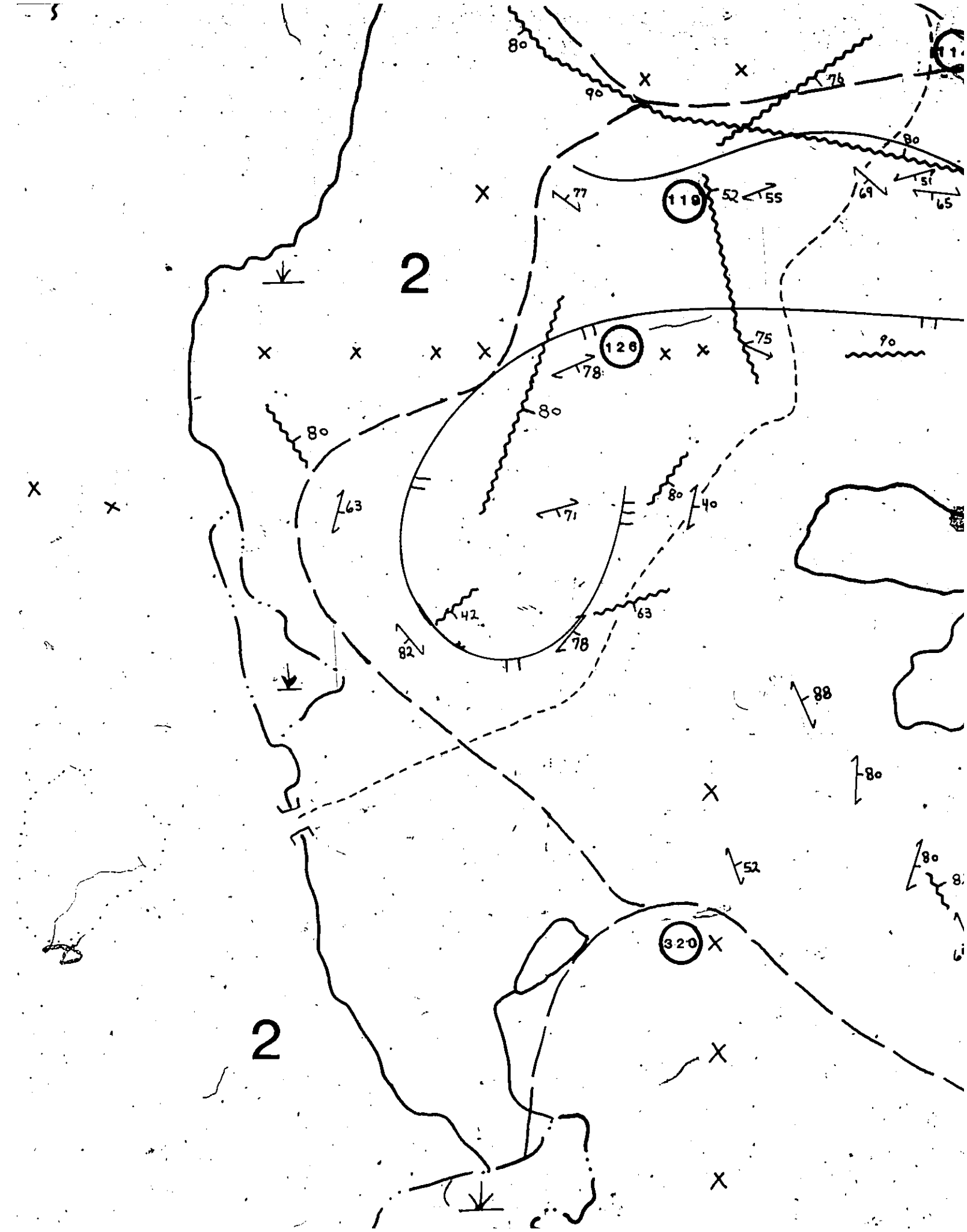
80
90
74
80
77
110
52
55
69
51
65
2
126
75
90
78
80
80
63
71
80
40
42
63
82
78
88
80
52
80
320
2


3
114
118
126
320
90
76
49
80
77
52
55
69
51
65
51
52
75
90
60
78
60
65
40
80
71
80
40
63
78
80
88
80
55
90
52
80
82
65
60

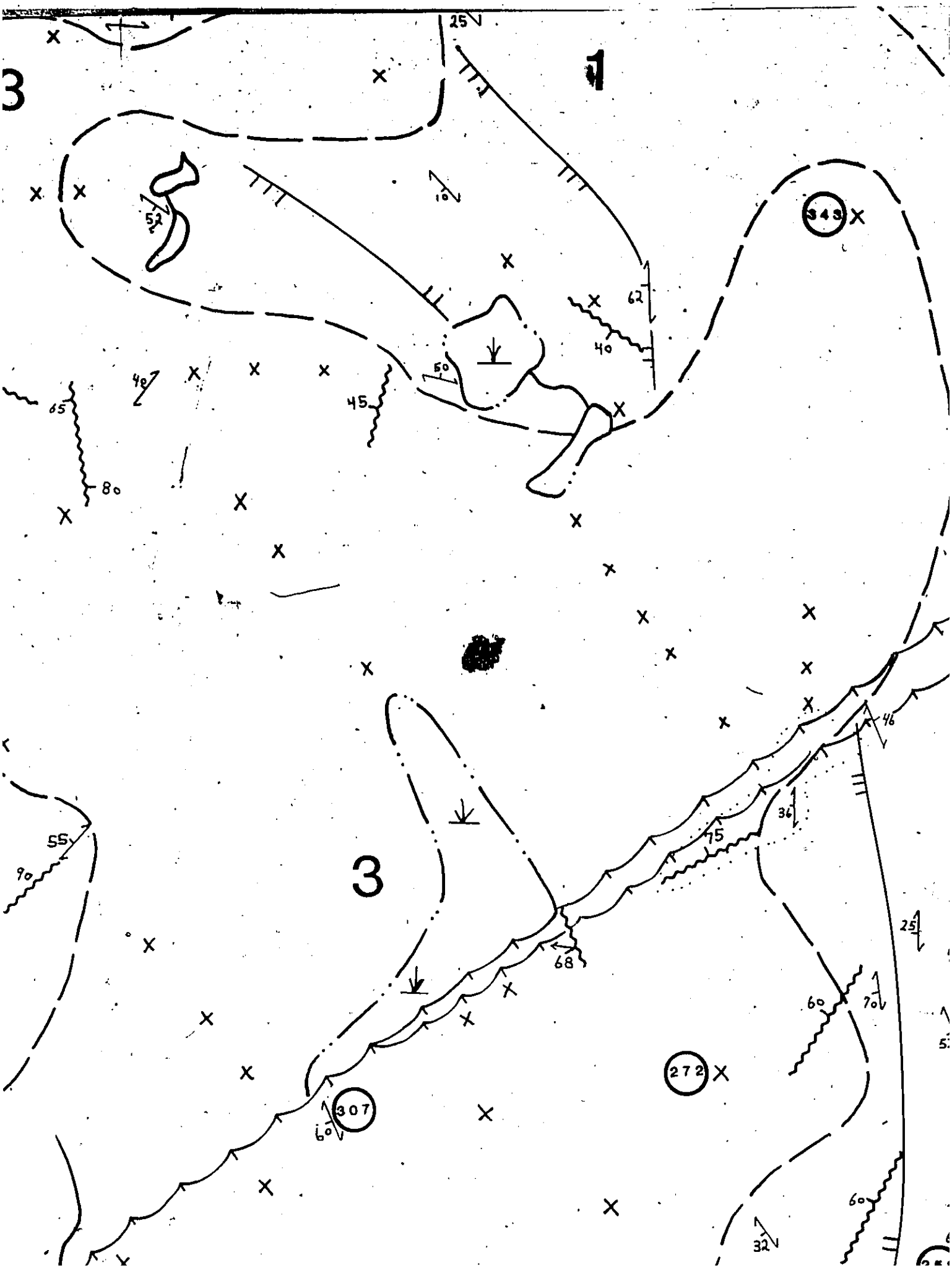
3
1
25
52
10
343
62
40
48
50
65
45
80
3
55
90
46
36
75
68
25
60
70
272
307
60
60
32

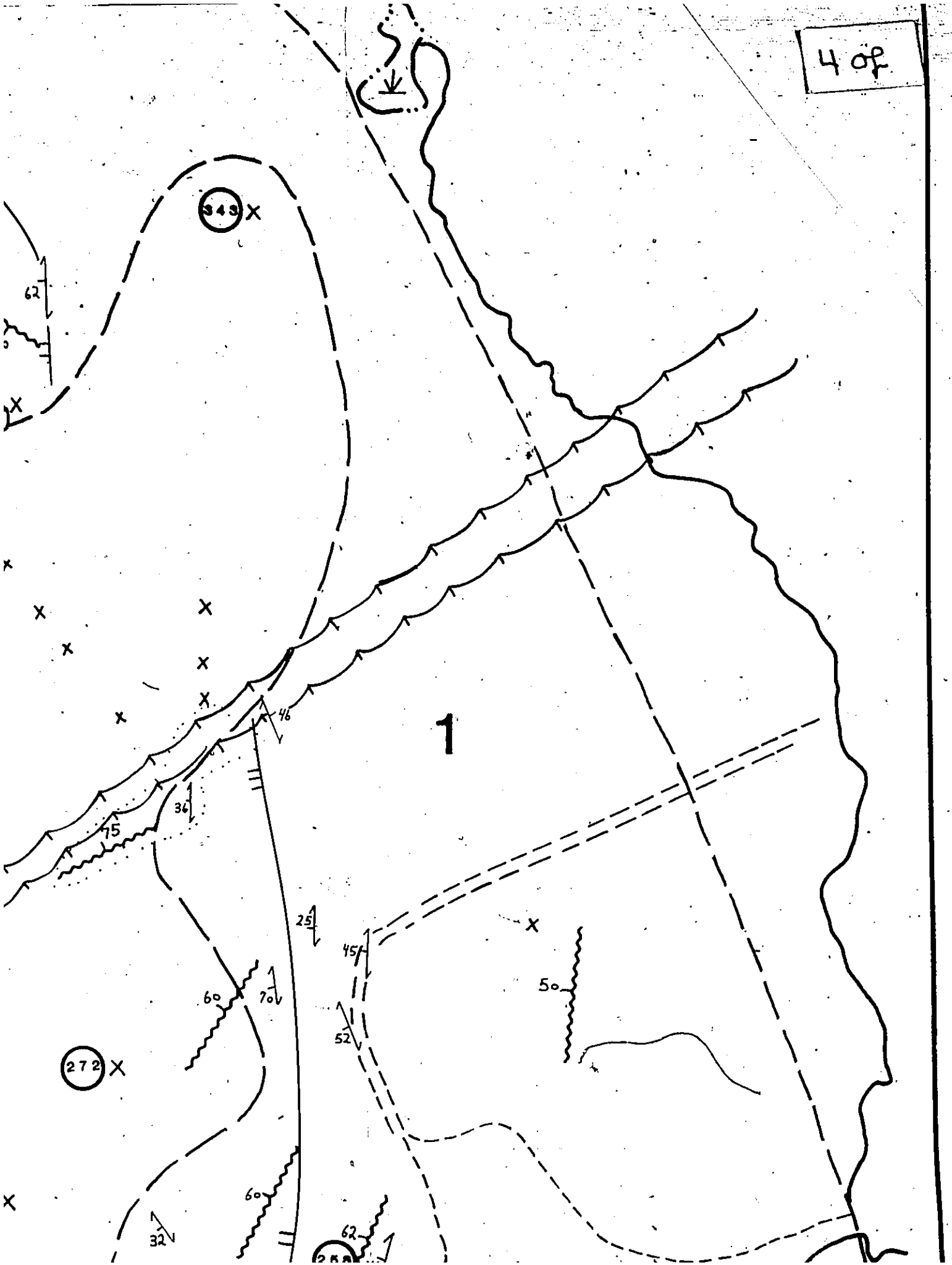
4 of
343
62
46
1
36
75
25
45
50
52
60
70
272
60
32
62

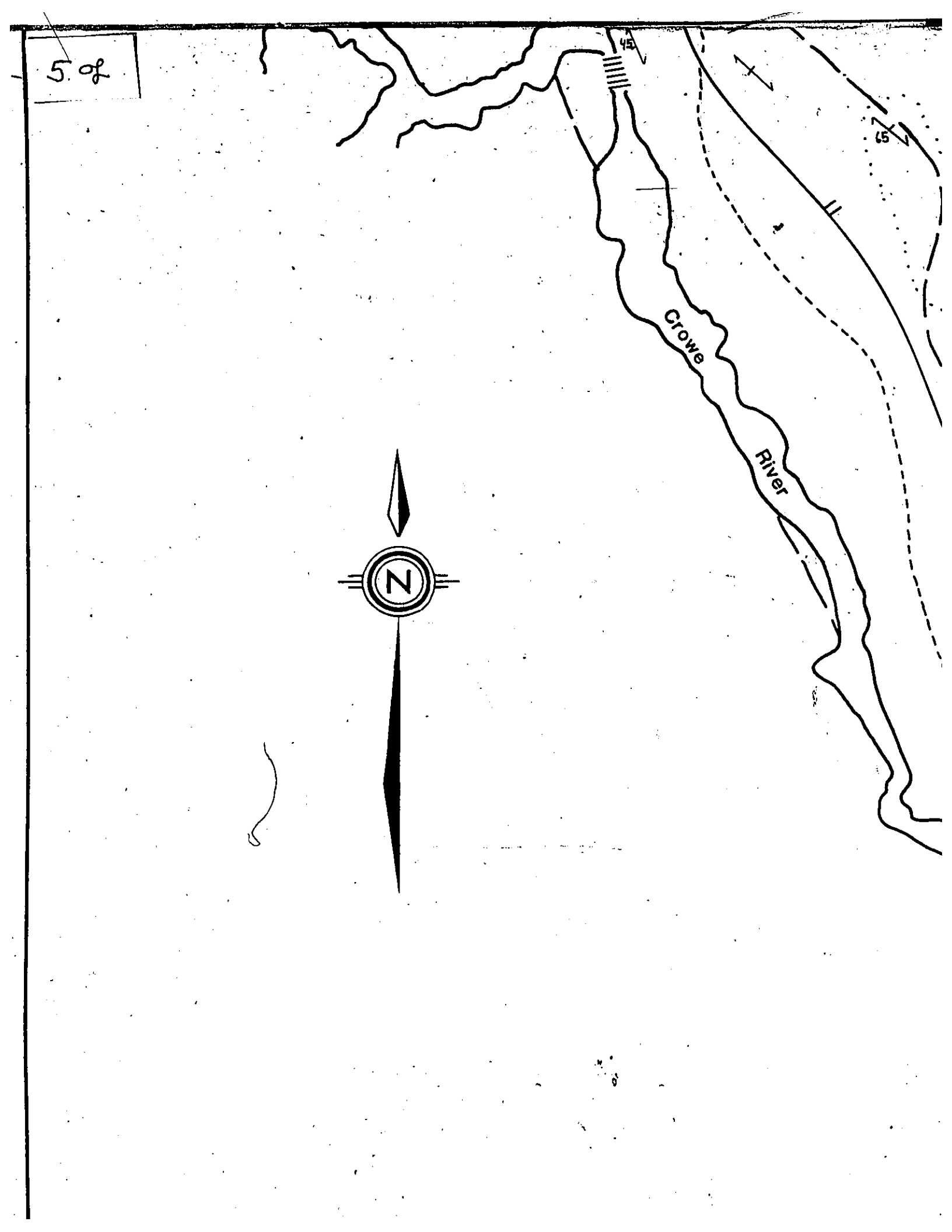
5 of
45
65
Crowe
River
N

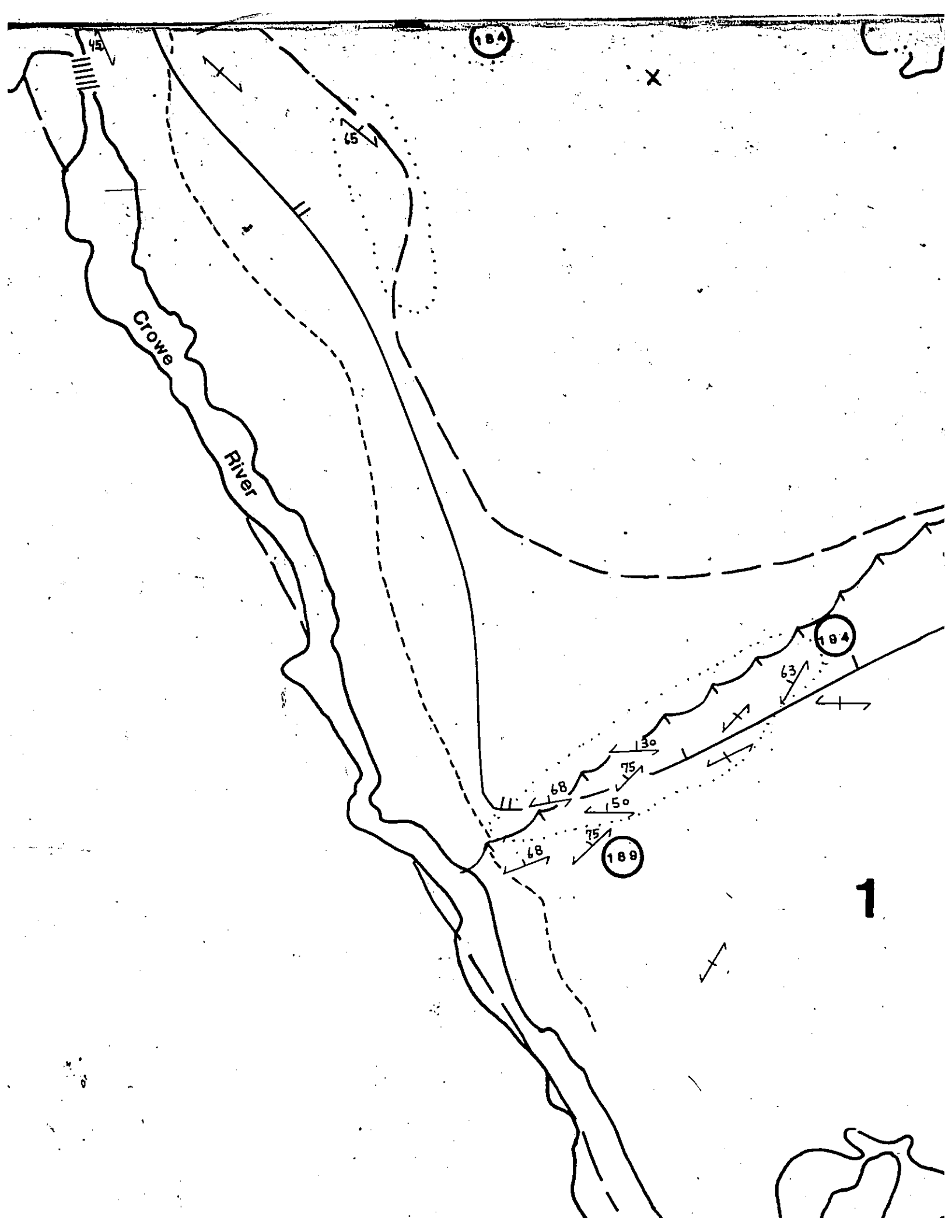
45
184
65
Crowe
River
184
63
30
75
68
50
75
68
188
1

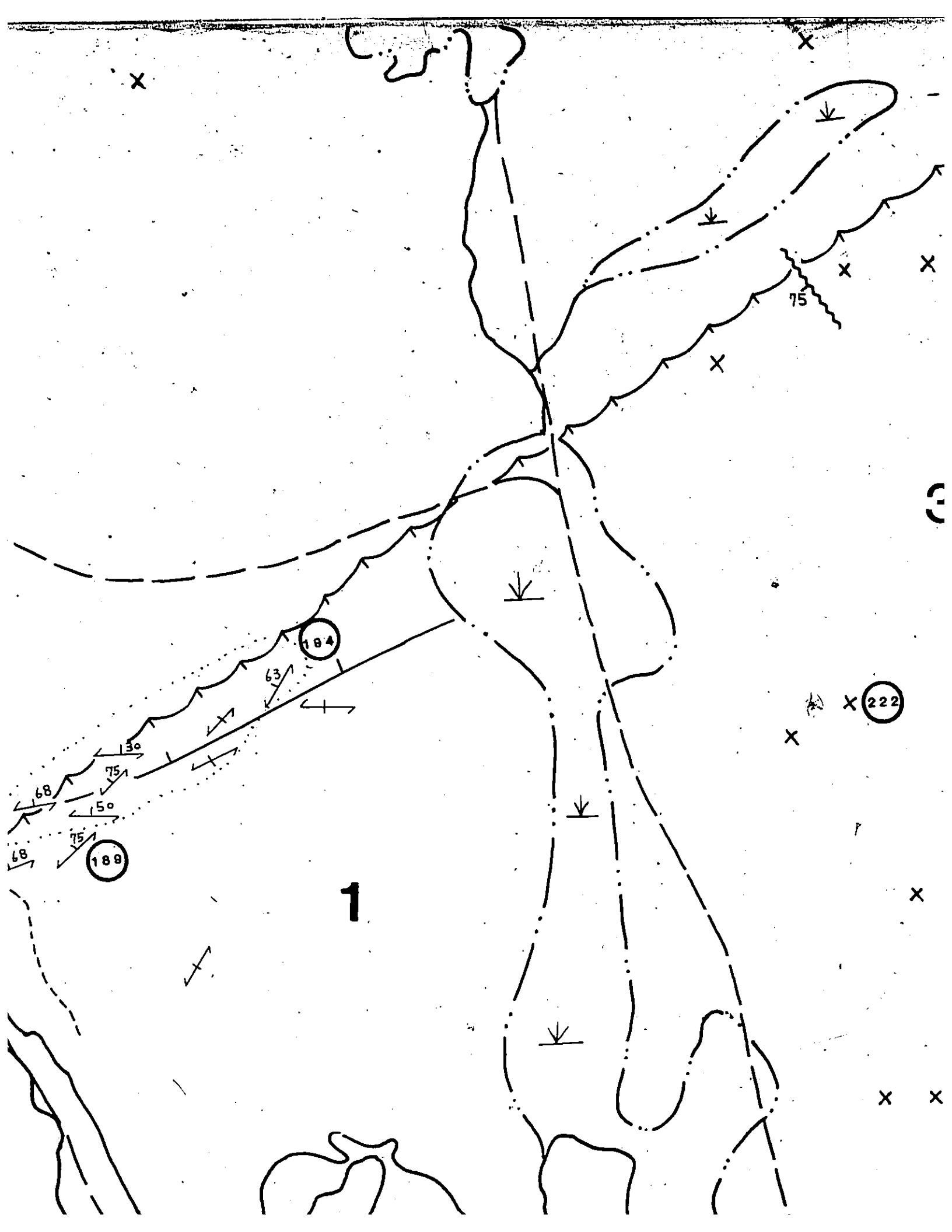
75
184
63
222
30
75
68
150
75
68
189
1

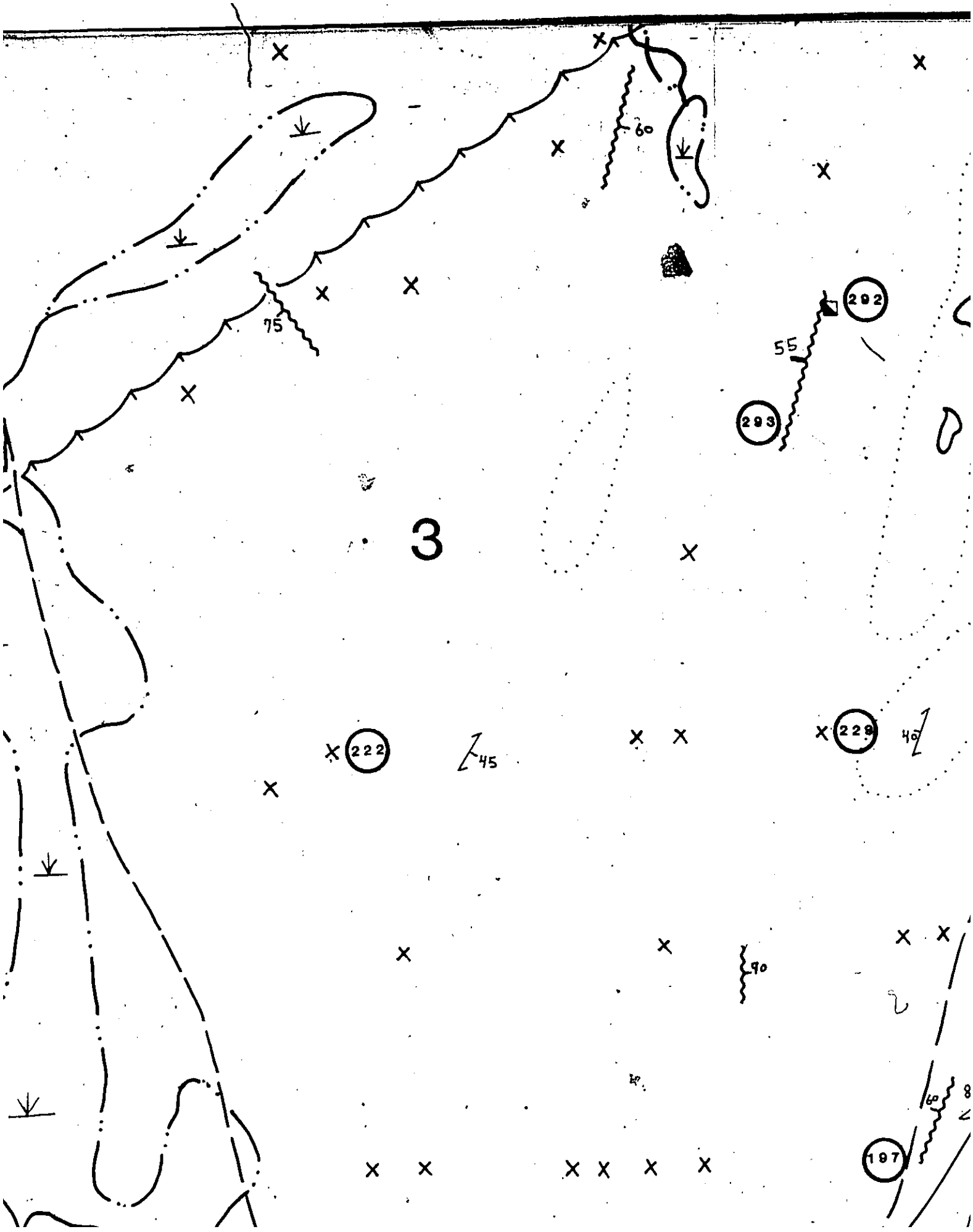
60
75
292
55
293
3
222
45
229
40
90
60
197

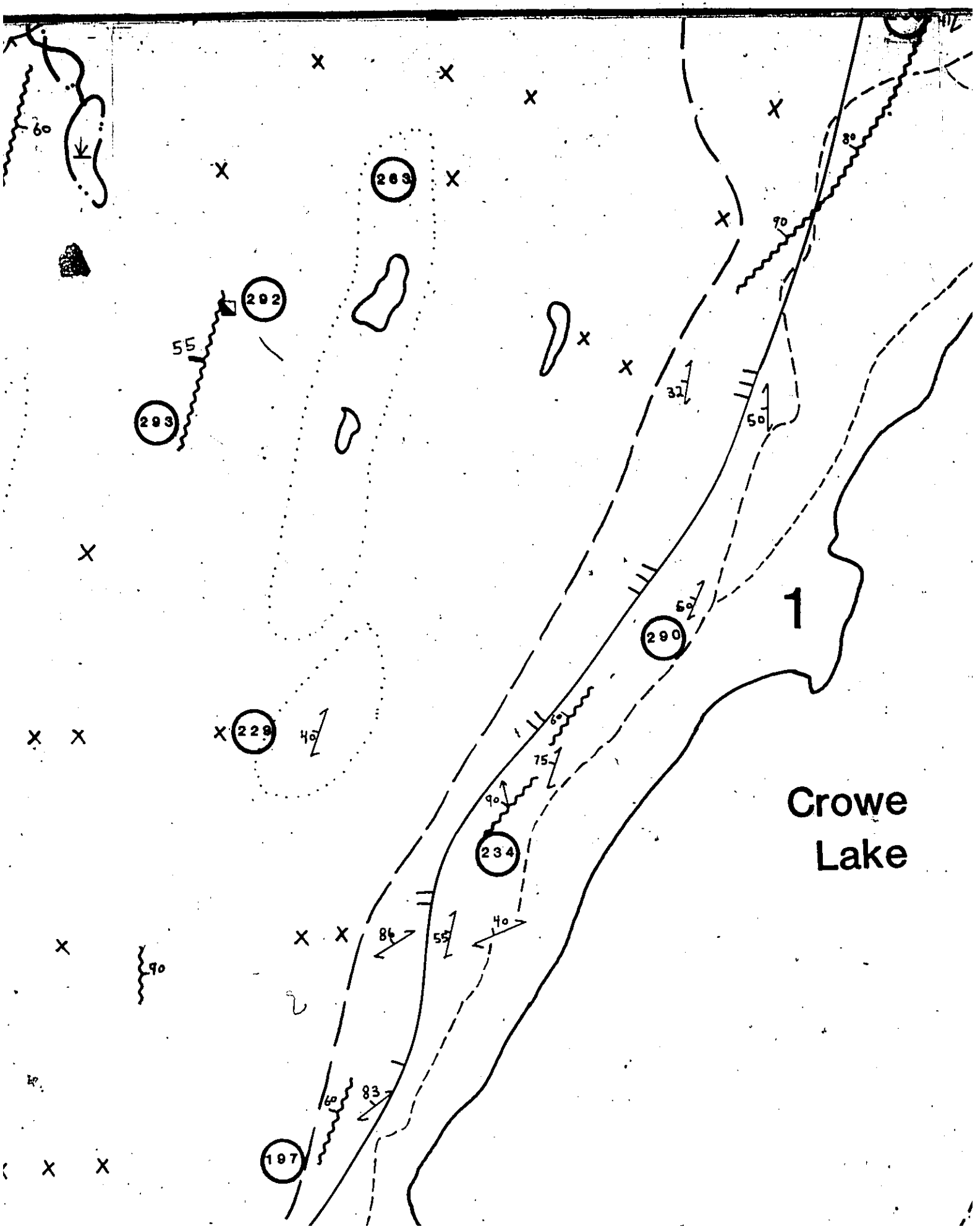
60
283
292
55
293
90
80
32
50
290
60
1
229
40
60
75
90
234
Crowe
Lake
86
55
40
90
60
83
197

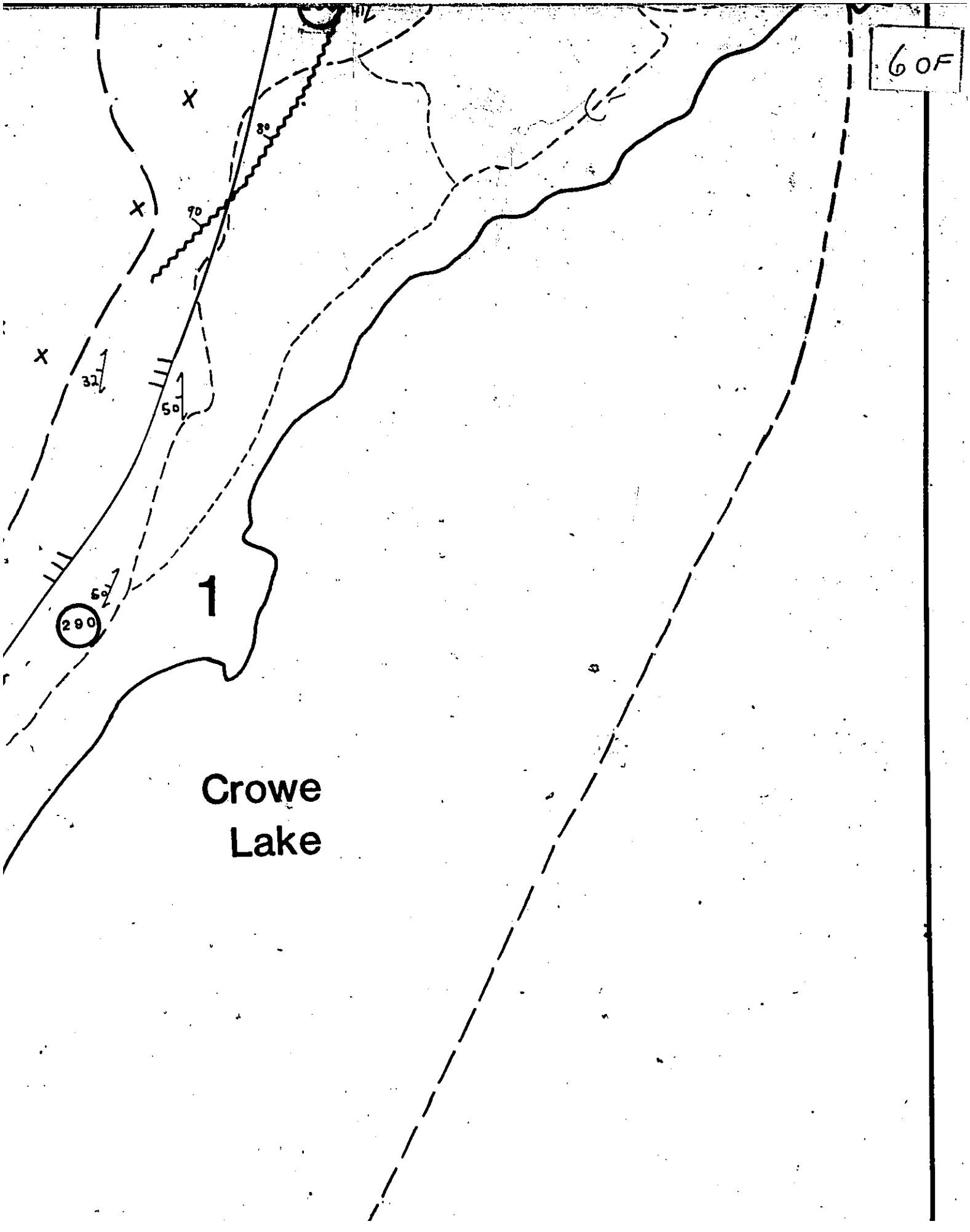
6 OF
X
X
X
80
90
32
50
50
290
1
Crowe
Lake

LEGEND

UNIT 3 Pegmatoid gabbro

UNIT 2 Fine-grained massive gabbro

UNIT 1 Medium-grained layered gabbro

Geologic boundary, defined, approximate, assumed

Shear zone strike and dip , pitch of striation

Strike and dip of foliation

Trend of primary layering, dip: <60, 60-80, 80-90, 90

Outcrop, area of abundant outcrop

Mine shaft (numbered if refered to in text)

Outcrop or sample location
refered to with the prefix CG-81

Swamp

Road, paved unpaved

Power line

GEND

o ---------- 3

ssive gabbro ---------- 2

ayered gabbro ---------- 1

ed, approximate, assumed ----

, pitch of striation ----------

----

ring, dip:<60,60-80,80-90,90

nt outcrop ----------

efered to in text) ----------

on

(CG-81 ----------

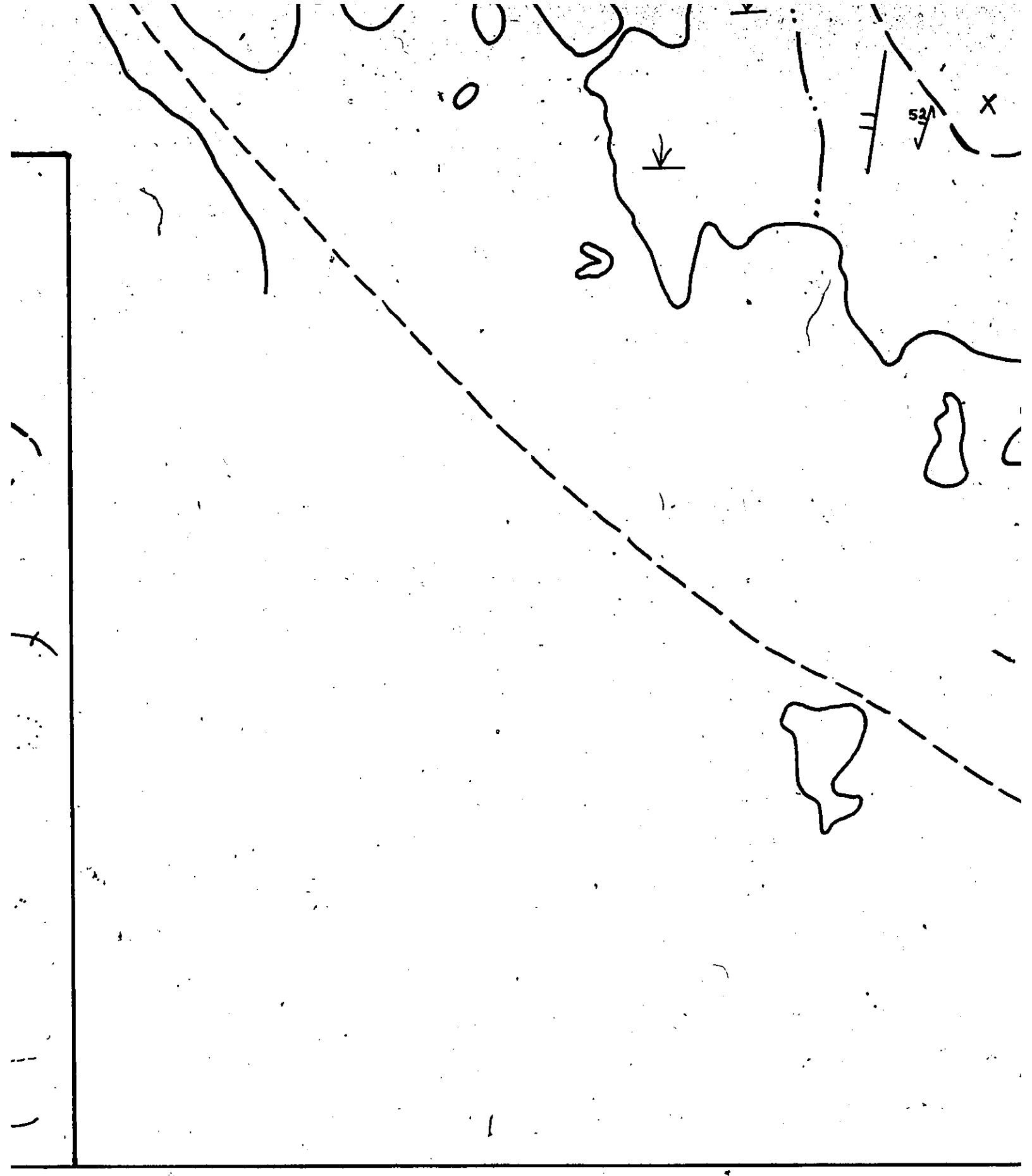
521

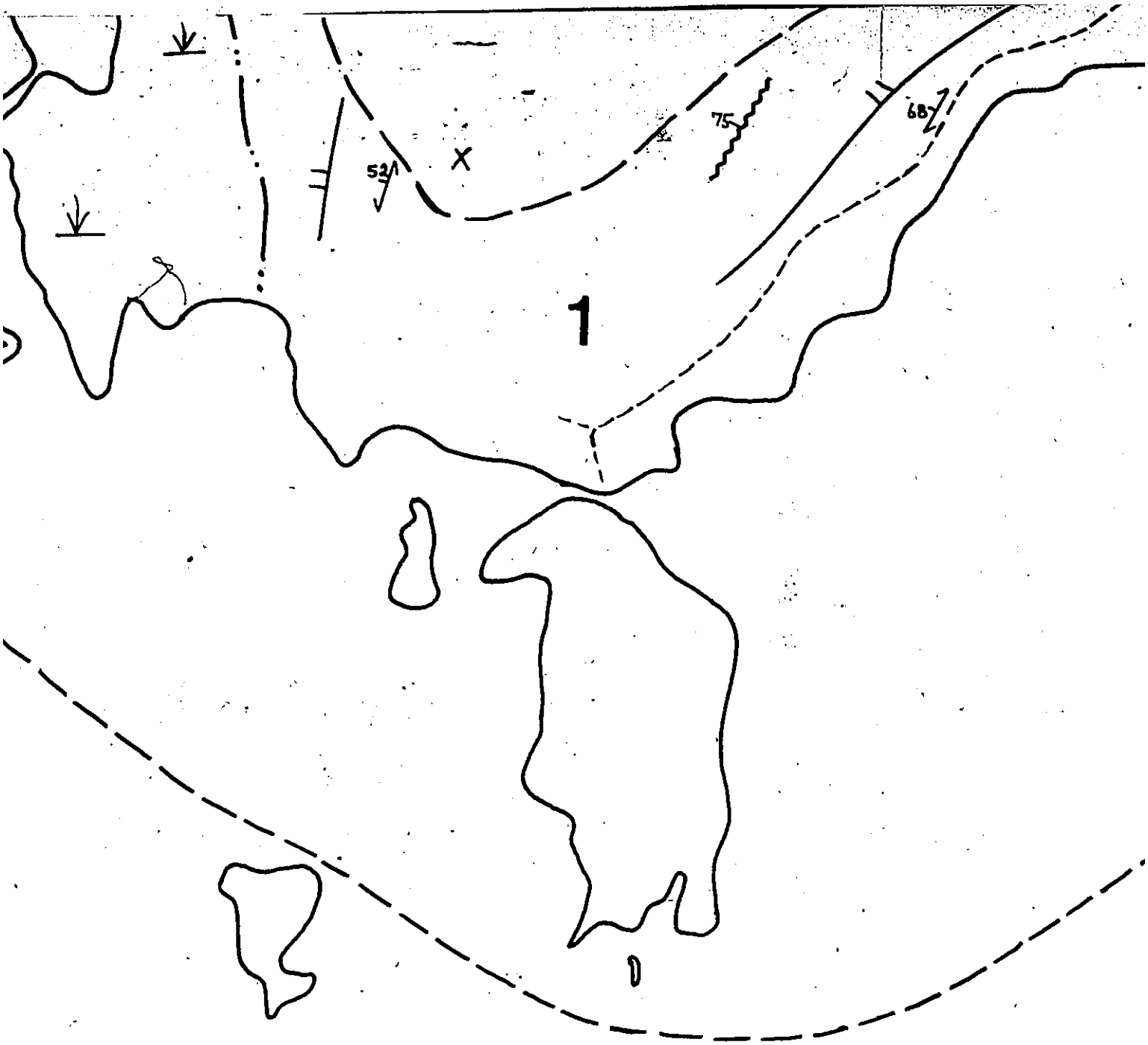
75
68
52
X
1

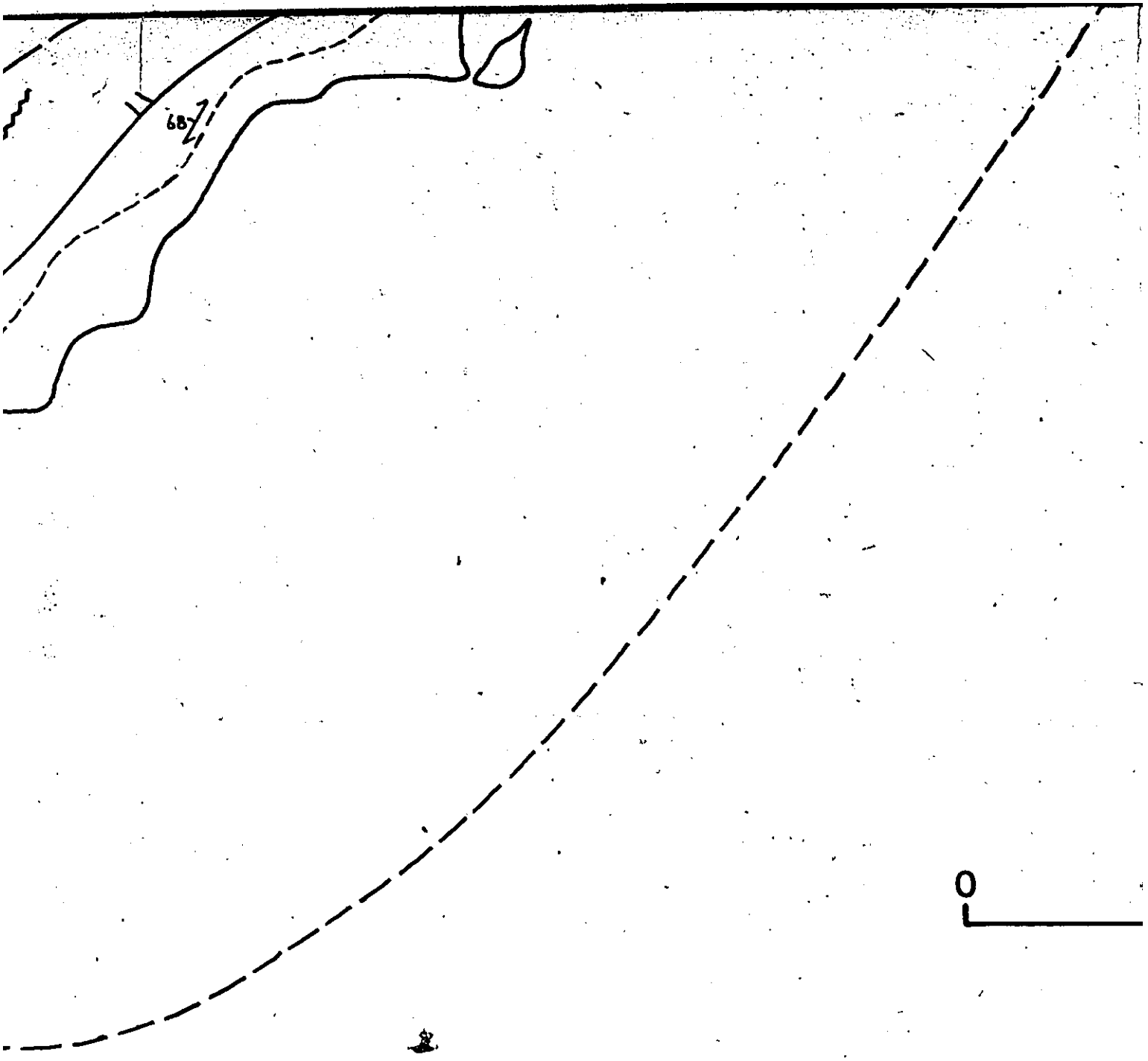
68
0


0
1
kilometres